

2013-12-20

Design of Endothelial Progenitor Cellular Constructs for Therapeutic Angiogenesis Applications

Ximena Vial

University of Miami, x.vial@umiami.edu

Follow this and additional works at: https://scholarlyrepository.miami.edu/oa_dissertations

Recommended Citation

Vial, Ximena, "Design of Endothelial Progenitor Cellular Constructs for Therapeutic Angiogenesis Applications" (2013). *Open Access Dissertations*. 1146.

https://scholarlyrepository.miami.edu/oa_dissertations/1146

This Open access is brought to you for free and open access by the Electronic Theses and Dissertations at Scholarly Repository. It has been accepted for inclusion in Open Access Dissertations by an authorized administrator of Scholarly Repository. For more information, please contact repository.library@miami.edu.

UNIVERSITY OF MIAMI

DESIGN OF ENDOTHELIAL PROGENITOR CELLULAR CONSTRUCTS FOR
THERAPEUTIC ANGIOGENESIS APPLICATIONS

By

Ximena Vial

A DISSERTATION

Submitted to the Faculty
of the University of Miami
in partial fulfillment of the requirements for
the degree of Doctor of Philosophy

Coral Gables, Florida

December 2013

©2013
Ximena Vial
All Rights Reserved

UNIVERSITY OF MIAMI

A dissertation submitted in partial fulfillment of
the requirements for the degree of
Doctor of Philosophy

DESIGN OF ENDOTHELIAL PROGENITOR CELLULAR CONSTRUCTS FOR
THERAPEUTIC ANGIOGENESIS APPLICATIONS

Ximena Vial

Approved:

Fotios M. Andreopoulos, Ph.D.
Professor of Biomedical Engineering

Edward Dauer, M.D.
Professor of Biomedical
Engineering

Si Pham, M.D.
Professor of Surgery

Herman Cheung, Ph.D.
Professor of Biomedical
Engineering

Roberto Vazquez-Padron
Professor of Surgery

M. Brian Blake, Ph.D.
Dean of the Graduate
School

VIAL, XIMENA
Design Of Endothelial Progenitor
Cellular Constructs For Therapeutic
Angiogenesis Applications

(Ph.D., Biomedical Engineering)
(December 2013)

Abstract of a dissertation at the University of Miami.

Dissertation supervised by Professor Fotios M. Andreopoulos
No. of pages in text. (162)

The goal of therapeutic angiogenesis is the development of functional and mature vasculature by combining biological and physical cues that mimic the native extracellular matrix. In this study we evaluated if immobilizing vascular endothelial growth factor (VEGF) gradients and SDF-1 α on gelatin nanofibrous scaffolds with different fiber orientations (i.e. random or aligned) influence the angiogenic potential of endothelial progenitor cells (EPCs) and human umbilical vein endothelial cells (HUVECs). Both cell types successfully adhered onto gelatin B scaffolds. VEGF gradients alone or combined with SDF-1 α as well as fiber orientation had a pronounced effect on cell behavior, morphology and orientation. Cells organized themselves parallel to the fibers of the electrospun scaffolds with the aligned orientation and developed a spindle-like morphology. Conversely, cells cultured on scaffolds with random fiber orientation, did not display directionality and appeared to have a rounder shape. Cell migration and capillary formation were found to be dependent on VEGF gradients, SDF-1 α presentation and cell type. These findings indicate that electrospun scaffolds are capable of regulating spatial growth factor presentation and influence cellular organization.

Table of Contents

List of Figures	v
List of Tables	viii
Chapter 1: Background and Significance	1
1.1 Vascular Biology and Pathophysiology	2
1.2 Angiogenesis.....	3
1.3 Current Strategies in Therapeutic Angiogenesis	8
1.4 Vascular Tissue Engineering.....	14
1.5 Angiogenic Growth Factor Delivery Strategies in Vascular Tissue Engineering	17
1.6 Guided Angiogenesis and Spatial-Temporal Delivery of Growth Factors..	19
1.7 Specific Aims.....	22
Chapter 2: Synthesis and Characterization of Nanofibrous Scaffolds with Defined Architectural and Biological Cues	25
2.1 Experimental Approach	28
2.1.1 Scaffold Fabrication and Crosslinking	28
2.1.2 Characterization of Nanofibrous Scaffolds: Morphological Characteristics, Degree of Swelling, Degradation Rate and Cytotoxicity	30
2.1.2.1 Evaluation of Fiber Morphology as a Function of Electrospinning Parameters.....	30
2.1.2.2 Effect of Crosslinking on Scaffold Morphology, Swelling and Degradation.....	30
2.1.2.3 Growth Factor Gradient Immobilization and Formation	32
2.1.2.4 Growth Factor Release Profile	33
2.1.2.5 Evaluation of Cell Proliferation and Morphology as a Function of Scaffold Architecture and Growth Factor Immobilization Pattern	34
2.2 Results and Discussion	34
2.2.1 Scaffold Morphology as a Function of Electrospinning Parameters	34
2.2.2 Effects of Crosslinking on Scaffold Morphology, Swelling and Degradation.....	35
2.2.3 Growth Factor Release Profile	36
2.2.4 Cell Proliferation and Morphology as a Function of Scaffold Architecture and Growth Factor Gradient.....	40

2.3 Conclusions.....	44
Chapter 3: Determine the Effect of VEGF Releasing Electrospun Scaffolds on Cellular Behavior (i.e. Proliferation and Migration) In Vitro.....	46
3.1 Experimental Approach.....	48
3.1.1 Live Cell Imaging Design and Setup Mechanims.....	48
3.1.2 HUVEC and EPC cell culture.....	50
3.1.3 Cell Density and Tubular Formation as a Function of Time and Scaffold Morphology.....	51
3.1.4 Cell Proliferation as a Function of Time and Scaffold Morphology.....	52
3.1.5 Cell Migration Evaluation.....	52
3.1.6 Cell Morphology.....	53
3.1.7 Immunohistochemistry.....	54
3.2 Results and Discussion.....	54
3.3 Conclusions.....	73
Chapter 4: Develop EPC-Seeded Vascular Sheets and Determine Capillary Formation as a Function of Construct Parameters and Co-administration of VEGF and SDF-1α.....	74
4.1 Experimental Approach.....	76
4.1.1 EPC cell culture.....	76
4.1.2 Cell Density and Proliferation as a Function of VEGF and SDF-1 α Delivery.....	76
4.1.3 Capillary Formation as a Function of VEGF and SDF-1 α Activity.....	78
4.1.4 Cell Migration Evaluation.....	78
4.1.5 Cell Morphology.....	80
4.1.6 Immunohistochemistry.....	80
4.2 Results and Discussion.....	81
4.3 Conclusions.....	93
Chapter 5: Conclusions and Future Directions.....	94
References.....	97
Appendices.....	109
Appendix I.....	110
Appendix II.....	122

List of Figures

Figure 1.1: Endothelial cells and vascular network assembly.....	5
Figure 1.2: Sprouting Angiogenesis.....	6
Figure 1.3: PLGA in growth factor delivery: the sequential release of dual factors has been examined by embedding PDGF-incorporated particles in a PLGA foam that have VEGF dispersed within	10
Figure 1.4: Cardiac tissue patches form human cardiac muscle and integrated human microvessels in rodent hearts	12
Figure 1.5: Schematic demonstrating a combination strategy for the delivery of HGF and BMNCs (bone marrow mononuclear cells) using a PEGylated fibrin biomatrix.....	14
Figure 1.6: Advanced synergistic tissue engineering approaches for cardiac regeneration	17
Figure 1.7: Schematic drawing of selected model systems for the delivery of two growth factors (GFs, i.e. GF1 and GF2)	21
Figure 2.1: Scanning electron microscopy images (SEM) of electrospun scaffolds	29
Figure 2.2: Diagrammatic representation of scaffold preparation and cell seeding	32
Figure 2.3: FITC-Albumin gradient distribution within gelatin electrospun scaffolds	33
Figure 2.4: Representative SEM image used to assess fiber diameters	36
Figure 2.5: Changes in scaffold architecture and fiber dimensions as a function of glutaraldehyde crosslinking	37
Figure 2.6: Degree of swelling and degradation kinetics as a function of GA vapor exposure time	38
Figure 2.7: Evaluation of the degree of swelling as a function of scaffold architecture (i.e. Aligned fiber scaffolds vs. Random fiber scaffolds) and Comparison between the release profiles of FITC-albumin from aligned fiber scaffolds and random fiber scaffolds	39
Figure 2.8: HUVEC proliferation as a function of scaffold topography – Aligned versus Random	41

Figure 2.9: Cytoskeleton arrangement of HUVECs on electrospun gelatin scaffolds	42
Figure 2.10: Cell density and proliferation as a function of scaffold topography .	44
Figure 3.1: Diagrammatic representation of well plate incubator components ...	48
Figure 3.2: Diagrammatic representation of well plate incubator connections....	49
Figure 3.3: Diagrammatic representation of chamber placement	50
Figure 3.4: EPC and HUVEC morphological response to nanotopography and VEGF gradients (Circularity)	57
Figure 3.5: Images of time-lapse video utilized for cell tracking	59
Figure 3.6: Migration velocity as a function of VEGF gradients and scaffold topography	60
Figure 3.7: Effective displacement as a function of VEGF gradients and scaffold topography	61
Figure 3.8: Cellular migration paths as a function of scaffold topography	62
Figure 3.9: Cell density as a function of VEGF gradients and scaffold topography	65
Figure 3.10: EPC and HUVEC proliferation as a function of VEGF gradients and scaffold topography	67
Figure 3.11: Effect of VEGF gradient and scaffold nanotopography on tubular formation	69
Figure 3.12: EPC and HUVEC immunohistochemistry evaluating expression of von Willebrand factor and VE-Cadherin as a function of VEGF gradients and scaffold topography	70
Figure 4.1: Diagrammatic representation of scaffold preparation and cell seeding	77
Figure 4.2: EPC response to the co-administration of VEGF gradients and SDF-1 α (Circularity)	82
Figure 4.3: Migration velocity as a function of the co-delivery of VEGF gradients and SDF-1 α	84
Figure 4.4: Effective displacement as a function of the co-delivery of VEGF gradients and SDF-1 α	84
Figure 4.5: Cellular migration paths as a function of co-administration of VEGF gradients and SDF-1 α	85

Figure 4.6: Cell density as a function of co-delivery of VEGF gradients and SDF-1 α	86
Figure 4.7: EPC proliferation as a function of co-administration of VEGF gradients and SDF-1 α	87
Figure 4.8: Tubular formation as a function of co-administration of VEGF gradients and SDF-1 α	89
Figure 4.9: EPC and HUVEC immunohistochemistry evaluating expression of von Willebrand factor and VE-Cadherin as a function of VEGF gradients and scaffold topography	90

List of Tables

Table 1.1: Matrices and Scaffolds for single angiogenic growth factor delivery. Adapted from Matrices and scaffolds for drug delivery in vascular tissue engineering.....	8
Table 2.1: Groups of electrospun 10% (Group A ₁₅ -C ₁₅) and 5% (Group D ₁₅ - F ₁₅) gelatin B in 1,1,1,3,3,3 hexafluoro-2-propanol nanofibrous scaffolds at different parameters	29

CHAPTER 1: BACKGROUND AND SIGNIFICANCE

1.1 Vascular Biology and Pathophysiology

The main function of vasculature is to maintain oxygen homeostasis by modulating O₂ delivery and exchange, in order to meet the demands imposed by cells [1-3]. Hence, understanding the fundamentals of vascular biology provides a foundation to fathom both normal functions of organ systems and their pathophysiological states. Briefly, capillaries consist of monolayers of endothelial cells juxtaposed with pericytes. Unlike larger vessels, pericytes do not to form a continuous sheath around microvessels. On the other hand, veins and arteries have a tri-laminar structure: The intima consists of endothelial cells, pericytes and a basement membrane, the middle layer or tunica media is composed principally of smooth muscle cells and the outer layer or adventitia consists of fibroblasts, mast cells, nerve terminals and extracellular matrix. Furthermore, arterioles and medium-size muscular arteries consist of thick and prominent tunica media in relation to the adventitia, where the muscular tone regulates both blood pressure and flow through the arterial networks. On the other hand, larger elastic arteries have a structured tunica media composed of concentric bands of smooth-muscle cells interspersed with elastin-rich extracellular matrix [1-3].

These types of arteries (i.e. muscular and elastic) are commonly affected by occlusions (i.e. atherosclerosis) and can lead to ischemia to the heart, brain or limbs resulting in infarction. In clinical disorders such as peripheral arterial disease (PAD), stenosis in the aorta or arteries of the extremities is

characteristic. Briefly, large and medium-sized vessels are occluded by segmental lesions that include atherosclerotic plaques (calcium deposition), thinning of the media, irregular destruction of muscle and elastic fibers, fragmentation of the internal elastic lamina, and thrombi composed of platelets and fibrin. Generally, said atherosclerotic lesions involve sites such as the abdominal aorta and iliac arteries, the femoral and popliteal arteries, and the more distal vessels (i.e. tibial and peroneal arteries). In other words, locations where there is increased turbulence and altered shear stress, which in turn leads to constant intimal injury (i.e. arterial branch points) [1-3].

Treatments for PAD include therapies to reduce the risk of associated cardiovascular events and improvement of limb symptoms (i.e. prevents progression to critical limb ischemia, and preserves limb viability) [2,4,5]. Patients should initiate treatment by modifying risk factors (i.e. smoking, diet, etc) in combination with an antiplatelet medication (e.g. aspirin, clopidogrel) and statins, in order to improve cardiovascular outcomes and avoid the risk of myocardial infarction, stroke and even death. However, in patients with symptoms refractory to pharmacological treatment and lifestyle modifications, revascularization interventions should improve long term survival and provide relief of symptoms [2,4,5].

Revascularization procedures include catheter-based (e.g. percutaneous transluminal angiography (PTA), stent placement, and atherectomy) and surgical interventions (e.g. peripheral artery bypass) [2,4,5]. The protocol for revascularization procedure depends on the location and extent of the occlusion

and medical condition of the patient. Despite advancement in revascularization procedures, a large number of patients (100,000- 200,000) have unfavorable occlusive patterns, diffuse coronary atherosclerosis, small distant vessels and comorbidities that prevent the utilization of any of these procedures [5] . Therefore, an alternative approach towards revascularization (i.e. therapeutic angiogenesis) could benefit these patients, whom otherwise are not candidates for conventional revascularization methods [2,4,5] .

1.2 Angiogenesis

Under normal adult physiological conditions a plethora of molecules (i.e. stimulators and inhibitors) regulate angiogenic homeostasis in order to maintain an angiostatic state. Angiogenic stimulation results from the release of growth factors within the microenvironment, leading to endothelial cell activation, proliferation, migration, tube formation, stabilization and maturation. On the other hand, angiogenic inhibitors hinder signaling pathways within endothelial cells in order to circumvent the development of unwanted vasculature. Angiogenic growth factors such as VEGF1 and FGF2 are considered stimulators of the angiogenic process as well as essential for the initial growth phase of angiogenesis [5-8]. Furthermore, growth factors such as TGF- β 3, PDGF- β 4, and angiopoietin-1 are required for vasculature stabilization. Additional angiogenic stimulators (e.g. G-

¹ VEGF- *Vascular endothelial growth factor*

² FGF- *Fibroblast growth factor*

³ TGF- β - *Transforming growth factor- β*

⁴ PDGF- β – *Platelet-derived growth factor- β*

CSF, HGF, PD-ECGF5) and inhibitors (e.g. TSP-1, TIMPs, hCG6) affect this process through feedback loops and interactions with the extracellular matrix [5,6,9], contributing to the abovementioned angiogenic homeostasis by regulating the expression and activity of both angiogenic and angiostatic growth factors [9] .

Upregulation of angiogenic growth factors due to, for example, ischemia, alters this regulatory balance, where interactions between growth factors, receptors, cells (i.e. endothelial and mesenchymal) and the extracellular matrix lead to neovascularization. Three processes within the body are known to induce new vessel formation (Figure 1.1): Angiogenesis, vasculogenesis and arteriogenesis [3].

In angiogenesis, new capillaries are established from the extension of preexisting vessels through a process that involves the activation, migration and proliferation of endothelial cells under the direction of local angiogenic stimulus (i.e. hypoxia, ischemia or inflammation). Subsequently, neovascularization occurs by either sprouting or intussusception. Briefly, in intussusception (splitting angiogenesis), splitting of the lumen in preexisting vessels is achieved through the insertion of interstitial cellular pillars. Local vasculature is then partitioned via stabilization and growth of these pillars, leading to vascular remodeling and an increase in the

⁵ G-CSF- Granulocyte colony-stimulating growth factor, HGF- Hepatocyte growth factor, PD-ECGF- Platelet-derived endothelial cell growth factor

⁶ TSP-1- Thrombospondin - 1, TIMPs – Metalloproteinase inhibitors, hCG- Human chorionic gonadotropin.

number of vessels without the need of an equivalent increase in the number of endothelial cells [3].

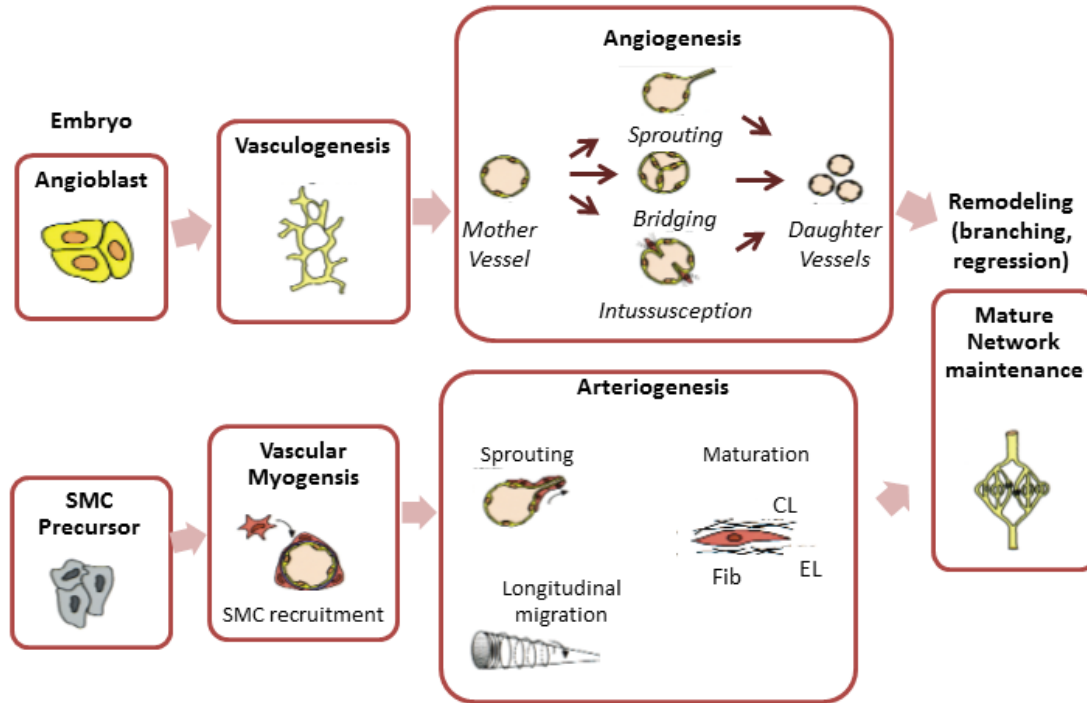


Figure 1.1 – Endothelial precursors (angioblasts) in the embryo assemble a primitive network (vasculogenesis), which in turn expands and is remodeled (angiogenesis). Smooth muscle cells cover endothelial cells during vascular myogenesis, and stabilize vessels during arteriogenesis. CL: collagen; EL: elastin; Fib: fibrillin (Fib). **Adapted from: Carmeliet, Mechanisms of angiogenesis and arteriogenesis, Nature Medicine 6, 389 – 395 (2000)**

Conversely, in sprouting angiogenesis (Figure 1.2) vascularization is a result of budding and extension of already formed vasculature. Briefly, when an angiogenic stimulus (i.e. hypoxia, ischemia or inflammation) is induced, a transient upregulation of angiogenic growth factors is triggered, which activates neighboring endothelial cells and recruits endothelial progenitor cells [5,9-11]. These migrating endothelial cells degrade the basement membrane of a parent vessel and begin

to lay down extracellular matrix. Subsequently, endothelial cells proliferate and begin to form connections with neighboring vasculature through a complex process of sprouting, branching and regression, in order to pattern a capillary network. Further cell-cell and cell-matrix interactions guide capillary extensions and aid in the stabilization of vasculature via the recruitment of pericytes and smooth muscle cells. Once tubules are formed, vessels are sealed via cell-cell junctions forming a capillary loop through where blood is perfused [5,12-14].

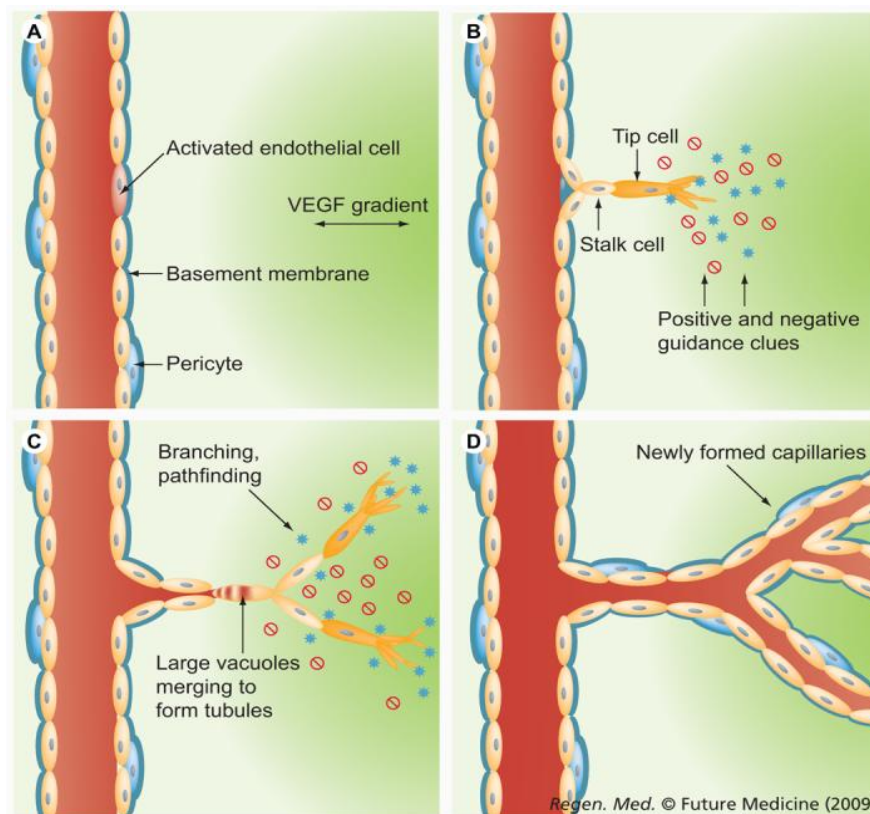


Figure 1.2 – Sprouting Angiogenesis. (A) Endothelial cells are activated through angiogenic cues and a tip cell is selected. (B) Tip cell degrades basement membrane and migrates within the parent vessel (C) Angiogenic cues control guidance and morphogenesis, large vacuoles form and merge to make tubules. (D) Deposition of basement membrane to stabilize newly formed endothelial tubules. Adapted from: Carmeliet, *Mechanisms of angiogenesis and arteriogenesis*, *Nature Medicine* 6, 389 – 395 (2000)

On the contrary, in vasculogenesis angioblasts or endothelial progenitor cells (circulating or residing in bone marrow) guide the de novo development of a simple vascular network (i.e. primary capillary plexus). Subsequently, this primary capillary plexus expands through branching, forming and remodeling a complex vascular system. Although vasculogenesis was considered to be an embryonic process, the paradigm for postnatal vasculogenesis has been revised due to recent studies that have demonstrated how endothelial progenitor cells circulating in peripheral blood of adult animals proliferate in response to an ischemic event, home and become incorporated within areas of neovascularization augmenting vasculature formation [5,6,8,11,14-16].

A third neovascularization process, arteriogenesis, is deemed to give rise to medium sized arteries through the remodeling of preexisting collateral vessels. Moreover, arteriogenesis is thought to be the result of changes in shear stress within an occluded vessel, leading to functional alterations within the vascular endothelium, modifications in cell-cell and cell-matrix interactions, as well as contributions to growth factor upregulation. Briefly, to adjust the blood flow as a function of tissue perfusion, the injured vasculature becomes covered by a muscular coat, endowing viscoelastic and vasomotor properties to the remodeled blood vessels [5,11-13]. Despite the fact that angiogenesis, vasculogenesis and arteriogenesis are relevant to the development of neovascularization strategies; angiogenesis has been the basis of research for the treatment of ischemic pathologies [5].

1.3 Current Strategies In Therapeutic Angiogenesis

Therapeutic angiogenesis seeks to mirror, support or augment natural mechanisms within the body that result in collateral vessel formation [6,9]. Strategies for therapeutic angiogenesis rest on inducing the development of new vasculature through the administration of bioactive agents such as angiogenic molecules (e.g. bFGF, VEGF), genes or cells [6,9,17]. Furthermore, the delivery of said angiogenic agents can be done either through a single or a combination dose of growth factor (s), gene (s) or cell (s) [7,11,17,18] .

The simplest strategy consists of injecting a single angiogenic growth factor or encoded gene to the affected site [6]. Several studies have demonstrated (Table 1.1) that administering a single growth factor or encoded gene can aid in restoring blood flow within ischemic areas [6,7,9,18].

Matrix/Scaffold	Growth factor
Fibrin	VEGF bFGF SDF-1
Collagen	VEGF
Gelatin	VEGF bFGF TGF- β HGF
Alginate	VEGF bFGF
PLGA/PEG	VEGF

Table 1.1 – Matrices and Scaffolds for single angiogenic growth factor delivery. Adapted from Matrices and scaffolds for drug delivery in vascular tissue engineering Zhang, G.; Suggs, L. J.; Advanced Drug Delivery Reviews, 2007

Growth factors such as VEGF and bFGF have been evaluated extensively in both animal and human studies. Although results were promising, the data has not demonstrated significant benefits in the defined endpoints (i.e. survival, improvements in quality of life, relief of symptoms) [7]. The limited success of these studies may be due to insufficient or excess delivery or dosing of the growth factor (e.g. VEGF, bFGF), which in turn may result in vascular networks that do not follow the hierarchical branching pattern of normal vasculature [7,18].

To overcome the issue of immature or malformed vasculature, combination therapies have been investigated (Figure 1.3). Said approaches involve two or more growth factors such as bFGF and PDGF [19], bFGF and VEGF-A and VEGF-C [20] , or angiopoietin-1 and VEGF [21]. Combination therapies are designed based on either the synergism between therapeutic effects or complementary functions (i.e. initiation and maturation of blood vessels) of the growth factors [18] . Although multiple growth factor delivery attempts to mimic biological mechanisms in angiogenesis, issues regarding dosages, rates, localization and modes of delivery for each bioactive factor have yet to be resolved [7,18] .

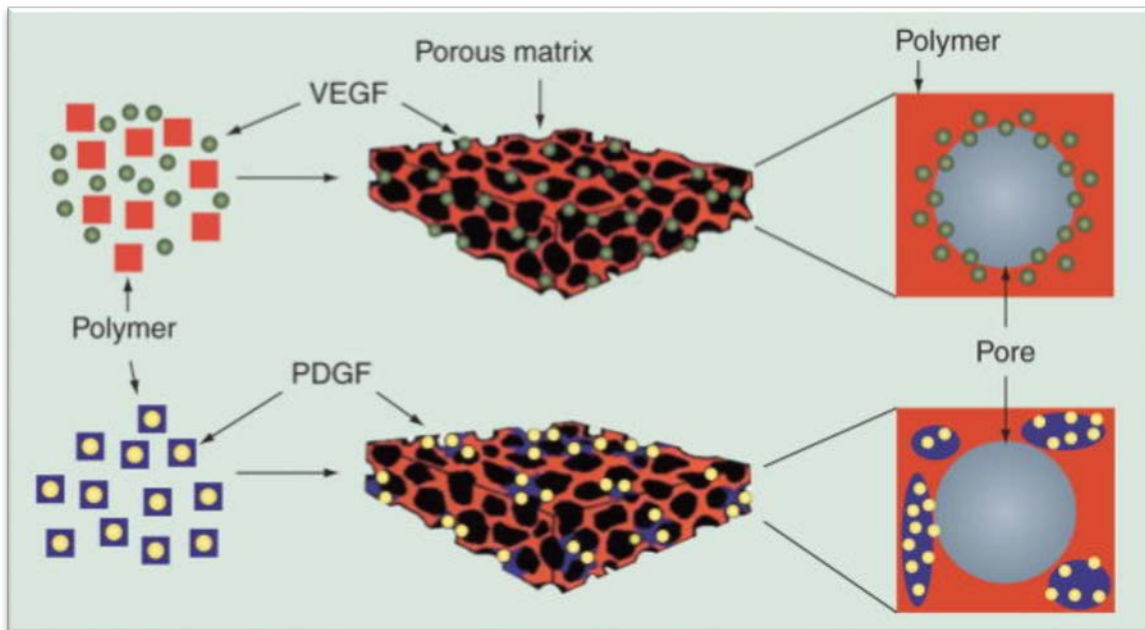


Figure 1.3- PLGA in growth factor delivery: the sequential release of dual factors has been examined by embedding PDGF-incorporated particles in a PLGA foam that have VEGF dispersed within. Poly(lactic acid-co-glycolic acid) (PLGA) scaffolds enable different release kinetics of growth factors. VEGF is incorporated into a porous PLGA scaffold by mixing with PLGA followed by processing into a scaffold. This approach results in VEGF absorption on the scaffold. On the other hand, PDGF is incorporated by pre-encapsulation of PDGF into PLGA microspheres followed by processing into a scaffold. Compared with VEGF, PDGF has a significantly slower release kinetic. These two approaches can be combined to deliver dual factors with distinct kinetics.

Furthermore, disadvantages such as short-half life in vivo, costs and manufacturing difficulty have lead researchers towards utilizing gene therapy in order to prolong and precisely localize the delivery of angiogenic growth factors [7,22]. Briefly, gene transfer utilizes either viral or non-viral vectors to introduce genes into target cells in furtherance of achieving high levels of sustained gene expression [5,23]. Due to safety concerns non-viral vectors have become an attractive option, however, they are less efficient at inducing gene expression

compared to viral vectors [5,7]. To overcome this inadequacy, large quantities of the non-viral vectors (i.e. plasmid) can be administered to induce angiogenesis. Despite providing a precise mode of delivery, there are concerns with gene transfer regarding vector-induced cytotoxicity (e.g. deleterious inflammatory response) [5].

Consequently, cell based strategies for revascularization have been evaluated. Due to stem and progenitor cell identification, potential for a new therapeutic option has emerged (Figure 1.4) [6,24]. The utilization of stem or progenitor cells in angiogenesis is driven by two rationales: Cell phenotypic plasticity and cellular recruitment via cytokines [6,25]. Adult stem cells have the capability of differentiating into functional vascular cells if given specific biological cues, cell types such as mesenchymal stem cells (MSCs), hematopoietic stem cells (HSCs) and endothelial progenitor cells (EPCs) have demonstrated said potential for differentiation [6,7,24]. However, to achieve new vessel formation, a relatively large amount of cells is required; leading to evaluate cellular recruitment and mobilization via growth factors [24] as circumvention to this issue. In brief, during an ischemic event, bone-marrow derived stem and progenitor cells are recruited to the injured area, growth factors such as granulocyte colony stimulating factor (G-CSF) and granulocyte-macrophage colony stimulating factor (GM-CSF) have been shown to promote cellular mobilization and subsequent homing in ischemic tissues [7,24,26].

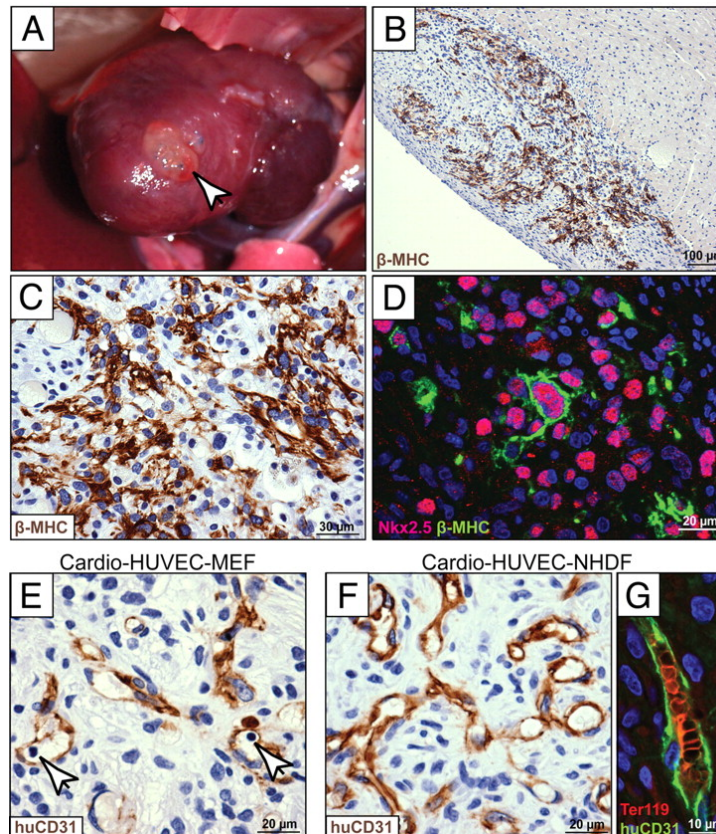


Figure 1.4- Cardiac tissue patches form human cardiac muscle and integrated human microvessels in rodent hearts. Cardio-HUVEC-MEF or cardio-HUVEC-NHDF patches were implanted onto nude rat hearts for 1 week. (A) Gross examination of the heart immediately after sacrifice demonstrated that patches (arrow) attached with sutures were firmly adhered to the heart. (B) Patches had significant β -MHC-positive human cardiac muscle tissue (brown immunostaining; representative cardio-HUVEC-MEF patch). (C) A higher-magnification image of the graft from B shows that β -MHC-positive cardiomyocytes were relatively small and had immature sarcomeric organization, and that (D) grafts contained Nkx2.5-positive (pink nuclei) cardiac progenitor cells that had not yet matured to express β -MHC (green). CD31-positive endothelial cells in animals implanted with cardio-HUVEC-MEF (E) or cardio-HUVEC-NHDF (F and G) patches frequently formed vessel-like lumens that contained leukocytes (arrows in E) and Ter-119-positive red blood cells (G), indicating that grafted human vessels had connected with the host vasculature. Stevens, K. R., et al. "Physiological function and transplantation of scaffold-free and vascularized human cardiac muscle tissue." *Proceedings of the National Academy of Sciences* 106.39 (2009): 16568-16573.

As mentioned earlier, neovascularization involves a harmonious interplay between cells and cytokines. Multiple growth factors play a role in vessel formation; these are tightly regulated and are presented at specific times [8,11,27]. Current growth factor and gene delivery strategies have failed to mirror the angiogenic process due to either insufficient or undetermined dosing. Studies have demonstrated injecting angiogenic growth factors leads to a transient elevation of the growth factor followed by unstable capillary formation [6,7,17,27,28]. Furthermore, the mechanisms involved in angiogenic processes have not been characterized sufficiently in areas such as cell based therapies [6,7,24,29]. These challenges, among others, could be addressed through combination therapies (Figure 1.5) (e.g. dual growth factor delivery, growth factor and cellular therapy) in conjunction with delivery matrices, microspheres or scaffolds [6,7,9,24,29-31].

Although the selection of a cell type and a matrix to reconstruct a specific tissue are the main requirements of tissue engineering, one essential component for successful tissue regeneration is the microenvironment (i.e. spatial and temporal) in which cells interact. Orchestrated interactions between cytokines, cells and extracellular matrices define this microenvironment [31]. Consequently, integrative approaches that combine encapsulated or tethered angiogenic growth factors, cells and 3-D microenvironments have been proposed in order to mimic in vivo mechanisms [31-34].

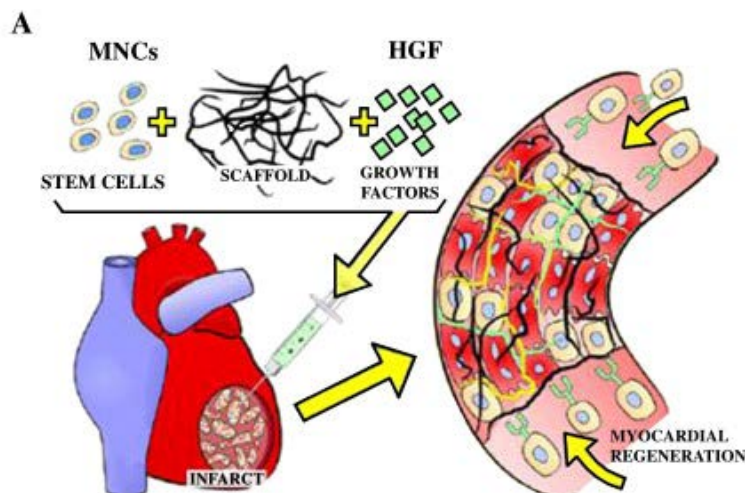


Figure 1.5- Schematic demonstrating a combination strategy for the delivery of HGF and BMNCs (bone marrow mononuclear cells) using a PEGylated fibrin biomatrix. Delivery was evaluated in a murine infarct model. Cell retention rate was significantly increased when delivered by injectable biomatrix compared with direct injection. The nuclei of transplanted BMNCs were stained blue by X-gal and the slides were counterstained by eosin (red). By direct injection only a few cells were detected at the peri-scar region. **Zhang et al. Enhancing efficacy of cell transplantation in hearts with post infarction LV remodeling by injectable bio matrix, Tissue eng. 2008**

1.4 Vascular Tissue Engineering

In areas such as vascular tissue engineering, this integrative approach has become the foundation to develop and maintain mature, stable and functional vascular networks. Studies have demonstrated the importance of sustained localized delivery of precise doses of angiogenic cues to produce and maintain this functional vasculature [9,33,35,36]. Herein, a variety of release technologies have been utilized to both carry and delivery angiogenic growth factors. Parameters such as growth factor amount and type, and material properties can be altered in

order to tailor release profiles in response to physiological demands at the ischemic site. The rationale to this tailored approach is to create a feedback loop between the growth factor release profile and the in vivo microenvironment, ensuing vascular repair and growth and preventing unwanted side-effects [9,37].

Furthermore, delivery vehicles for angiogenic biomolecules provide means to protect, improve bioavailability and reduce the amount of protein required to achieve a desired effect [31,38]. Thus, delivery strategies should enable retention, stability and uniformity of the biomolecule, and control the spatial-temporal delivery for a sufficient period to allow neovascularization [6,33,39]. Conversely, delivery systems can also serve as a provisional extracellular matrix to garner and foster cells, as well as guide cellular migration within the matrix while preserving surface area in which vascular networks can grow [33,40]. Considerations such as cellular adhesion, physical and chemical properties, and degradation rates should be taken into account if the tissue engineered construct should be utilized to mimic vascular extracellular matrix [6,41].

Therefore, strategies for vascular tissue engineering have focused on developing 3-D systems (i.e. matrices, scaffolds) utilizing biomaterials (i.e. natural or synthetic) to incorporate angiogenic growth factors or extracellular matrix proteins that regulate vascular cell behavior (i.e. adhesion, migration, proliferation) or both, in order to entice and support vascular network development, as well as release the angiogenic biomolecules in a tunable manner. To achieve this, biomaterials have been modified to enhance their physical and chemical properties, and to improve the efficiency of growth factor delivery and bioactivity [7,30,31,33,34,36,41]

leading to biomimetic matrices that provide greater control over cellular responses, angiogenic cue delivery and vascular network guidance.

However, to mimic the physiological process of angiogenesis, it is critical to understand the timing and release of growth factors in vivo, which in turn, will provide release profile guidelines to develop a delivery vehicle that will entice and control the degree of vascularization within the tissue (Figure 1.6) [42]. Angiogenesis is an intricate process that involves a plethora of morphogens, in order to initiate, mature and stabilize new functional vasculature. These include pro-angiogenic factors such as VEGF, bFGF and PDGF, in addition to other families of growth factors/ growth factor receptors such as angiopoietins and ephrins, which aid in stabilizing newly formed capillaries [6,8,10,43,44] . Briefly, in vasculogenesis, specific concentration gradients and threshold levels of VEGF, activate receptors to induce angioblasts to form the primary capillary plexus, conversely, sprouting angiogenesis is induced by angiopoietins which in turn modulate VEGF activity in order to direct angiogenesis [45,46]. Subsequently, PDGF and TGF – β regulate the recruitment of vascular smooth muscle cells and pericytes in order to stabilize immature vessels and generate extracellular matrix [8,47]. Moreover, matrix metalloproteinase influence cell migration and differentiation via pro-angiogenic factors within the matrix, in order to regulate branching and remodeling of the new vasculature [8]. Consequently, delivery approaches should utilize this knowledge to delineate the specific concentrations and, temporal and spatial expression profiles of cytokines to achieve the development of functional vasculature [48] .

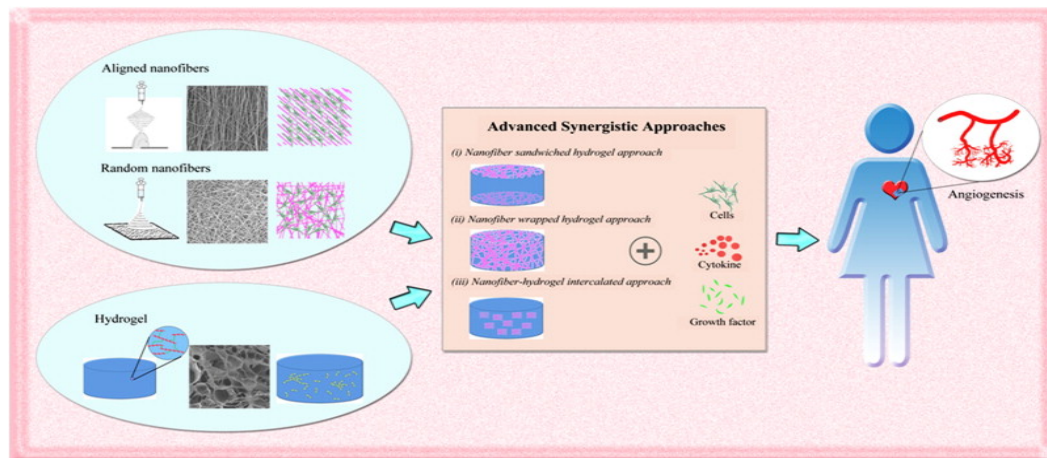


Figure 1.6- Advanced synergistic tissue engineering approaches for cardiac regeneration. Prabhakaran, Molamma P., et al. "Biomimetic material strategies for cardiac tissue engineering." *Materials Science and Engineering: C* 31.3 (2011): 503-513.

1.5 Angiogenic Growth Factor Delivery Strategies in Vascular Tissue Engineering

Several strategies have been developed to mimic the in vivo release profiles of angiogenic cytokines, these approaches range from incorporation through adsorption to encapsulation. Single-factor delivery strategies have focused on a broad array of different cytokines, materials, delivery methods, and means of incorporation. Natural biopolymers (i.e. Fibrin, collagen, gelatin, and alginate) have been utilized successfully to load angiogenic growth factors via coating or adsorption, as they are well-characterized and may contain native ECM molecules [48]. Collagen sponges coated with PDGF were implanted into full-thickness

excision wounds in rats; results demonstrated increased fibroblast infiltration and enhanced capillary formation [49,50]. Tabata et al. demonstrated that controlled release of bFGF is caused by biodegradation of gelatin hydrogels, thus promoting vascularization dependent on water content of said hydrogel [51]. Conversely, synthetic scaffolds such as PLGA (copolymer of D,L-lactide and glycolide) have been utilized to deliver VEGF to enhance neovascularization [52].

Furthermore, advances in protein modification techniques have led to the incorporation of angiogenic cytokines into scaffolds via fusion proteins or coupling utilizing 1-ethyl-3-(3-dimethylaminopropyl)- carbodiimide (EDC) and N-hydroxysuccinimide (NHS) chemistry. Zisch et al. developed a fibrin-binding VEGF fusion protein and incorporated it into fibrin during coagulation. The study demonstrated VEGF could be retained within the fibrin matrix until tissue remodeling had taken place [53]. Similarly, bFGF and fibrin-binding peptide Kringle1, or PDGF and collagen-binding domains fusion proteins have been utilized to link bFGF or PDGF to fibrin or collagen hydrogels, respectively, both studies showed said scaffolds promoted neovascularization in vivo [54,55]. Alternatively, heparin has been incorporated into collagen matrices via carbodiimides. Subsequently, the heparinized collagen matrices were enhanced by immobilization VEGF through the heparin-binding domain. Results demonstrated loading of heparinized matrices with VEGF increased angiogenic potential [56-58].

Although there has been success in delivering angiogenic cytokines either through adsorption, coating and surface tethering, there still remains a problem with

localized delivery and release kinetics. Thus, microspheres with encapsulated angiogenic growth factors have been either incorporated into scaffolds or utilized for targeted delivery (i.e. catheter based therapy). Perets et al. incorporated bFGF loaded PLGA poly (lactic-co-glycolic acid) microspheres within a porous alginate scaffold in order to control release profiles, results demonstrated enhanced vascularization in rats [59]. Similarly, Richardson et al. developed a 3-D construct composed of PDGF loaded microspheres and a VEGF immobilized PLGA scaffold. This dual delivery approach allowed the release of the cytokines at different rates in order to promote larger and mature vasculature. Several studies have elucidated that vascular development under the guidance of a dual delivery strategies is superior when compared to single growth factor therapy [31,38,60-64].

1.6 Guided Angiogenesis and Spatial-Temporal Delivery of Growth Factors

Releasing growth factors as a function of time has been the main focus for vascular tissue engineering approaches, however, the role of growth factor concentration and spatial-temporal profiles are crucial in the recreation of angiogenic processes. The formation of mature and functional vasculature in vivo is the result of angiogenic growth factors acting in spatial-temporal gradients to regulate vessel properties (i.e. density, size and distribution), architecture and patterning. Moreover, seeing that undirected vessel growth leads to haphazard vascular patterning, spatial control is essential in order to avoid vessel instability and therefore inadequate vascular network functionality [38,65]. Studies have addressed the need for spatial-temporal delivery by either incorporating single growth factors within fibrin [66] or PLGA [67] films, or by utilizing individual delivery

vehicles (e.g. microspheres, hydrogels and scaffolds) [68,69]. However, any strategy that attempts to mimic in vivo angiogenic processes should not be limited to the delivery of a single growth factor; rather it should deliver at least two synergistic angiogenic cytokines, at optimized ratios and in a specific spatial-temporal profile, in order to entice mature and functional vessel development [31]. With this concept in mind, the design of delivery strategies for angiogenic growth factors has aimed to either provide spatially or zonally (i.e. gradients) distinct cues within a 3-D construct [70].

Strategies to control spatial gradients incorporate growth factors in predetermined sites within a scaffold in order to provide specific signaling cues (Figure 1.7). Neovascularization was achieved by spatially segregating VEGF within one region and VEGF/PDGF within an adjacent region of a porous bi-layered PLGA scaffold. Moreover, the controlled delivery utilizing this PLGA scaffold regulated vessel density, size and maturity in vivo [38]. More recently, studies have shown patterned surfaces influence cell behavior, yielding to the development of constructs with growth factor patterning gradients [70-72]. Miller et al. utilized inkjet printing to immobilize patterns of FGF-2 at different concentrations upon fibrin substrates. Cells initially grew randomly across both the patterned and non-patterned surface; however, over time cells began to migrate to the patterned regions, leaving the non-patterned areas empty. Additionally, cells located upon FGF-2 patterns survived longer compared to the cells located off patterns [71]. Herein, guided angiogenesis could be achieved by combining controlled zonal release of angiogenic cytokines and a patterned specific 3-D construct.

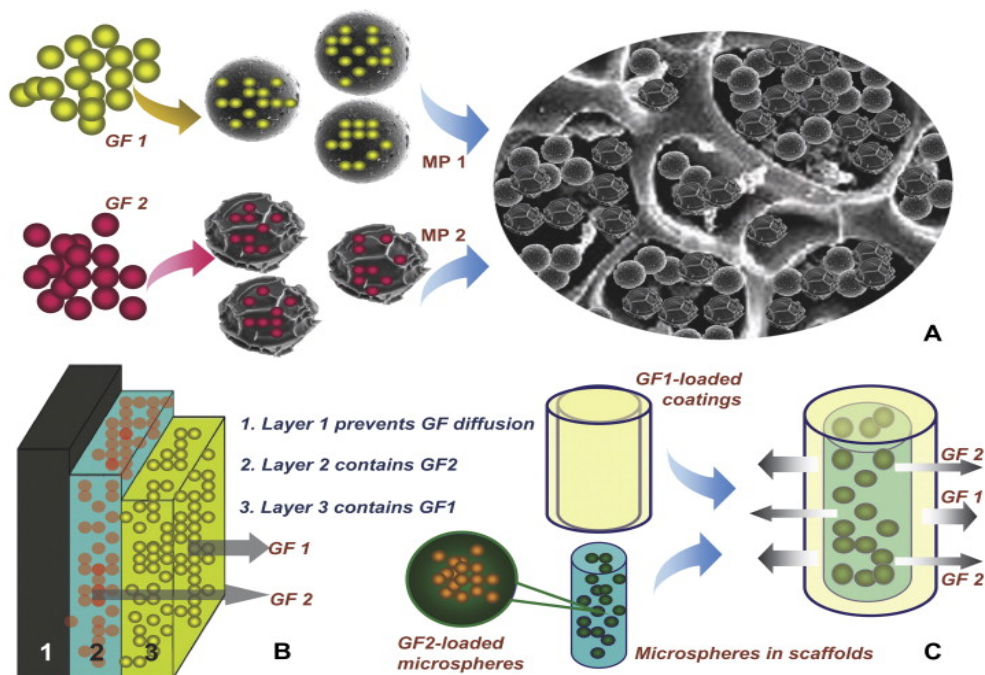


Figure 1.7- Schematic drawing of selected model systems for the delivery of two growth factors (GFs, i.e. GF1 and GF2). (A) A microsphere-based system in which two types of microencapsulated GFs (MP1 and MP2) are entrapped in scaffolding materials enables simultaneous delivery and release of dual GFs from one delivery platform (B) A multi-layer system can be used to mimic a double coated scaffold (layer 1 does not contain GFs and does not allow diffusion of the model proteins, layer 3 contains GF1, and layer 2 contains GF2) (C) A core-shell system: A composite scaffold for the sequential release of two GFs, where the scaffolding rod (core) and the synthetic shell were prepared separately and combined just before implantation to a wound site (illustration is not to scale).

1.7 Specific Aims

Vascular ischemic disorders remain the major cause of disability and death in developed societies. Predictions estimate that by the year 2020 cardiovascular diseases (i.e. Atherosclerosis) will become the leading cause of health care burden in western societies [3] despite improvement in surgical and minimally invasive techniques to restore blood flow in underperfused areas of the heart and limbs [6,9,73]. Therapeutic angiogenesis seeks to promote revascularization through the delivery of bioactive agents (e.g. growth factors, cells) [17,73]. Studies have shown controlled and localized delivery of multiple growth factors is required to produce functional vasculature [6,7,38]. A number of sustained and localized growth factor delivery strategies have been developed, however neither vasculature patterning nor organization has been achieved successfully [38,73-75]. Furthermore, studies have demonstrated growth factor type, concentration and mode of presentation (spatial and temporal) are critical in promoting mature and stable vasculature. Both type and concentration of angiogenic cytokines will affect the extent of cellular signaling and thus cellular behavior (e.g. proliferation, migration, differentiation) [6,9,34,37,38,40,76]. Moreover, physiologically, angiogenic growth factors are presented at specific time points and locations, and in different concentrations, therefore, sequential and spatial delivery of these cytokines is critical in establishing patterned and stable neovascularization, in addition to avoiding undesirable side effects at distant sites. Herein, elucidation of how spatial and temporal presentation affects angiogenesis and vascular development is important

for the development of promising therapeutic angiogenic strategies [6,9,10,30,31,34,35,38,40,41,75,77].

The **long-term** goal of this project is to develop three-dimensional cellular sheets with distinct architectural and biological cues that promote directed angiogenesis.

In order to address this goal, the following specific aims will be pursued:

AIM 1: Synthesis and characterization of nanofibrous scaffolds with defined architectural and biological cues

Gelatin based electrospun scaffolds with well-defined fiber architecture will be fabricated based on a novel electrospinning approach developed in our laboratory. Vascular endothelial growth factor (VEGF), a well-known angiogenic growth factor will be immobilized onto the surface of the nanofibrous construct via means of physical immobilization.

AIM 2: Determine the effect of VEGF releasing electrospun scaffolds on cellular behavior (i.e. proliferation and migration) in vitro

HUVECs and EPCs will be seeded onto the constructs and migration velocities will be determined as a function of fiber orientation and VEGF spatial and temporal delivery. Specifically, VEGF gradients will be established on the surface of the electrospun constructs and cell velocity profiles and effective displacement will be evaluated.

AIM 3: Develop EPC-seeded vascular sheets and determine capillary formation and directionality as a function of construct parameters and co-administration of VEGF and SDF-1 α

SDF-1 α and VEGF will be immobilized onto the surface of aligned electrospun scaffolds to evaluate if the co-delivery of these cytokines will provide the necessary cues to entice EPC attachment, proliferation and migration within nanofibrous scaffolds and promote vessel development and directionality.

CHAPTER 2: SYNTHESIS AND CHARACTERIZATION OF NANOFIBROUS SCAFFOLDS WITH DEFINED ARCHITECTURAL AND BIOLOGICAL CUES

Electrospinning is a fabrication technique that utilizes electrical charges to assemble polymer mats with different fiber diameters and architectures ranging from micrometer down nanometer scale [78,79]. This process has gained much attention not only because of its versatility in spinning a wide variety of polymeric fibers but also due to its ability to consistently produce uniform fibers that otherwise would be difficult to achieve by using standard mechanical fiber-spinning techniques. Electrospun fiber scaffolds also offer several advantages such as, an extremely high surface-to-volume ratio, tunable porosity, malleability to conform to a wide variety of sizes and shapes and the ability to control the nanofiber composition to achieve the desired results from its properties and functionality. A major challenge encountered in using electrospun scaffolds for tissue engineering is the non-uniform cellular distribution and lack of cellular migration in the scaffold with increasing depth under normal passive seeding conditions [80].

Three important factors influence cellular behavior: scaffold chemistry, mechanical properties, and architecture. Naturally occurring ECM, is composed of various proteins and sugars, this blend of materials provides mechanical properties that are ideal for supporting cells and tissue and promotes specific biomolecular activity among cells. Materials can be designed to mimic the tensile and compressive properties of certain tissues, and coatings can impart proper surface chemistry. Although biomaterial development has evolved one of the real challenges is creating the proper architecture through balancing both porosity and pore size [79-81].

Techniques such as salt leaching and lyophilization generate highly porous scaffolds, however these fail to create the proper void size. Pores in such artificial ECMs are often on the order of hundreds of microns, and cells merely stretch along a flat surface instead of engaging multiple attachment points in a 3D environment. Studies have shown that it is very difficult to identify “optimal” pore diameter for tissue growth, as varying pore diameters often lead to varying porosities, mechanical properties, available surface area, and other variables that have been shown to affect cell growth [72,78,81,82][72,82][72,82].

Electrospun scaffold have been shown to provide large porosities (>70%) and a nanofibrous structure capable of allowing cells to bridge voids and attach to multiple fibers in a truly 3D environment, making them ideal candidates for tissue engineering applications [81]. A plethora of biodegradable polymers have already been electrospun with tissue engineering in mind [83-86]. The effect of fiber diameter on cell proliferation has also been evaluated, with the general conclusion that smaller fibers seem to entice cellular replication and signaling [87,88].

Constructing electrospun nanofibrous mats into specific designs – such as a hollow conduit for nerve regeneration or multiple stacks of materials to mimic tiered layers of tissue – has also shown promising success [89]. There has been little work, however, on the effect of scaffold architecture. Electrospun scaffold architecture is an interesting challenge, in that there are few effective means to vary independently basic morphological parameters: porosity, pore diameter, and fiber diameter. The effect of these morphological parameters on cellular behavior is of particular relevance, as the utilization of space is a key concern when utilizing

electrospun scaffolds as tissue engineering templates, because cellular population and tissue formation usually occurs only on the scaffold periphery [90]. Previous studies have utilized different methods to increase cell infiltration include spinning mixed populations of micro and nano-sized fibers, [91] electrospinning in the presence of cells, [92] spinning with sacrificial fibers, [93] including poragens during fiber collection, [94] and photopatterning, [95] all of which have shown some degree of success in increasing initial cell infiltration into the scaffold. However, these methods have focused on initial scaffold porosity and do not actually direct cells into the scaffold [93].

Directed cell migration is critical during several different physiological processes such as tissue development, tumorigenesis, and wound healing. Common approaches to direct cells include topographical patterning (e.g. aligned channels and fibers) and immobilization of growth factors or cytokines [95-99]. Studies have shown spatiotemporal delivery of growth factors (e.g. VEGF) has been useful in achieving enhanced cellular effects both in vitro and in vivo [75] via the interplay between scaffold and growth factor delivery profiles [31]. Furthermore, cellular directionality is highly regulated and strongly depends on growth factor gradients, cells exposed to gradients grow and migrate towards areas where growth factors have been immobilized [100,101].

In this study we utilized our nanofibrous gelatin electrospun scaffolds [102] with different fiber orientations (i.e. random or aligned) evaluate HUVEC behavior and their angiogenic potential as a function of construct parameters (i.e. morphological characteristics, fiber alignment, VEGF gradients).

2.1 Experimental Approach

2.1.1 Scaffold Fabrication and Crosslinking

Our laboratory has developed a novel electrospinning apparatus that allows us to design 3D scaffolds with different pattern arrangements, fiber densities and diameters. Briefly, gelatin B (Sigma Aldrich USA, Gelatin Type B from Bovine Skin G9391-500G) was dissolved at 10% w/v in 1,1,1,3,3,3 hexafluoro-2-propanol (Sigma Aldrich USA, Fluka HFIP 52512-100mL), the solution was loaded into a 5 mL syringe (Thomas Scientific USA, Henke Sass Wolf Norm-Ject 8939N52) and electrospun at specified parameters from a 22G blunt needle (Table 2.1). A total of 500 μ L was deposited onto aluminum covered glass slide and left to dry for 1 hour under vacuum (25 in Hg) at room temperature. Aligned fiber orientation was achieved by controlling the polarity of the collecting plates of our custom made electrospinning apparatus (Figure 2.1). Crosslinking of gelatin B nanofibrous scaffolds was performed with glutaraldehyde vapor (Sigma Aldrich USA, Glutaraldehyde Solution Grade II 25% in H₂O G6257-1L). Briefly, 2mL of 25% glutaraldehyde solution per scaffold was deposited in an airtight container that contained the electrospun scaffold still attached to the aluminum collector. Scaffolds were crosslinked at various times (15 min to 2 hrs) in room temperature and then washed for 1 hour in 100mM glycine solution (Sigma Aldrich) to block any unreacted aldehyde groups.

Group	Voltage (kV)	N-t-C (cm)	Feed Rate (ml/hr)
A ₁₅	15	10	1
B ₁₅			4
C ₁₅			8
D ₁₅		15	1
E ₁₅			4
F ₁₅			8

Table 2.1: Groups of electrospun 10% (Group A₁₅-C₁₅) and 5% (Group D₁₅-F₁₅) gelatin B in 1,1,1,3,3,3 hexafluoro-2-propanol nanofibrous scaffolds at different parameters. Subscripts on sample ID's refer to kV used.

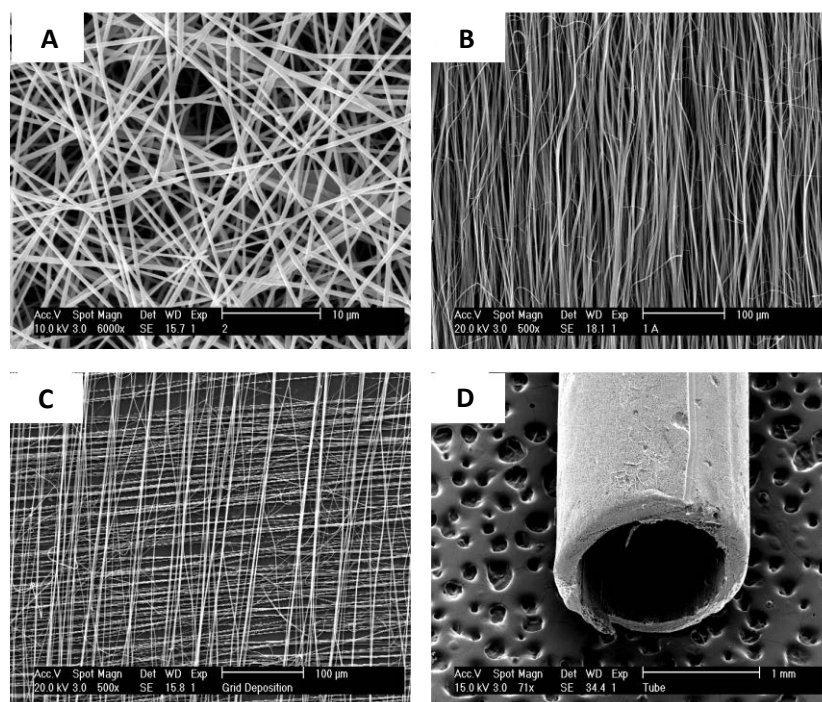


Figure 2.1: Scanning electron microscopy images (SEM) of electrospun scaffolds with (A) random fiber orientation (B) aligned fiber orientation (C) gridded fiber alignment and (D) tubular morphology.

2.1.2 Characterization of Nanofibrous Scaffolds: Morphological Characteristics, Degree of Swelling, Degradation Rate and Cytotoxicity

2.1.2.1 Evaluation of Fiber Morphology as a Function Of Electrospinning Parameters

Scanning Electron Microscopy (SEM) was utilized to evaluate fiber orientation and morphology of electrospun scaffolds as a function of electrospinning parameters, such as N-t-C (cm), electric potential amplitude (kV), feed rate (ml/hr), electrode polarity (+/-) and polymer concentration (wt%). Briefly, said parameters were varied and 500 μ L of electrospun polymer was collected, crosslinked, cut to 1cm x 1cm (dimensions) and imaged at 12kV (Table 2.1). The dimensions of the fibers were assessed by evaluating 20 random individual fibers from 3 SEM images using ImageJ software (Table 2.1, Figure 2.1). Fiber orientation and alignment was determined by edge-based image processing techniques as described by Montero et al. (82)

2.1.2.2 Effect of Crosslinking on Scaffold Morphology, Swelling and Degradation

Nanofibrous scaffold topographical characteristics were assessed as a result of the crosslinking conditions utilizing SEM. Briefly, both aligned and random scaffolds were electrospun under parameters B₁₅ and crosslinked with glutaraldehyde vapor for one hour. Subsequent to crosslinking and washing, 3 SEM images per group were assessed for changes in fiber diameter and morphology utilizing ImageJ.

Degree of swelling was evaluated as a function of crosslinking time. Electrospun scaffolds were crosslinked with glutaraldehyde vapor, washed with glycine and PBS, and then submerged in Di H₂O for 24 h to allow for complete swelling. Scaffolds were then weighed and their wet weights were recorded (W_w). Subsequently, wet scaffolds were placed in a vacuum oven and allowed to dry for 1 h at 25in Hg and 60 °C. After complete drying, scaffolds were weighed and their weight recorded as dry weight (W_d). Degrees of swelling were calculated with the following formula:

$$DS = \frac{W_s - W_d}{W_d}$$

Furthermore, over a period of one week in a simulated biological fluid, degradation profile of electrospun scaffolds was evaluated as a function of GA crosslinking time (Range 1 to 24 hours). Briefly, crosslinked scaffolds were washed with glycine and PBS and their initial dried weight was recorded following by vacuum drying (25in Hg, at 50° C) for 1 hour. Scaffolds were placed in a 0.1mg/mL collagenase solution (Collagenase type I Calbiochem Cat# 234153) and weight loss was recorded at specified time points.

2.1.2.3 Growth Factor Gradient Immobilization and Formation

To determine the effect of scaffold design in controlling spatial-temporal VEGF delivery and promoting vessel development and patterning, we have established a protocol to physically immobilize VEGF with different cytokine gradients (Figure 2.2). As proof of concept we have immobilized FITC-albumin within the electrospun scaffolds and assessed gradient distribution of the protein utilizing fluorescent microscopy (Figure 2.3). Each scaffold region from left to right has a higher concentration of FITC-albumin with the highest being at the left section and the lowest at the right.

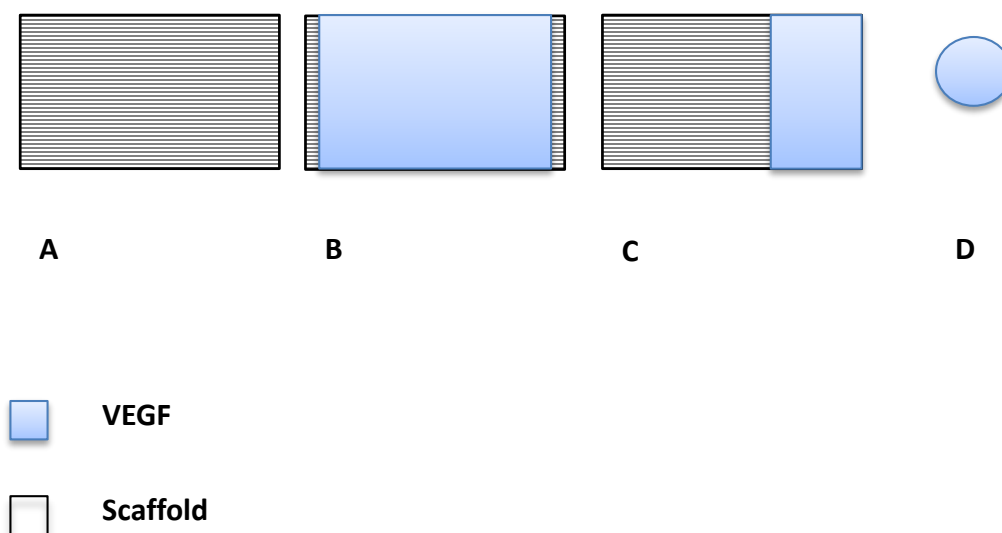


Figure 2.2: Diagrammatic representation of scaffold preparation and cell seeding.

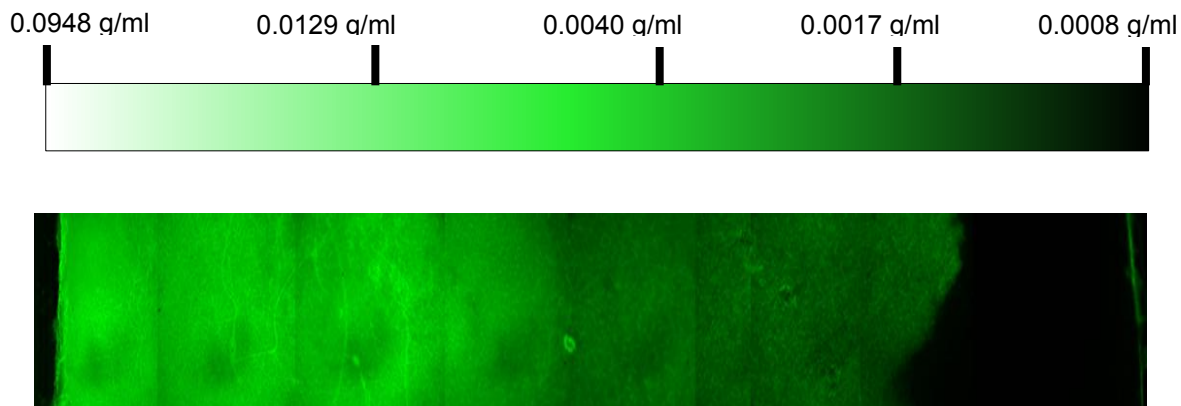


Figure 2.3: FITC-Albumin gradient distribution within gelatin electrospun scaffolds. By physically entrapping FITC-albumin we were able to immobilize a gradient of albumin concentration. Fluorescent images demonstrate that from left to right the concentration of FITC-albumin within the gelatin construct is decreased.

2.1.2.4 Growth Factor Release Profile

To assess release profiles, a 10 μ l aliquot of 10ng/ml model protein (FITC-albumin) solution was physically entrapped within the electrospun scaffolds. Subsequently, scaffolds were then submerged in PBS for 24 hours and data points were collected at 1, 5, 15, 30 and 60 min, and 24 hours. Samples were then diluted and analyzed as per protocol on a Beckman Coulter Plate Reader reading absorbance values at 450nm wavelength. This was performed in order to ensure the entrapped biomolecule was being released from the scaffolds in a time dependent manner and to evaluate release profile differences dependent on scaffold topography (i.e. random vs. aligned).

2.1.2.5 Evaluation of Cell Proliferation and Morphology as a Function of Scaffold Architecture and Growth Factor Immobilization Pattern

Gelatin is a natural material that has been utilized for several tissue engineering applications with minimum cytotoxicity [74,102]. The ability of cells to successfully adhere and proliferate was evaluated as a function of scaffold characteristics. Briefly, random and aligned scaffolds were adhered to the bottom of a 12- well plate utilizing fibrin glue. VEGF (10ng/ml) was physically entrapped on the scaffold for 20 min. HUVECs (Passages 2-4) were then seeded (50,000 cells/scaffold) and allowed to attach for 20 min @ 37 °C. Following cell attachment, each well was supplemented with 2 mL EGM-2 media (Lonza AG, Rockland, ME) and incubated at 37 °C and 5% CO₂ for 5 days. Subsequent to incubation, live cells were stained with 100 µL per well of 0.1 mg/mL calcein AM to assess cell density and morphology. To evaluate HUVEC proliferation on nanofiber scaffolds we utilized a Click-iT® EdU Kit (Invitrogen, Carlsbad, CA). Images of each scaffold were captured and then processed utilizing ImageJ and an add-on (Cell Counter) software.

2.2 Results and discussion

2.2.1 Scaffold Morphology as a Function of Electrospinning Parameters

Cell adhesion, proliferation, and differentiation have been shown to be significantly influenced by scaffold characteristics (e.g. fiber diameter and morphology) [83]. Several studies have demonstrated both cellular attachment and infiltration are predominantly affected by scaffold pore size and by individual fiber morphology

[84]. Herein, we evaluated the effect of electrospinning parameters (i.e. voltage, needle to collector distance, etc.) on scaffold fiber dimensions and orientation. Briefly, scaffolds were electrospun under a set of conditions in which gelatin concentration (5% or 10%), voltage amplitude (15kV or 20kV), needle-to-collector distance (10cm or 15cm), and feed rate (1, 4, or 8mL/hr) were varied. Fiber dimensions were determined using scanning electron microscopy. Results demonstrated, fiber diameters ranged from 0.15 μ m to 2 μ m and uniform nanofiber distribution was only achieved at specified fabrication conditions; electrospun scaffolds prepared under parameters B₁₅ (15kV, 10cm N-t-C, 4mL/hr feed rate) were highly uniform with 70% of their fiber diameter ranging between 750-850nm (Figure 2.4 A and B). In contrast, when the N-t-C was increased to 15 cm and the feed rate to 8 mL/hr (Table 2.1, F15) the fiber diameters of electrospun scaffolds ranged between 150-2000nm (Figure 2.4 C and D). Scaffolds prepared under the conditions described in B₁₅ (15kV, 10cm N-t-C, 4mL/hr feed rate) were utilized for the remainder of the described studies.

2.2.2 Effects of Crosslinking on Scaffold Morphology, Swelling and Degradation

Crosslinking methods utilized to control mechanical properties of tissue engineering scaffolds can considerably affect fiber morphology as well as scaffold architecture, which in turn can influence cellular behavior [85]. To tailor physicomechanical properties of gelatin scaffolds Glutaraldehyde vapor (GA) was used as a crosslinking agent. Briefly, electrospun scaffolds were crosslinked with GA and allowed to be exposed to the GA vapor for different time frames. Results

demonstrated, within one hour of GA crosslinking, scaffold architecture and fiber dimensions were not significantly affected in both aligned ($1 \pm 0.3\mu\text{m}$ to $1 \pm 0.2\mu\text{m}$) or random ($0.58 \pm 0.15\mu\text{m}$ to $0.83 \pm 0.14\mu\text{m}$) fiber scaffolds (Figure 2.5). There was a linear relationship between scaffold swelling and crosslinking time from 1 to 2 hours. Once crosslinking time exceeded two hours, small differences in degree of swelling were observed. Scaffolds crosslinked for 60, 90, 120 minutes, and 24 hours had degrees of swelling of 11.26 ± 0.68 , 6.23 ± 0.26 , 3.94 ± 0.67 , and 2.32 ± 0.48 respectively (Figure 2.6A).

2.2.3 Growth Factor Release Profile

Studies have demonstrated swelling profile differences among aligned and random fiber scaffolds, could influence cytokine release and loading profiles [86-88,103]. We determined there was a 33% increase in the amount of a model protein (FITC-albumin) released from aligned scaffolds in comparison to the amount that was released from random scaffolds over a period of 24hrs in vitro (Figure 2.7B).

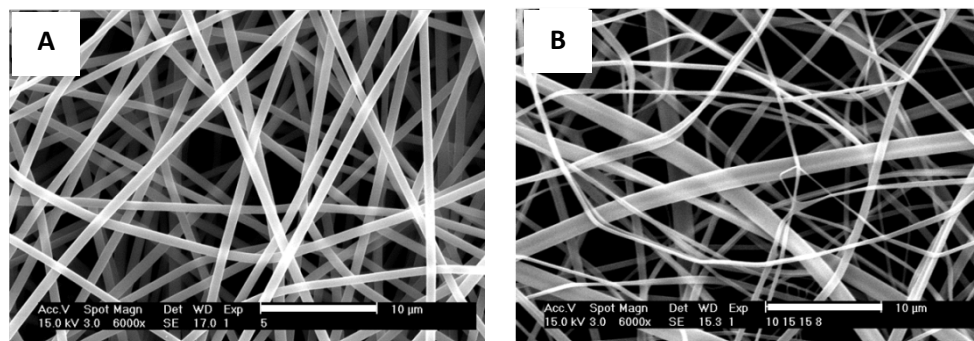


Figure 2.4: (A) Representative SEM image used to assess fiber diameters. Results yielded 5% of fibers diameters between $0.95\text{-}1.0\mu\text{m}$, 20% between $0.85\text{-}0.95\mu\text{m}$, 70% between $0.75\text{-}0.85\mu\text{m}$, and 5% between $0.65\text{-}0.75\mu\text{m}$ in diameter. (B) Representative SEM image used to assess fiber diameters. Results yielded 15% between $1.5\text{-}2\mu\text{m}$, 15% between $0.95\text{-}1.5\mu\text{m}$, 10% between $0.55\text{-}0.65\mu\text{m}$, 10% between $0.45\text{-}0.55\mu\text{m}$, 10% between $0.35\text{-}0.45\mu\text{m}$, 30% between $0.25\text{-}0.35\mu\text{m}$, 10% between $0.15\text{-}0.25\mu\text{m}$ in diameter.

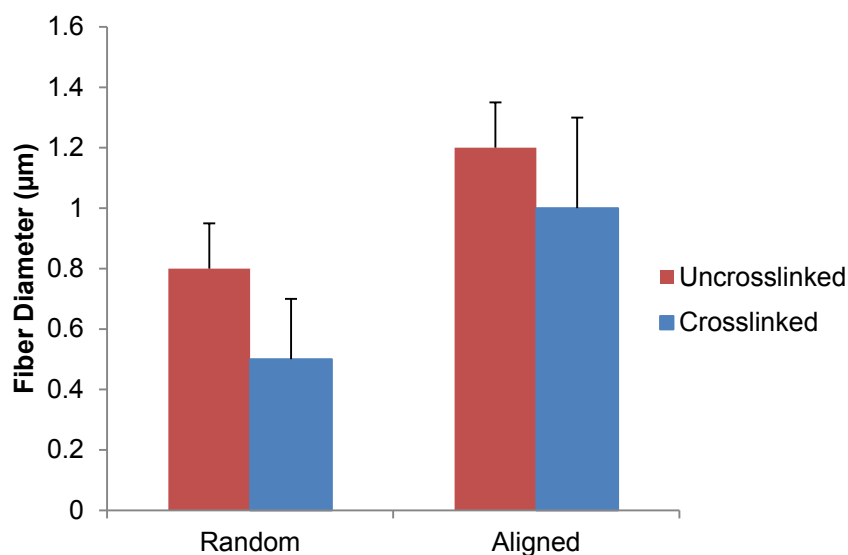
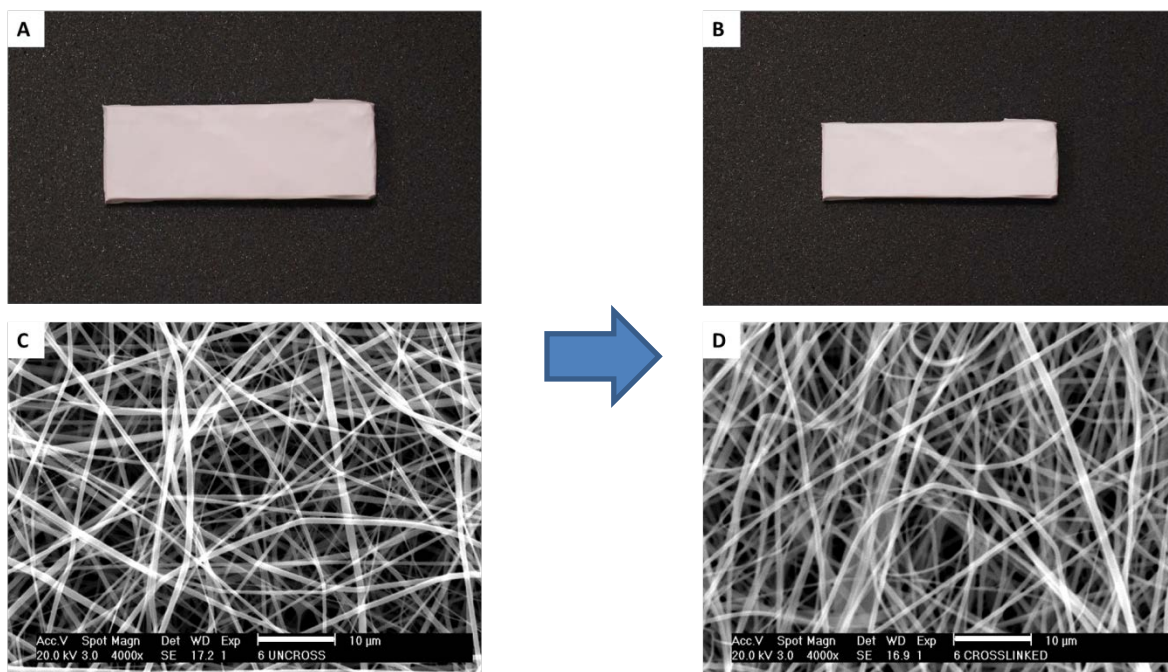


Figure 2.5: Changes in scaffold architecture and fiber dimensions as a function of glutaraldehyde crosslinking. Randomly deposited nanofibrous scaffolds (A) prior to crosslinking and (B) after crosslinking. SEM images of scaffold prior to crosslinking (C) and after crosslinking (D) used for assessing fiber diameters and morphology are shown. Crosslinking of 10% gelatin B nanofibers was achieved via glutaraldehyde vapor from a 25% GA solution at 2mL per 500µL of electrospun gelatin for one hour. (E) Bar graph of fiber diameters from all conditions, i.e. aligned not crosslinked, random not crosslinked, aligned crosslinked, and random crosslinked. Measurements were taken from three SEM images per condition, and twenty fibers per image.

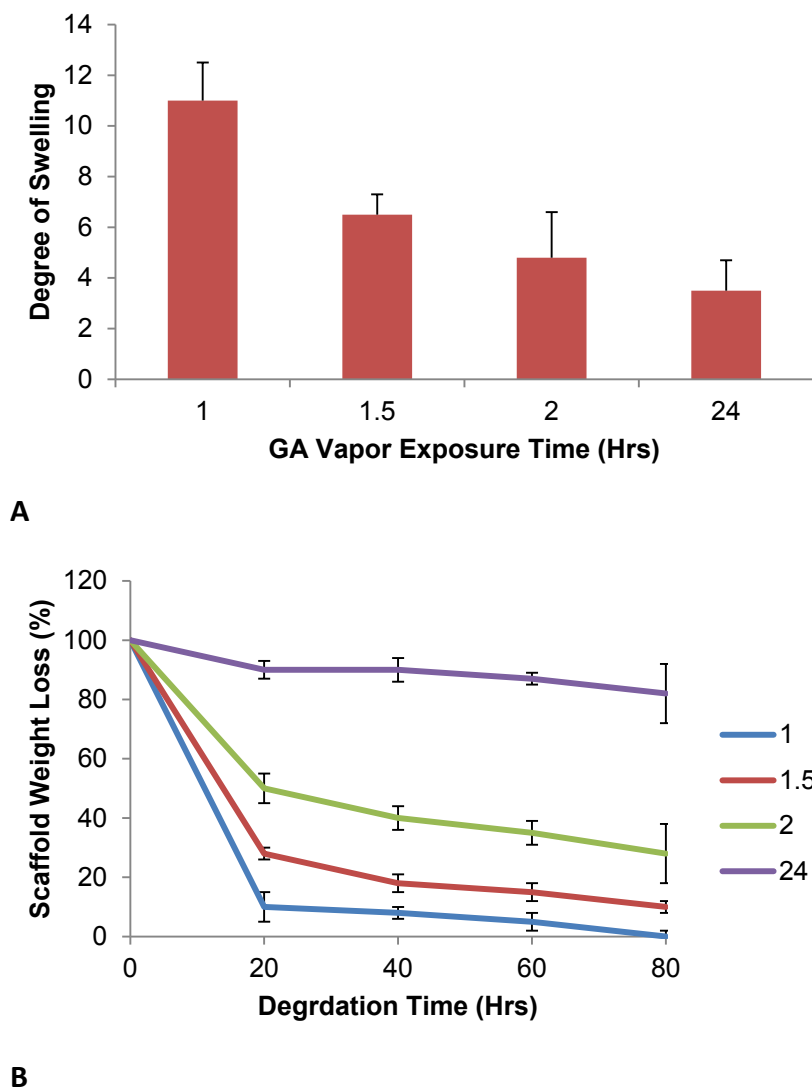
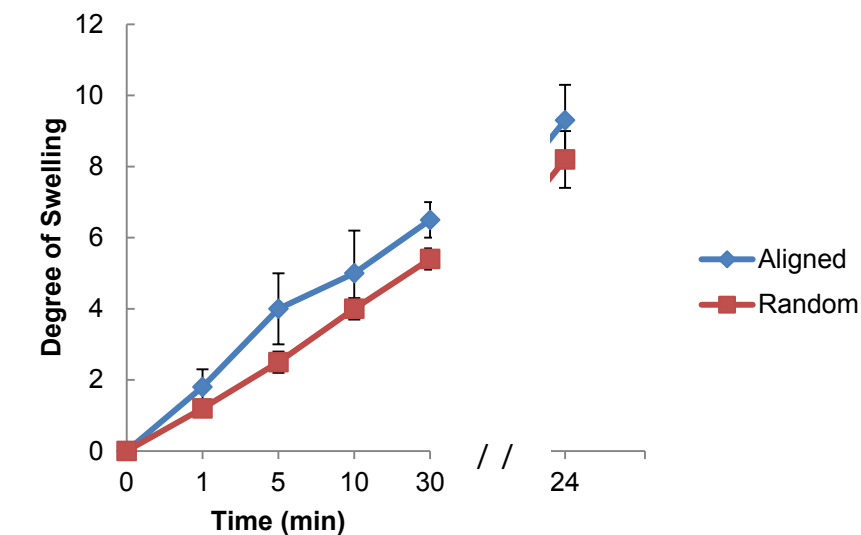
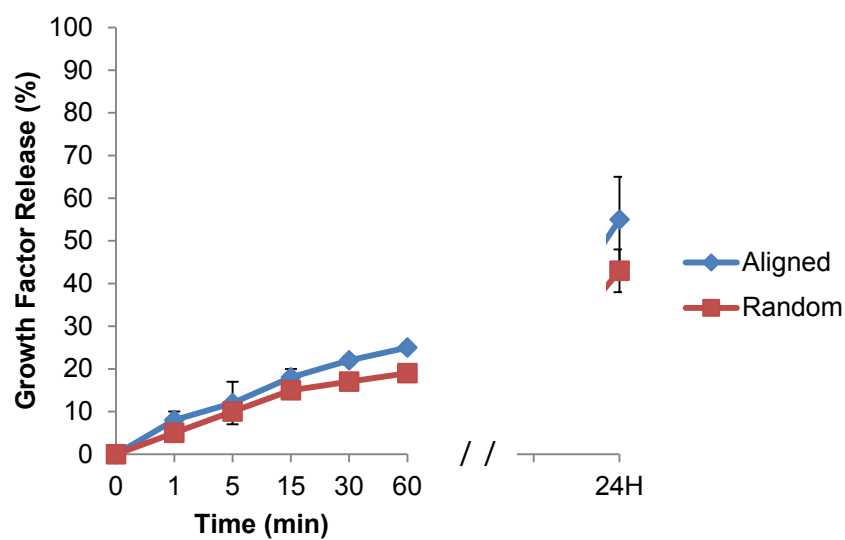


Figure 2.6: Degree of swelling and degradation kinetics as a function of GA vapor exposure time. (A) Electrospun scaffolds were crosslinked for 1, 1.5, 2, and 24 hours degrees of swelling ranged from of 11.25 ± 0.69 to 3.32 ± 0.48 respectively. (B) Degradation kinetics of electrospun scaffolds as a function of GA vapor exposure time. Samples were degraded in 0.1mg/mL collagenase solution in PBS



A



B

Figure 2.7: (A) Evaluation of the degree of swelling as a function of scaffold architecture (i.e. Aligned fiber scaffolds vs. Random fiber scaffolds) and (B) Comparison between the release profiles of FITC-albumin from aligned fiber scaffolds and random fiber scaffolds. Aligned and random scaffolds were electrospun under parameters B_{15} (Table 1) and crosslinked with glutaraldehyde vapor for one hour.

2.2.4 Cell Proliferation and Morphology as a Function Of Scaffold Architecture and Growth Factor Gradient

Several authors have demonstrated tissue engineering construct parameters (i.e. morphological characteristics, fiber alignment, GF gradients) can significantly influence cellular behavior [88]. Preliminary results demonstrated HUVECs adhered successfully onto 3-D electrospun gelatin B scaffolds (Figure 2.8). Briefly, cell density on the surface of the gelatin scaffolds was determined to be 158 ± 11 cells/mm² while at the control groups (2-D culture plates) was determined to be 320 ± 152 cells/mm². Subsequently, we evaluated the effect of nanotopographical cues and VEGF gradients immobilized onto gelatin nanofibrous scaffolds on HUVEC alignment, density and proliferation. We identified nanofiber alignment (random vs. aligned) had a pronounced effect on individual cell morphology (Figure 2.9).

HUVECs responded to aligned scaffold morphology through elongation and organization parallel to the nanofibers (Figure 2.9B). Conversely, cells seeded on random fiber scaffolds exhibited a rounded morphology, lower proliferation rates and reduced migration (Figure 2.9C). This cellular response of HUVECs to aligned or random fibers is in concord with our previous studies [102] and several others [100,104-108]. Nanoscopic topography is known to influence cell behavior and morphology via contact guidance [83,84,109,110]. This difference in cellular response could be a result of gap size between fibers; the larger the gaps between fibers the less cell-cell interactions will occur, hindering cellular processes [85]. Aligned fibers presented cells with smaller gaps between fibers and increased surface area which allowed for HUVECs to attach and spread more easily

compared to random fibers. This cell infiltration was evident from fluorescent microscopic images taken at various scaffold depths in the random fiber orientation groups, while minimum infiltration was observed in the aligned nanofibrous scaffolds. Similar findings on the effect of fiber orientation of electrospun scaffolds on pore size and cellular infiltration have been reported by others [85,90].

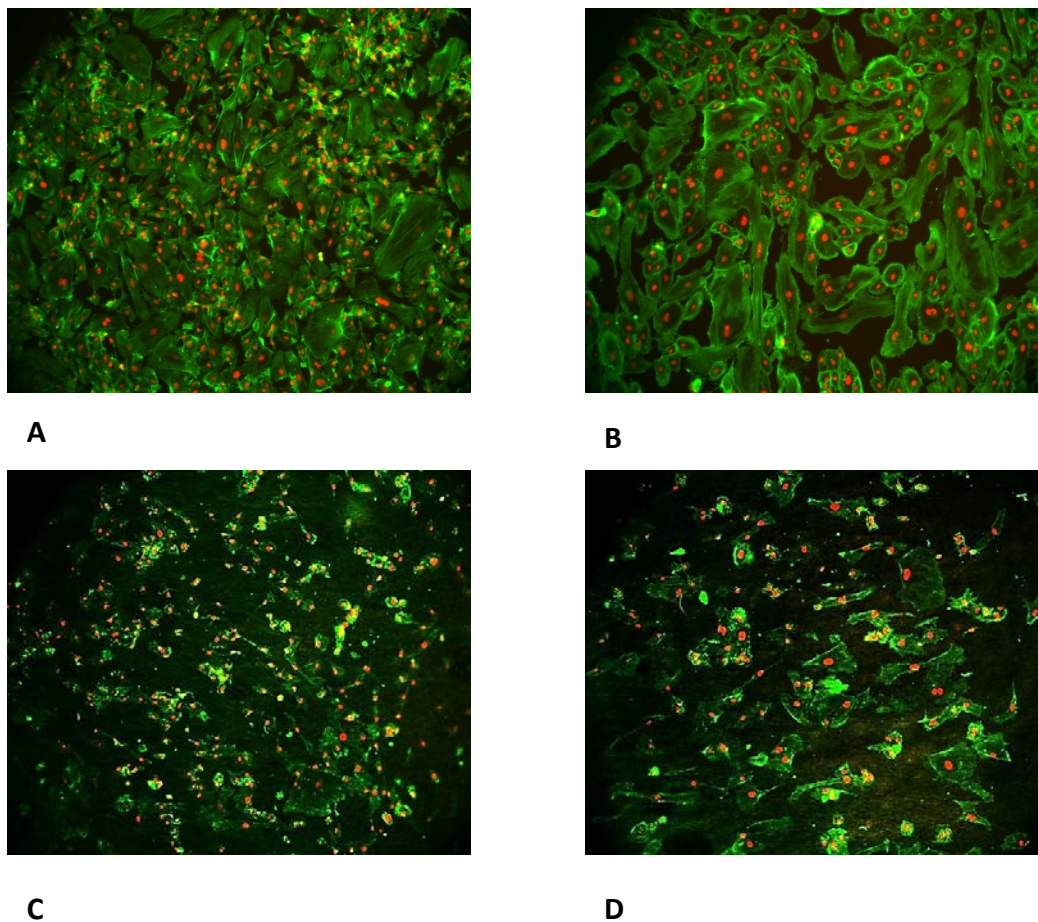


Figure 2.8: HUVEC proliferation as a function of scaffold topography – Aligned versus Random. Assessment was performed after 5 days in culture using a calcein AM stain and fluorescent microscopy. Representative fluorescent images (10X magnification) of cells growing on 2-D wells (A and B) and electrospun scaffolds (C and D) with random fiber orientation loaded with 10ng/mL of VEGF.

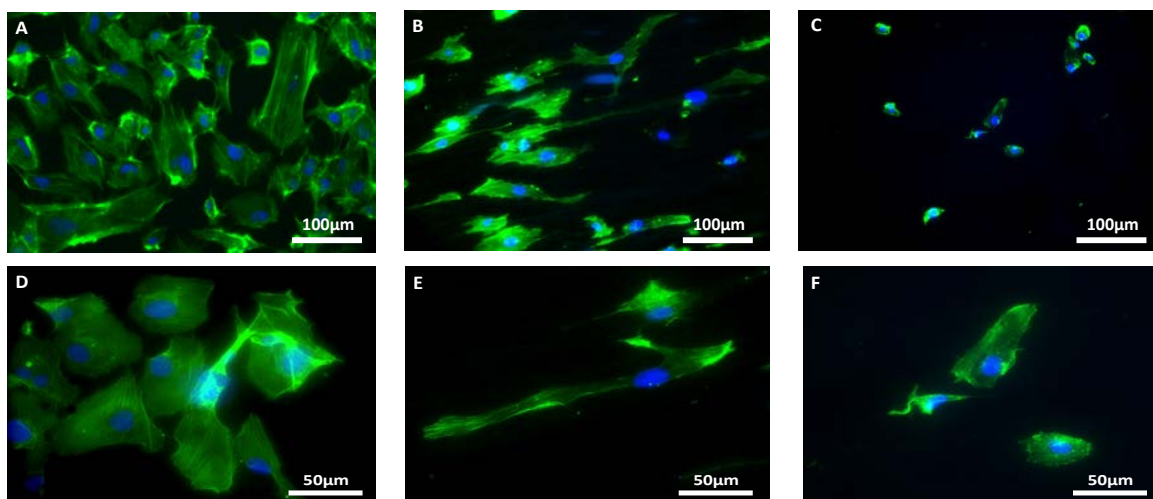
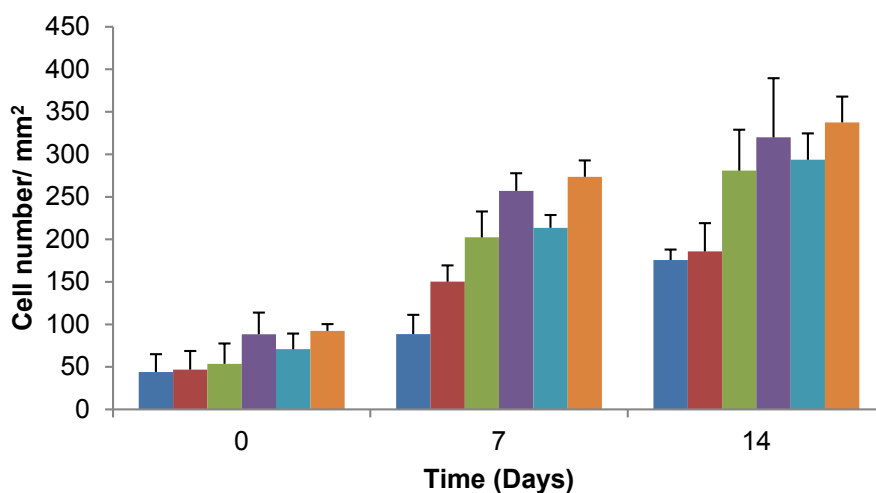
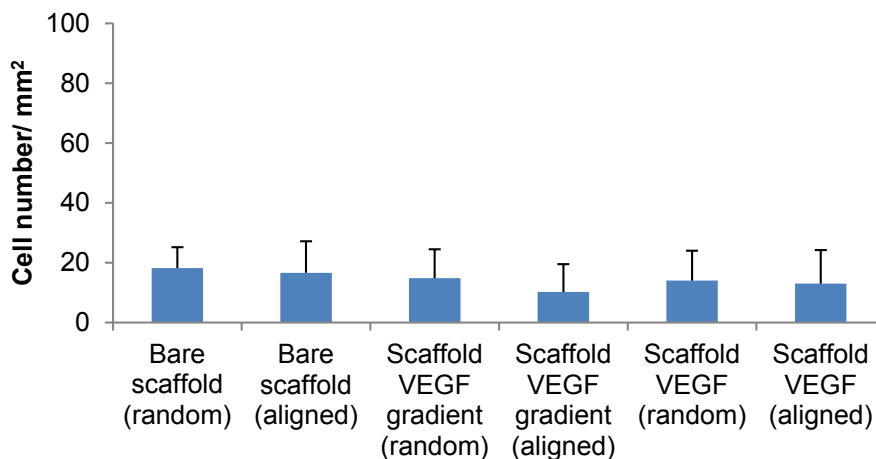


Figure 2.9: Cytoskeleton arrangement of HUVECs on electrospun gelatin scaffolds. (A & D) Bare well, (B & E) Aligned fiber orientation, and (C & F) Random fiber orientation (A, B, and C all taken at 20X magnification while D, E, and F taken at 40X magnification). 10,000 cells were added to each well containing scaffolds (1 cm diameter, 24-well plates) and the cells were incubated at 37 °C/5 %CO₂ for 5 days. Following incubation, the cells were stained with Alexa Fluor 488 Phalloidin and DAPI per manufacturer's protocol, and the cell-scaffolds were imaged with a fluorescent microscope to assess the effect of the scaffold's fiber orientation on cell morphology.

We also found that in addition to fiber architecture, HUVEC behavior was also dependent on growth factor growth factor delivery profile. Results demonstrated cells migrated up the VEGF concentration gradient, yielding to higher cell densities, and changes in cellular morphology and proliferation rates (Figures 2.10). The number of HUVECs that migrated (Figure 2.10A) up the VEGF gradient after 14 days of incubation was of 298 ± 13.4 cells/mm² in the case of aligned constructs while for the randomly orientated constructs it was of 158 ± 11 cells/mm² ($p < 0.05$). HUVECs resulted in higher proliferation rates (Figure 2.10B) when cells were cultured on aligned fibers (14.8 ± 5.19 cells/mm²) compared to $10.2 \pm$

4.11 cells/ mm² when seeded on random fibers ($p < 0.05$). Studies have demonstrated migration of endothelial cells and sprouting vessels are dependent on VEGF gradient shape [100]. Cells cultured on exponential gradients show increased chemotactic response and directed capillary growth [86,100] compared to linear gradients [87]. Additionally, the combination of aligned fiber scaffolds and VEGF gradients enhanced cellular responses, resulting in higher cell densities and cellular elongation which lead to higher cell-cell interactions and contact guidance. In conclusion, HUVEC behavior was influenced by nanotopographical changes and VEGF gradient. Cells cultured on aligned fiber scaffolds in combination with VEGF gradients displayed significant changes and differences in proliferation, cell density and morphology compared to cells seeded on random fiber constructs.

**A**



B

Figure 2.10: Cell density and proliferation as a function of scaffold topography. Number of cells that migrated up the concentration gradient was higher when HUVECs were seeded on aligned fiber scaffolds (A) ($*p < 0.05$). Scaffold morphology influences cell proliferation. HUVEC proliferation (B) was reduced when cultured on random fiber scaffolds ($p > *0.05$).

2.3 Conclusions

In this study, we described a novel electrospinning approach to fabricate VEGF-loaded nanofibrous scaffolds with patterned fiber architecture and assessed their ability to direct cellular behavior. Electrospun gelatin scaffolds with variable fiber orientation, dimensions and rate of degradation were produced by controlling the fabrication parameters (i.e. needle-to-collector distance, electric field, electrode polarity, glutaraldehyde crosslinking, etc.). HUVEC behavior was influenced by nanotopographical changes and VEGF gradients. Cells cultured on aligned fiber scaffolds in combination with VEGF gradients displayed significant changes and differences in proliferation, cell displacement and morphology compared to cells seeded on random fiber constructs. These results suggest the combinatory effect

of electrospun aligned fiber scaffolds, VEGF gradients and HUVECs could be a potential tissue engineering approach to direct vascular patterning. This is particularly important since the formation of new vessels in response to pro-angiogenic growth factor stimulation or matrix rearrangement is associated with the activation of quiescent endothelial cells which in part involves changes in cell morphology (i.e. elongation) and the formation of new contacts with the underlying substrate [39].

CHAPTER 3: DETERMINE THE EFFECT OF VEGF RELEASING ELECTROSPUN SCAFFOLDS ON CELLULAR BEHAVIOR (I.E. PROLIFERATION AND MIGRATION) IN VITRO

Tissue and organ (i.e. blood vessels, nerves, bone) development [99-102] often arise from the spatially and temporally tuned growth factor delivery profile. Angiogenesis is one of these types mechanisms controlled by an intricate cascade of events. The formation of mature new vascular networks are initiated by pro-angiogenic growth factors such as vascular endothelial growth factor (VEGF) mediated by different types of endothelial cells (i.e pericytes, smooth muscle cells) [104,105]. To regulate vessel density, size, and distribution to pattern vascular networks, VEGF and its isoforms [106], and other angiogenic growth factors act in spatial–temporal gradients. Spatial control over angiogenesis is especially important since unguided vessel growth may lead to incorrect vascular patterning, vessel instability and poor network functionality [107].

The biological mechanisms of angiogenesis suggest that strategies to develop new blood vessels may benefit from tailored spatial–temporal delivery of cytokines [108,109]. Traditionally, therapeutic angiogenic approaches for ischemic diseases (e.g. coronary artery disease, peripheral vascular disease) have focused on delivering bolus injections of single growth factors however; the lack of control over growth factor availability using this approach has limited its clinical success [108,109]. The need for spatial–temporal growth factor delivery strategies have been addressed by immobilizing single growth factors on substrates [18,31,33] or by encapsulating them in delivery vehicles [33,73,74]. However, with these approaches, the sustained and patterned release of

bioactive molecules remains a challenge. Therefore, we have electrospun scaffolds with different architectures that allow localized and sustained delivery of VEGF in distinct spatial distributions to evaluate vessel formation as a function of substrate characteristics. However, growth factor spatial-temporal delivery alone may not stimulate mature vessel development and subsequent patterning. The addition of endothelial cells (i.e. HUVECs or EPCs) may entice scaffold vascularization more effectively.

We previously described the synthesis of gelatin electrospun scaffolds for guided angiogenesis [102]; results demonstrated HUVEC morphology and orientation were affected by fiber orientation and growth factor growth factor delivery profile. Although HUVEC behavior was influenced by construct characteristics, tube-like structures were not well defined. Studies have demonstrated that although EPCs have undergone differentiation, they still possess properties of immature cells, thus suggesting greater angiogenic capabilities compared to mature endothelial cells (i.e. HUVECs) [88-90].

The goal of this aim is to determine the proper balance between physical (i.e. electrospun scaffold fiber architecture) and chemical (i.e. VEGF) cues for the purpose of achieving optimum EPC or HUVEC attachment, proliferation and migration within electrospun scaffolds. With a suitable balance, in conjunction with scaffold- cell (EPCs-HUVECs) interaction we can recreate vasculature networks by organizing cells into specific patterns.

3.1 Experimental Approach

3.1.1 Live imaging design and setup mechanism

To evaluate cellular behavior in real time we tailored our own microscope stage incubator. This system is composed of two subsystems, a well plate incubator system (Appendix I) and a visualization system. Our well plate incubator is composed by a chamber, control unit, preheating module and humidifying module (Figure 3.1).

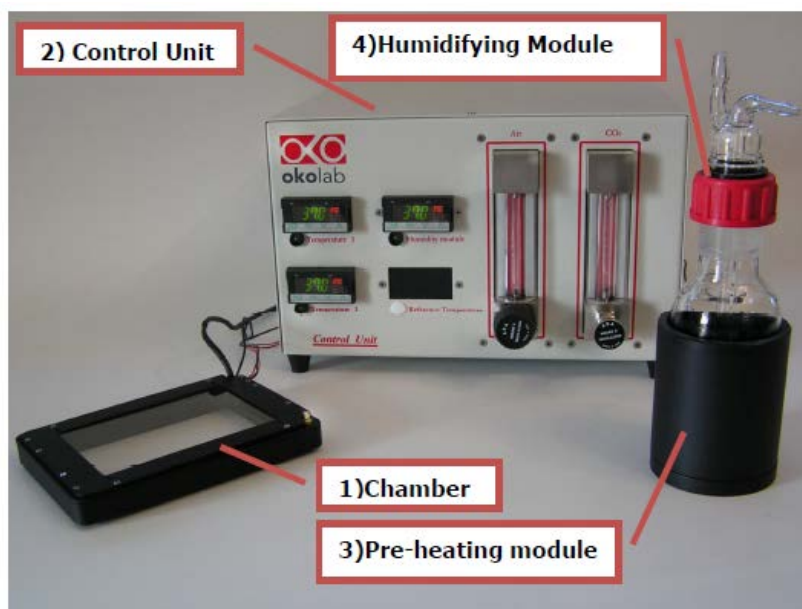


Figure 3.1: Diagrammatic representation of well plate incubator components

This system regulates chamber temperature, CO₂ and humidity. Briefly, chamber temperature is regulated by the combined action of two controllers acting on the power dissipated by the electric resistances, embedded both in the base and in the lid of the incubating chamber. CO₂ levels are maintained constant by mixing

CO₂ with air in the control unit, this mixture is continuously fed into the incubating chamber to control medium pH. Finally, the humidifying module helps prevent medium evaporation and avoid water condensation on glass and plastic surfaces. Figure 3.2 shows how the system is connected.

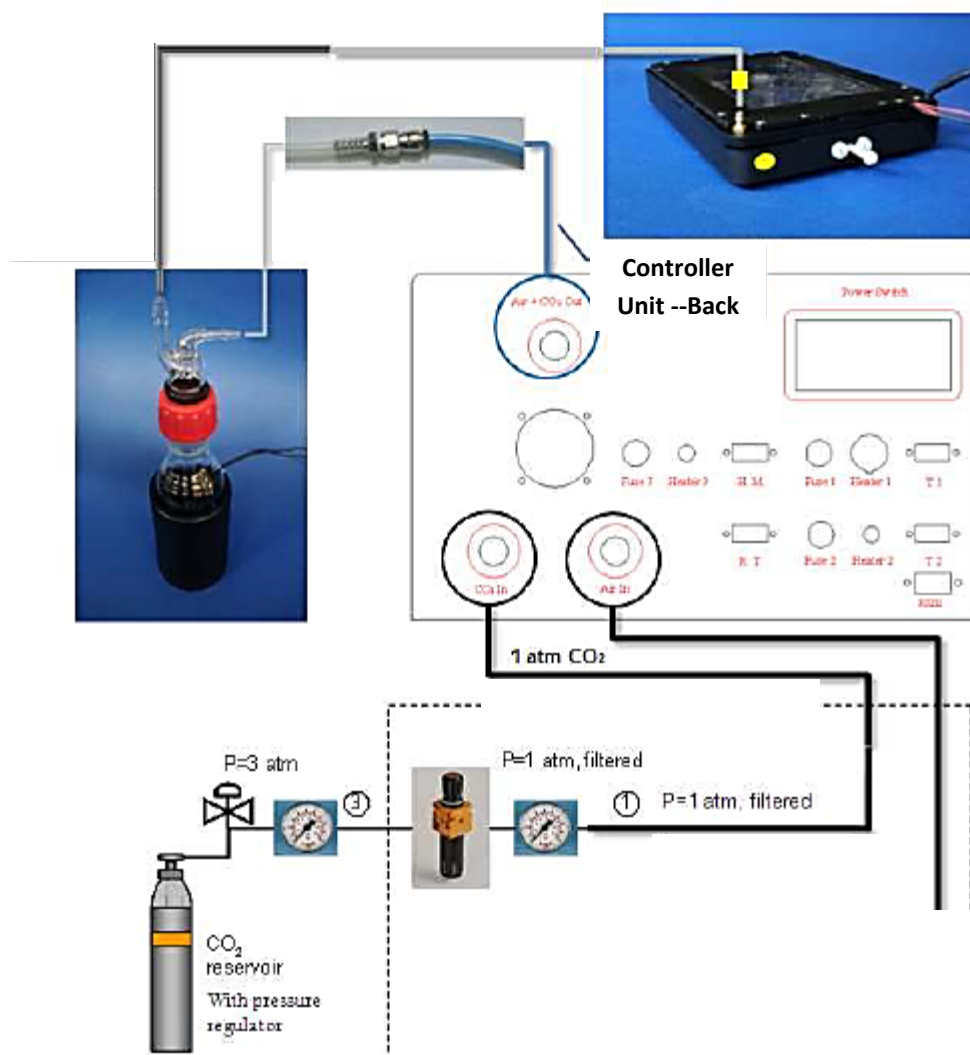


Figure 3.2: Diagrammatic representation of well plate incubator

Our visualization system is composed of Motic inverted microscope equipped with epi-fluorescence. A CCD camera is utilized to capture images and for time-lapse video. In order to obtain live cell images we place the chamber from our well plate incubator on top of the microscope's stage (Figure 3.3). Once situated properly our motic camera software is initiated and time-lapse video is obtained.



Figure 3.3: Diagrammatic representation of chamber placement

3.1.2 HUVEC and EPC cell culture

HUVECs were obtained from Lonza (Rockland, ME). Cell culture was maintained at 37°C and 5% CO₂ in endothelial basal media -2 (EBM-2, Lonza AG, Rockland, ME) supplemented with SingleQuotes growth factors. EPCs (Promocell, Germany) were processed according to manufacturer specifications, followed by seeding on type I collagen-coated plates. Cells were expanded in Endothelial Progenitor

Medium - Ready to use - (Promocell, Germany) and maintained at 37°C and 5% CO₂. At day 4 cells were passaged, seeded on type I collagen coated plates and cultured in EBM-2 (Lonza AG, Rockland, ME) supplemented with SingleQuotes growth factors. Passages 2-4 were utilized for all experiments.

3.1.3 Cell density and tubular formation as a function of time and scaffold morphology

Scaffolds were synthesized as previously described [102]. Random and aligned scaffolds were adhered to the bottom of a 12- well plate utilizing fibrin glue. VEGF (10ng/ml) was physically entrapped on the right side of the scaffold for 20 min. EPCs or HUVECs were then seeded (50,000 cells/scaffold) on the left side and allowed to attach for 20 min @ 37 °C (Figure 2.2). At day 7 and 14 scaffolds were stained with CalceinAm (Invitrogen, Carlsbad, CA) to assess cell density per unit area and tubular formation. Subsequently, images of each scaffold were captured utilizing a Motic AE 20/21 microscope (VWR, Radnor, PA) with a 4X-10X objective. To ensure each scaffold was observed in its entirety 15 images were taken per construct. The number of images per scaffold was defined as a function of total scaffold area (2 cm²) and microscope field of view (diameter 0.26 cm). To measure cell density per unit area we uploaded the images to ImageJ (NIH, Bethesda, MD) and utilizing particle analysis we determined the number of cells. To assess tubule length and number we identified and selected 5 cell clusters from where tubule growth was apparent and took measurements utilizing the measurement analysis tool from Image J. The total number of measurements was averaged to determine the overall tubular length per scaffold.

3.1.4 Cell proliferation as a function of time and scaffold morphology

EPC and HUVEC proliferation on nanofiber scaffolds was evaluated utilizing a Click-iT® EdU Alexa Fluor® 488 Imaging Kit (Invitrogen, Carlsbad, CA). Both types of cells were incubated with 10µl of EdU for 48 hrs subsequent to seeding on nanofibrous constructs. Cells were then fixed and permeabilized followed by the addition of the Click-iT® reaction cocktail. Images were taken to evaluate cell proliferation as a function of nanotopography and VEGF gradients.

3.1.5 Cell Migration Evaluation

Prior to cell seeding onto scaffolds, both EPCS and HUVECs were transfected with CellLight® Reagent *BacMam 2.0* (Baculovirus) following manufacturer's (Invitrogen, Carlsbad, CA) protocol. Subsequently, random and aligned scaffolds were placed on glass bottom dishes, VEGF (10ng/ml) was physically entrapped on the right side of the scaffold for 20 min. Transfected EPCs or HUVECs were then seeded (50,000 cells/scaffold) onto the left side of the scaffold and allowed to attach for 20 min @ 37 °C. Cells were incubated for 24 hrs before beginning time lapse imaging. Images were collected at 10min intervals for 24 hrs utilizing a Motic AE 20/21 microscope equipped with a stage incubator (OKO labs, Warner instruments, Hamden, CT). Cell migration was quantified manually by tracking the coordinates of 25 migrating cells using Motic Plus 2.0 software. Average migration velocity (V_{mig}) was calculated equation (a) The effective displacement (D_{migeff}) due to migration was calculated using equation (b). Additionally, using Image J plugin chemotaxis and migration tool (NIH- IBIDI, Bethesda, MD) cellular migration paths

were delineated and animated by manually tracking 3 cells per group over 25 successional coordinates.

(a) Average migration velocity (V_m)

$$V_m = \frac{\sum_{i=1}^n \sqrt{(x_i - x_{i-1})^2 + (y_i - y_{i-1})^2}}{\sum_{i=1}^n t_i}$$

(b) Displacement due to migration

$$D_{mig.eff} = \sqrt{(x_{fin} - x_o)^2 + (y_{fin} - y_o)^2}$$

3.1.6 Cell morphology

Images of cells were taken at 10X magnification to evaluate circularity at day 7 and 14. Perimeter and area measurements were calculated utilizing ImageJ software. Circularity was evaluated using formula below (c).

(c) Circularity

$$C = \frac{4\pi A}{P^2}$$

A is the approximate area of the cell and P is the perimeter of the cell. Circularity is described as a measurement that ranges between 0 and 1, where $0 < C \leq 1$ (In an elongated shape $C \rightarrow 0$ and in a circle $C \rightarrow 1$).

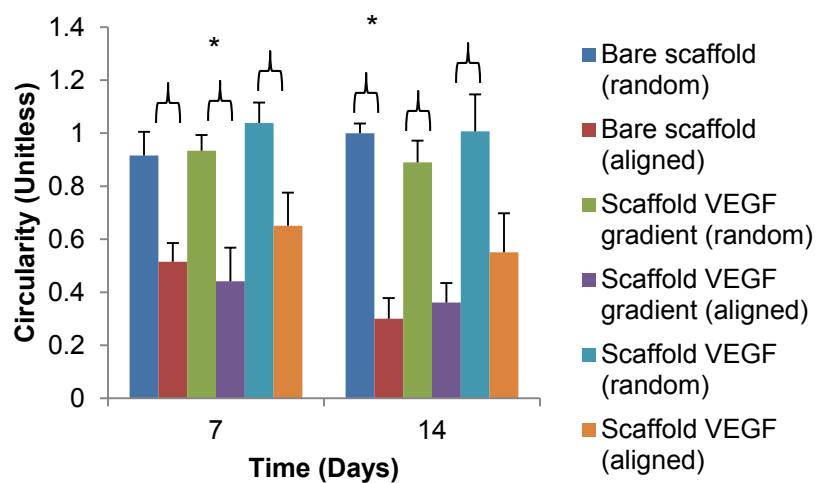
3.1.7 Immunohistochemistry

Cells were fixed in 4% paraformaldehyde, permeabilized with 0.1% Triton X-100 in PBS and stained for endothelial cell markers and cytoskeleton structure. Primary antibodies utilized were: anti-von Willenbrand Factor (Sigma) and anti-vascular endothelial cadherin (Chemicon). Subsequently cells were washed and incubated in their respective secondary antibodies: Alexa Fluor® 647 Goat Anti-Mouse IgG (H+L)- VE Cadherin (Invotrogen) and fluorescein F(ab') fragment goat anti-rabbit IgG (H+L)- von Willenbrand Factor. Subsequently cells were viewed using a Motic AE 20/21 microscope equipped with Motic Plus 2.0 software. Fluorescence intensity was determined by using ImageJ (NIH, Bethesda, MD). Photos were converted to grey scale and in each picture five representative vessels were selected. The integrated density (product of area and mean grey value) was calculated for each selected area. Additionally, the mean average value was subtracted from five background intensities per image (mean grey value_{background}). The average fluorescence intensity (mean grey value_{vessels}) was calculated (CFCT: integrated fluorescence density) whereby the total vessel area multiplied with mean grey value_{background} was subtracted from the average fluorescence intensity and summarized as the corrected total cell fluorescence.

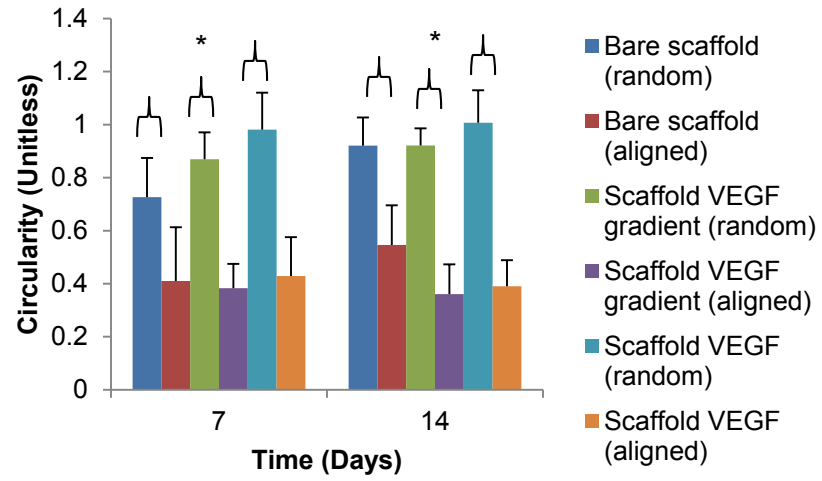
3.2 Results and Discussion

In this study, VEGF concentration gradients were immobilized on nanofibrous gelatin electrospun scaffolds to compare EPC and HUVEC behavior and their angiogenic potential as a function of construct parameters (i.e. morphological

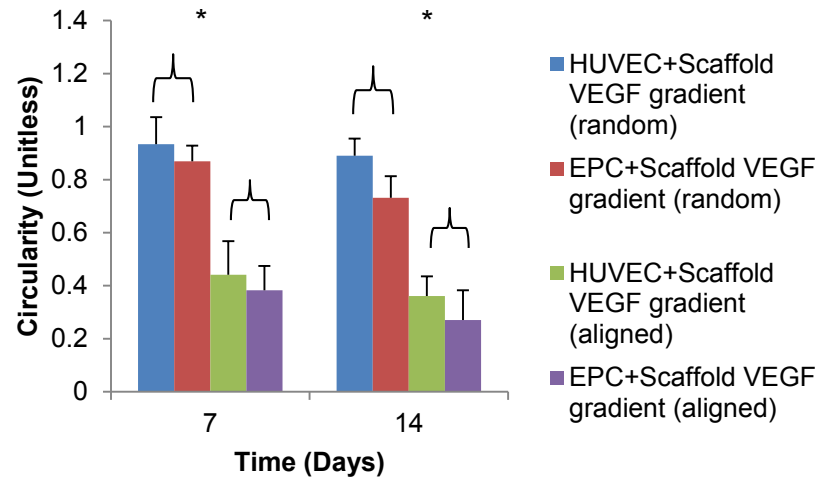
characteristics, fiber alignment, VEGF gradients). We found that both EPC and HUVEC behavior (adhesion, proliferation and migration) were highly dependent on VEGF gradient presentation. After a 14 day period, average circularity (Figure 3.4) showed both EPCs and HUVECs seeded on aligned fiber scaffolds had increased alignment and elongation compared to cells seeded on random fiber scaffolds, which displayed a rounded morphology ($p < 0.05$) (Figure 3.4A and B). There was no statistical significance when comparing gradient presentation to the controls (Bare and constant VEGF). When cell types were compared, the average circularity in all groups was reduced in EPCs in relation to HUVECs (Figure 3.4C and D). This was particularly evident in groups where VEGF gradients had been immobilized on aligned fiber scaffolds (Figure 3.4D) ($p < 0.05$) where the average circularity of EPCs was of 0.32 ± 0.06 and 0.40 ± 0.12 .



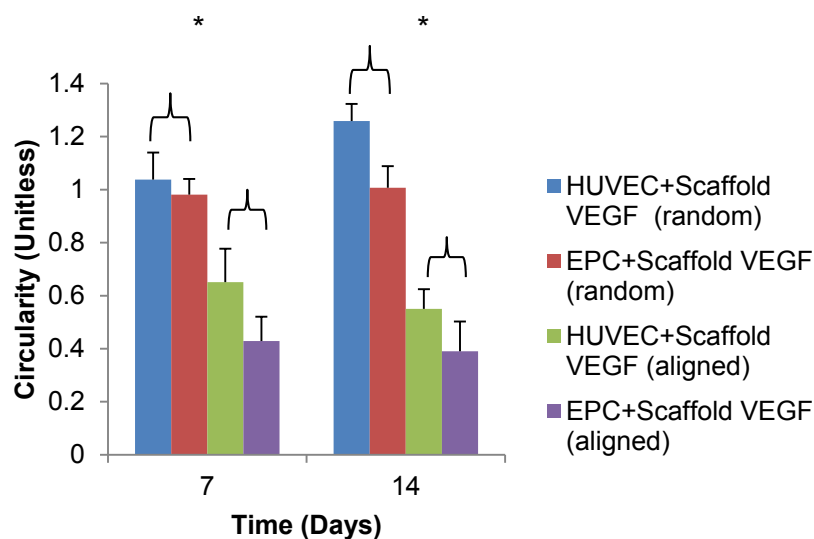
A



B



C



D

Figure 3.4: EPC and HUVEC morphological response to nanotopography and VEGF gradients (Circularity) (A) HUVECs (B) and EPCs cultured on random and aligned fiber scaffolds modified with VEGF gradients exhibited morphological changes. Both EPCs and HUVECs had reduced circularity when cultured on aligned fibers (* $p < 0.05$). Circularity differences were also observed when cell types were compared, EPCs seeded on random fiber scaffolds (C) and on aligned fiber scaffolds (D) had decreased circularity compared to HUVECs.

Furthermore, the rate of cell migration and effective displacement was higher up the VEGF concentration gradient in both cell types (Figure 3.5 -3.8). However, EPC migration was improved on aligned and random nanofibrous scaffolds when compared to HUVEC migration (Figure 3.6A and B). The average velocity of EPCs cultured on aligned fiber constructs was $0.43 \pm 0.08 \mu\text{m}/\text{min}$, while for HUVECs it was estimated at $0.34 \pm 0.05 \mu\text{m}/\text{min}$ ($p < 0.05$). Similarly, migration on random fibers was of $0.19 \pm 0.02 \mu\text{m}/\text{min}$ and $0.14 \pm 0.01 \mu\text{m}/\text{min}$, respectively ($p < 0.05$). As shown in figure 3.6 C and D, topographical cues in combination with VEGF

gradients also influenced cellular movement, HUVECs and EPCs migrated more rapidly when seeded on aligned fibers ($0.34 \pm 0.05 \mu\text{m}/\text{min}$ and $0.43 \pm 0.08 \mu\text{m}/\text{min}$, respectively) compared to random fibers ($0.14 \pm 0.01 \mu\text{m}/\text{min}$ and $0.19 \pm 0.02 \mu\text{m}/\text{min}$, respectively) ($p < 0.05$).

Results of effective displacement assessment demonstrated EPCs travelled further than HUVECs on both types of scaffolds (Figure 3.7 A and B). The effective migration distance of EPCs and HUVECs on aligned scaffolds was of $843 \pm 137 \mu\text{m}$ and $524 \pm 142 \mu\text{m}$ ($p < 0.05$), respectively, while displacement on random fiber scaffolds was of $351 \pm 124 \mu\text{m}$ and $319 \pm 120 \mu\text{m}$, respectively ($p < 0.05$). Furthermore, when comparing topographical characteristics, both HUVECs and EPCs ($843 \pm 137 \mu\text{m}$ and $351 \pm 124 \mu\text{m}$, respectively) had enhanced migration on aligned fiber scaffolds compared to random fibers ($524 \pm 142 \mu\text{m}$ and $319 \pm 120 \mu\text{m}$, respectively) ($p < 0.05$) (Figure 3.7 C and D). These results could indicate both HUVECs and EPCs migrate in a linear fashion when seeded on aligned substrates, however cellular migration path tracking demonstrated both types of cells migrated based on random walk (Figure 3.8). Results show the angle of cell path dispersion is smaller in aligned fiber scaffold groups (Figure 3.8 A and B) compared to those seeded on random fiber scaffolds (Figure 3.8 C and D). Briefly, the random walk dispersion angle of EPCs and HUVECs on aligned scaffolds was of 15° and 30° , respectively, while on random fiber scaffolds the angle was of 55° and 65° , respectively (Figure 3.8).

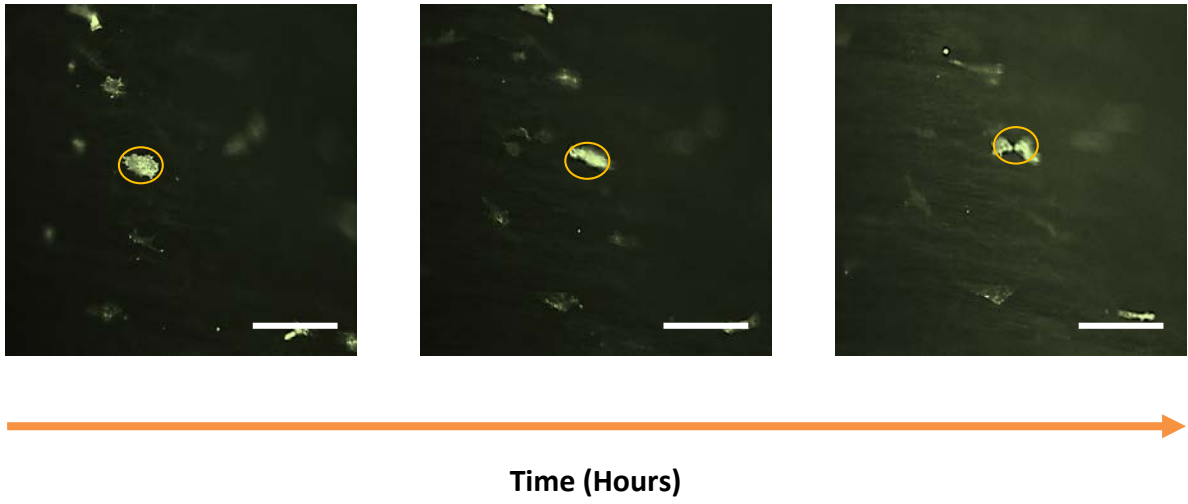


Figure 3.5: Images of time-lapse video utilized for cell tracking. Cell migration was quantified manually by tracking the coordinates of 25 migrating cells. Quantification of cell movement between frames of a temporal stack was obtained by utilizing manual tracking plugin from ImageJ in order to obtain migration paths (Figure 3.8) of each cell and then the data was exported to excel to calculate velocity and displacement as a function of time.

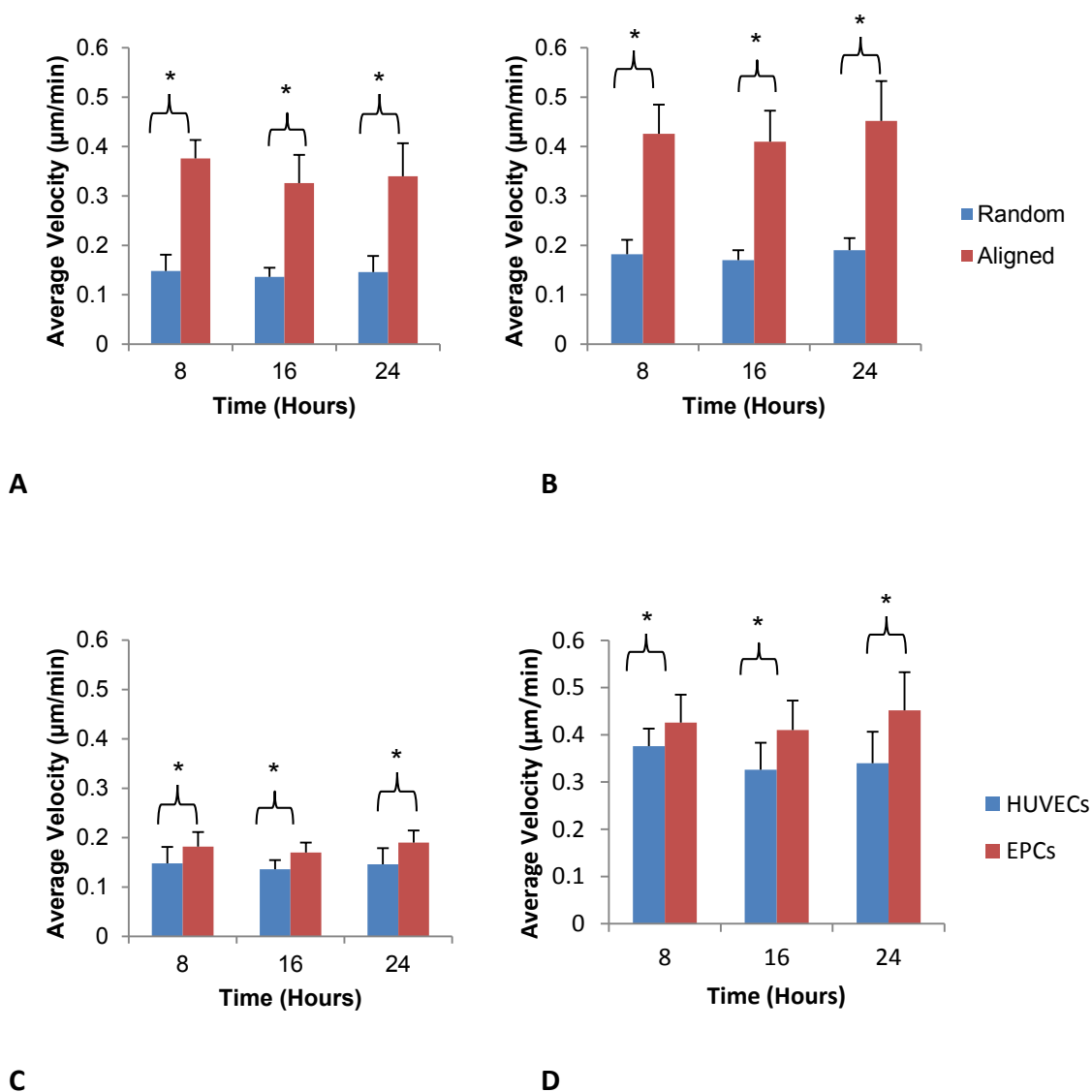


Figure 3.6: Migration velocity as a function of VEGF gradients and scaffold topography. Cell migration was found to be up the VEGF concentration gradient in all groups. HUVECS (A) and EPCs (B) seeded on aligned fiber scaffolds showed higher migration rates compared to cell cultured on random fiber constructs ($*p < 0.05$). Migration velocity differences were also observed when HUVECs were compared to EPCs, in both types of scaffolds (Random (C) and Aligned (D)), EPCs migrated faster ($*p < 0.05$).

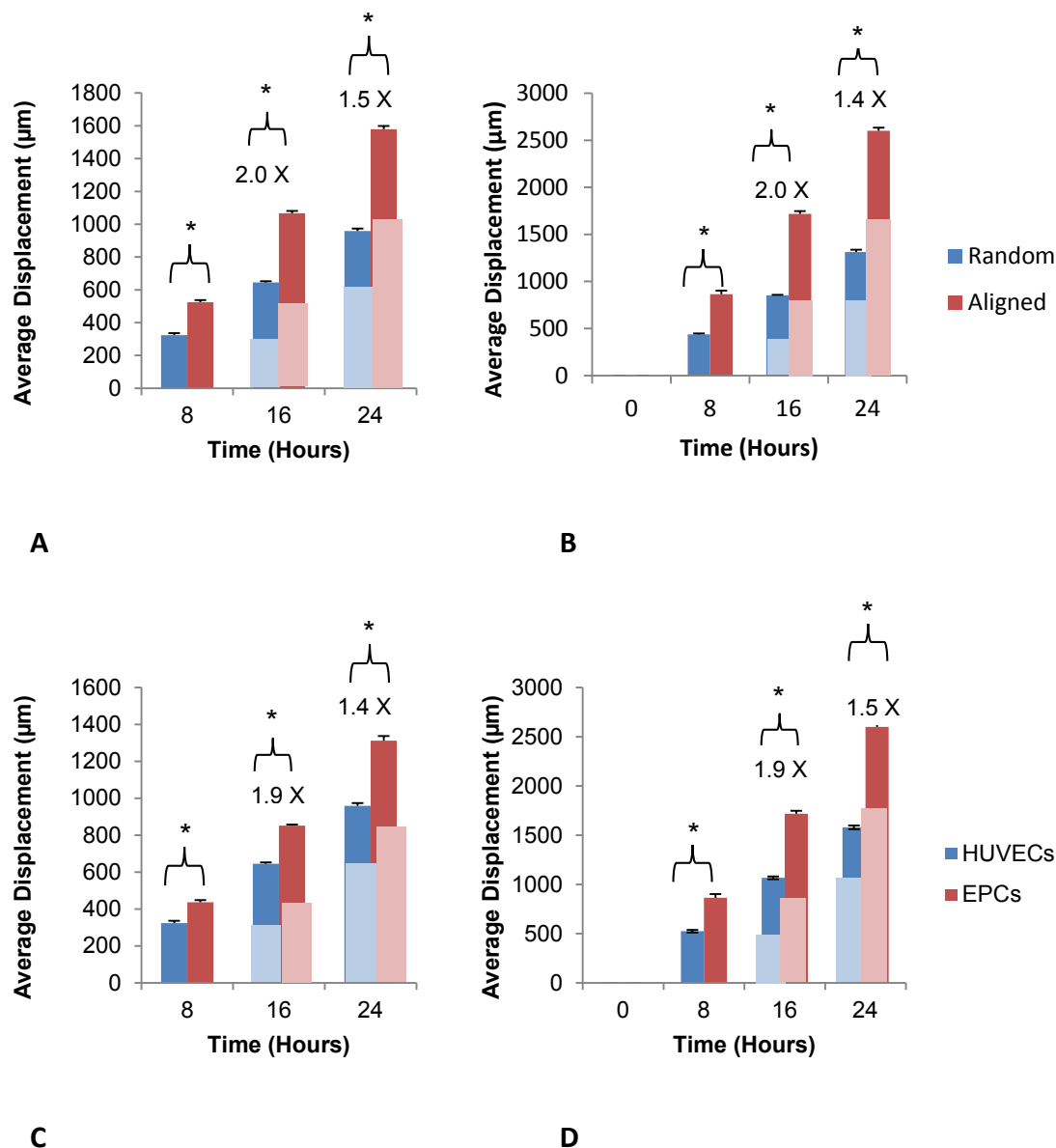


Figure 3.7: Effective displacement as a function of VEGF gradients and scaffold topography. HUVECs (A) and EPCs (B) seeded on aligned fiber scaffolds migrated further compared to cell cultured on random fiber constructs ($*p < 0.05$). Displacement differences were also observed when cell types were compared, EPCs seeded on random fiber scaffolds (D) and on aligned fiber scaffolds (E) had higher migration distances compared to HUVECs ($*p < 0.05$).

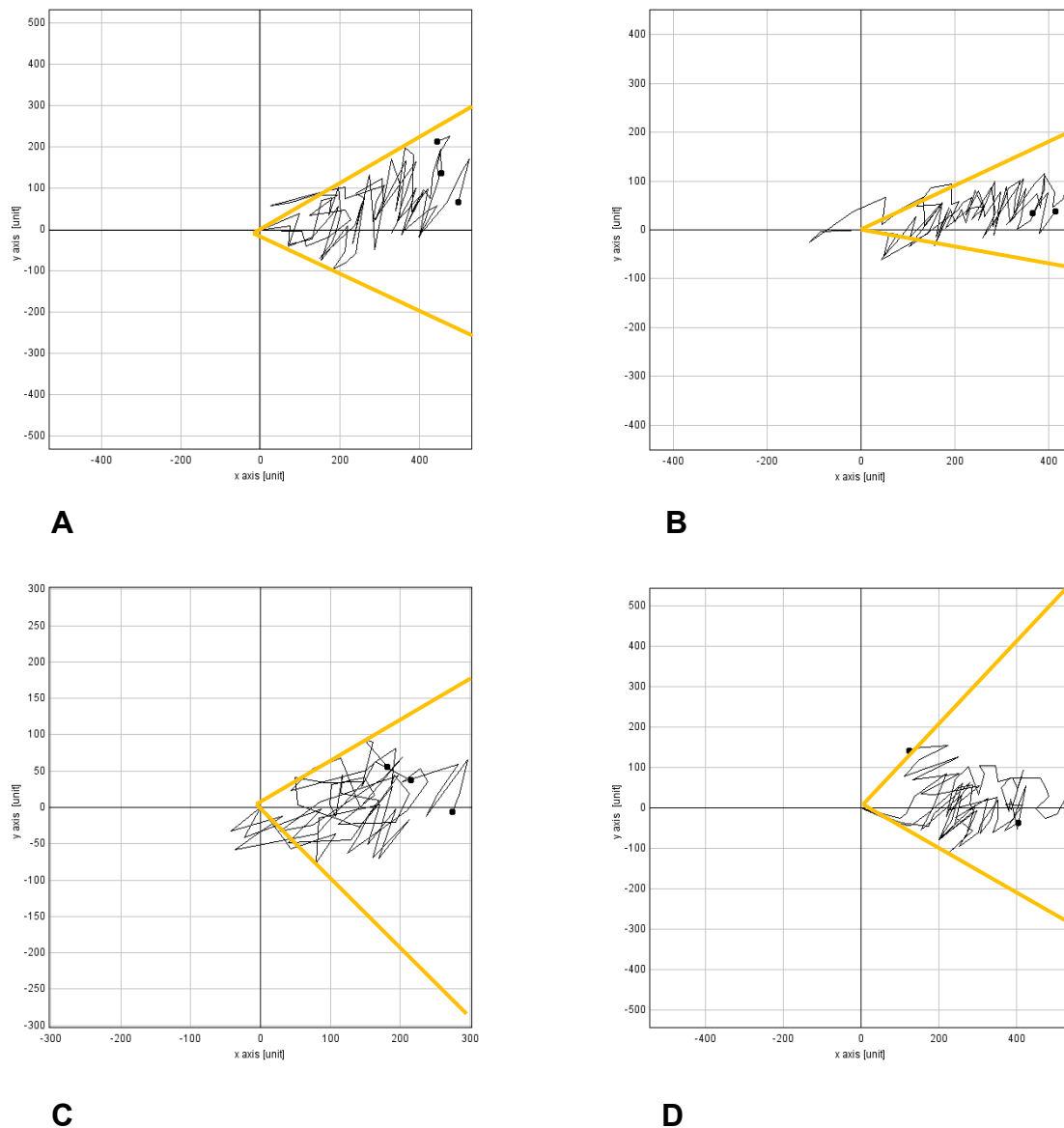
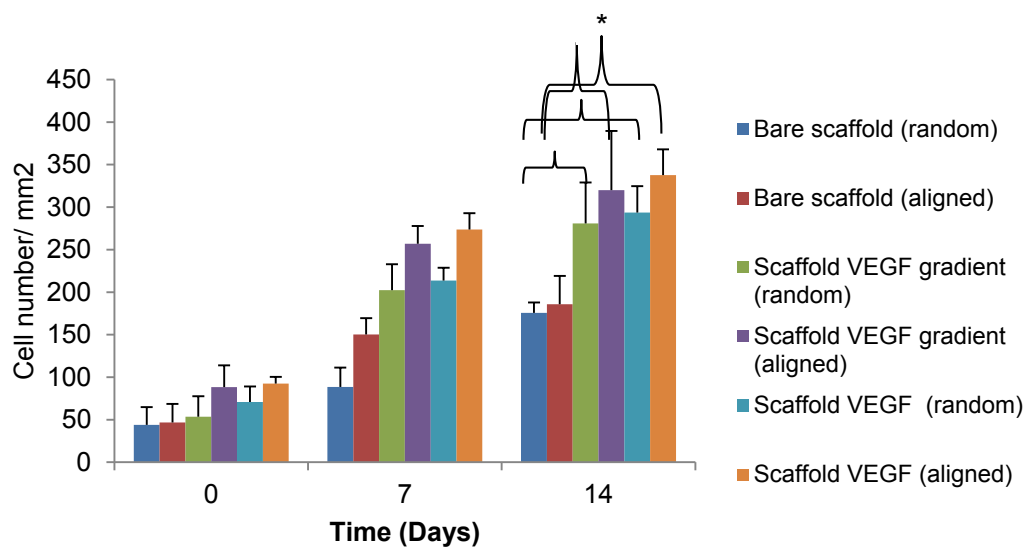
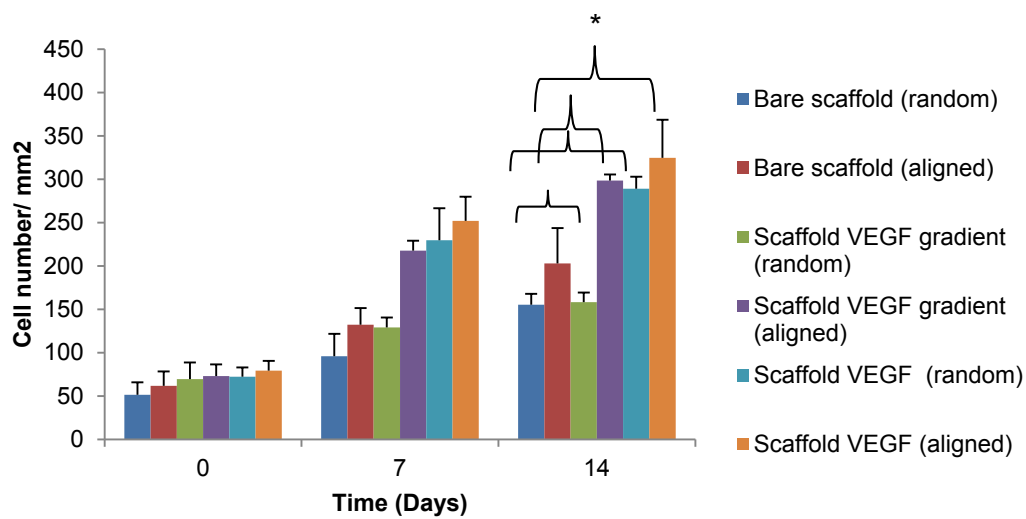


Figure 3.8: Cellular migration paths as a function of scaffold topography. HUVECs (A) and EPCs (B) seeded on aligned fiber scaffolds migrated further compared to cell cultured on random fiber constructs – HUVECs (C) and EPCs (D, despite cell movement was in a random walk fashion). Yellow lines show the angle of cellular path dispersion -- (A) 30° (B) 15° (C) 65° (D) 55°.

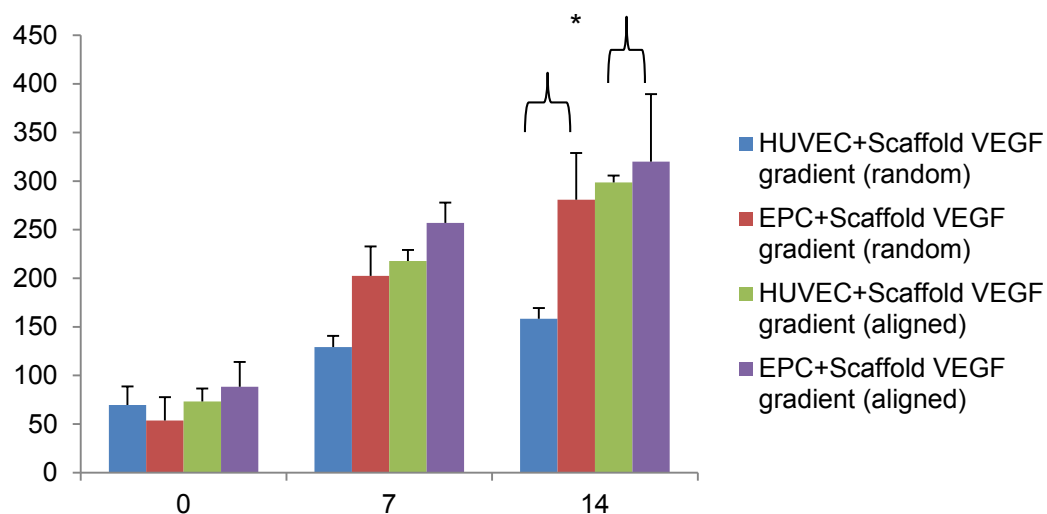
In both types of cells, cell proliferation rate and cell density (Figures 3.9 and 3.10) were a function of scaffold nanotopography and VEGF gradient. After 14 days of incubation, the number of EPCs and HUVECs that migrated (Figure 3.9A and B) towards the VEGF gradient was higher on aligned constructs (281 ± 48 and 158.4 ± 11 cells/ mm², respectively) compared to the randomly orientated constructs (320 ± 69.6 and 298.6 ± 67 cells/ mm², respectively) ($p < 0.05$). Similar results were observed when cell density on scaffolds with constant and gradient VEGF (Figure 3.9A and B) were compared to the control (Bare scaffold) ($p < 0.05$). Moreover, when comparing cell type (Figure 3.9C and D), EPC density (320 ± 26 cells/mm² and 298 ± 13.4 cells/mm²) was higher compared to HUVEC density (280 ± 24 cells/ mm² and 158 ± 11 cells/ mm²) on both aligned and random fiber oriented constructs. Although this behavior was observed in all groups, it was only significant in constructs with VEGF gradients (Figure 3.9). Cell proliferation rates (Figure 3.10) of EPCs seeded on aligned fiber scaffolds were increased in all groups compared to cells seeded on random fiber scaffolds ($p < 0.05$) (Figure 3.9B). Similarly, HUVECs resulted in higher proliferation rates (Figure 3.10A) when cells were cultured on aligned compared to random fiber scaffolds, however rates were not significantly different. When cell types were correlated (Figure 3.10C and D), EPCs were found to have higher proliferation rates in both types of scaffolds compared to HUVECs ($p < 0.05$), this was observed in all groups (Bare, Constant VEGF and VEGF gradient).



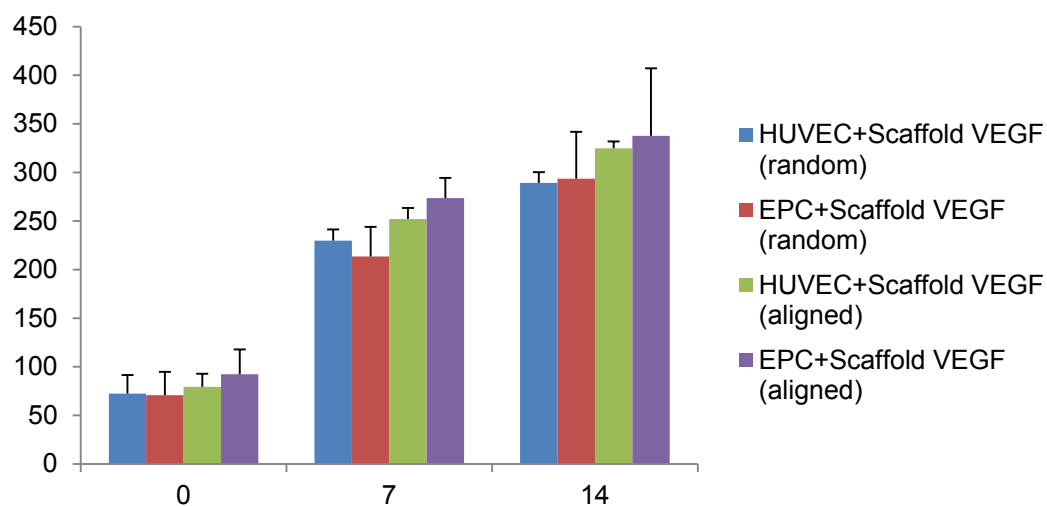
A



B

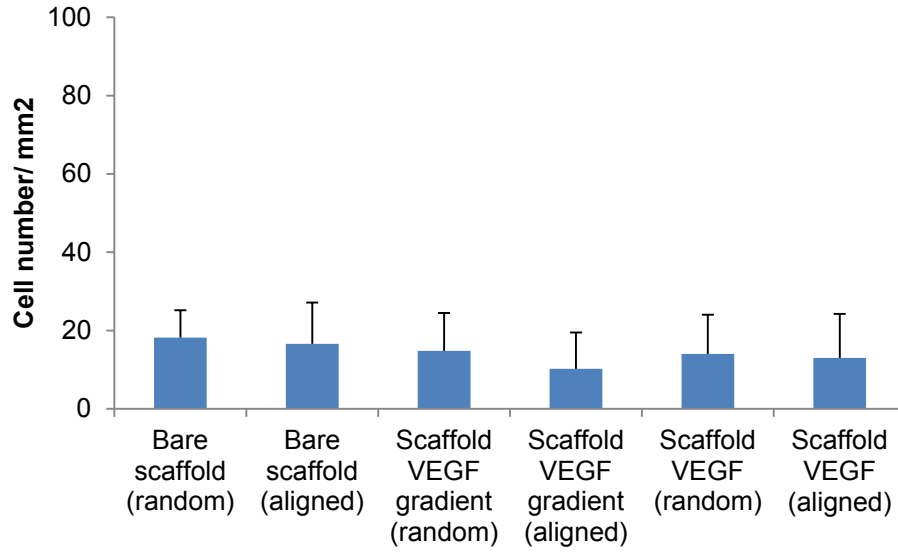
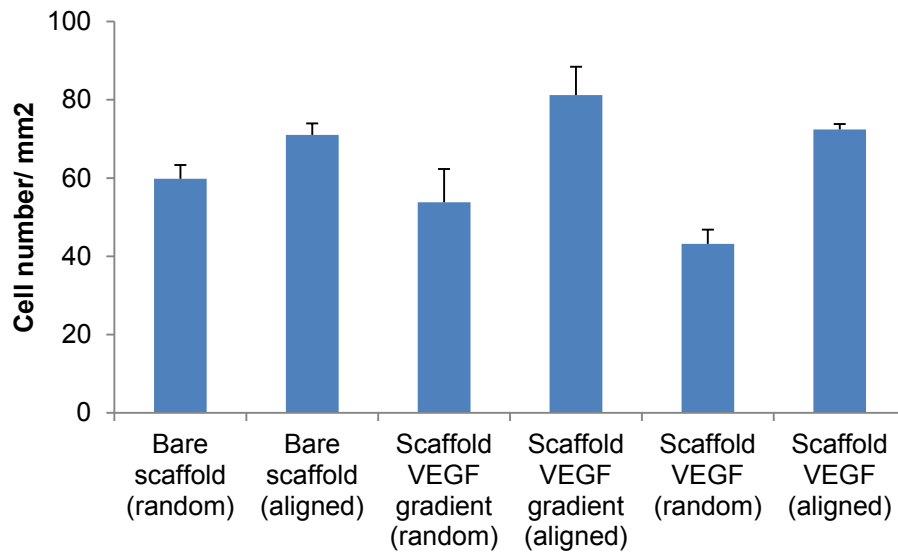


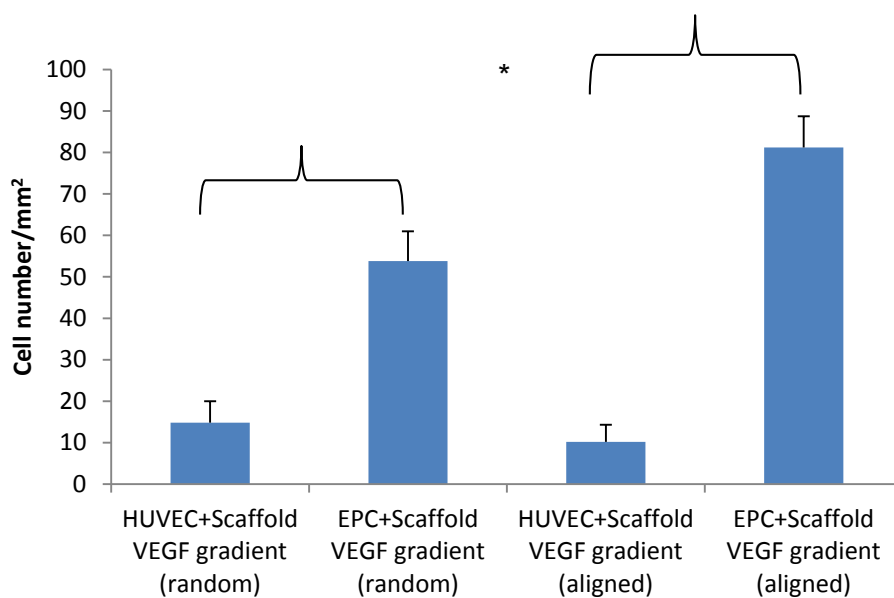
C



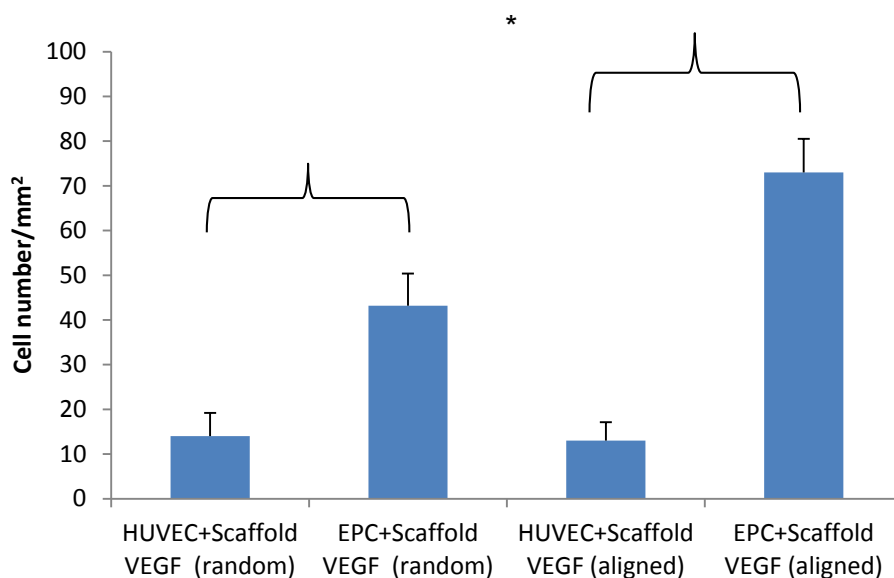
D

Figure 3.9: Cell density as a function of VEGF gradients and scaffold topography. Number of cells that migrated up the concentration gradient was higher when HUVECs (A) and EPCs (B) were seeded on aligned fiber scaffolds ($*p < 0.05$). Differences between HUVEC and EPC density were also observed. EPCs density on both random (C) and aligned (D) fiber constructs was higher compared to HUVEC density.

**A****B**



C



D

Figure 3.10: EPC and HUVEC proliferation as a function of VEGF gradients and scaffold topography. Scaffold morphology influences cell proliferation. HUVEC (A) and EPC (B) proliferation was reduced when cultured on random fiber scaffolds ($p > 0.05$). Proliferation rates were also found to be reduced in HUVECs compared to EPCs when seeded on both random (C) and aligned (D) fibers ($*p < 0.05$).

Scaffold architecture and the presence of a VEGF gradient affected EPC and HUVEC sprouting. Capillaries were found to elongate up the VEGF concentration gradient compared to surfaces containing a constant VEGF concentration. At day 7 tubules were apparent only in groups containing aligned fiber scaffolds (Figure 3.11A) which continued to elongate and align themselves parallel to the nanofibers over a 14 day period. Furthermore, average tubule length (Figure 3.11B) over a 14 day period was found to be greater in scaffolds seeded with EPCs ($485 \pm 29.4 \mu\text{m}$) compared to HUVECs ($256 \pm 63 \mu\text{m}$). Similar HUVEC and EPC behavior was observed when evaluating sprout number per unit area. At day 7 and 14 scaffolds seeded with EPCs developed a higher number of capillaries compared to scaffolds seeded with HUVECs (Figure 3.11C). Furthermore, the levels of protein expression of markers such as vWF were found to be similar in both types of cell cultures (Figure 3.12) and present in tubules formed within aligned fiber scaffolds.

VEGF gradients immobilized on nanofibrous scaffolds were investigated for their effects on EPC and HUVEC behavior. Gradients of VEGF have been shown to have potent chemotactic effects on endothelial cells compared to other types of angiogenic growth factors (e.g. bFGF) [106]. Furthermore, synthesis of a 3D polymeric scaffold in combination of gradients more accurately mimics native ECM, thus eliciting cell behavior that is conducive to the formation of new tissue, while providing spatial and temporal control of growth factor release [31,70,106].

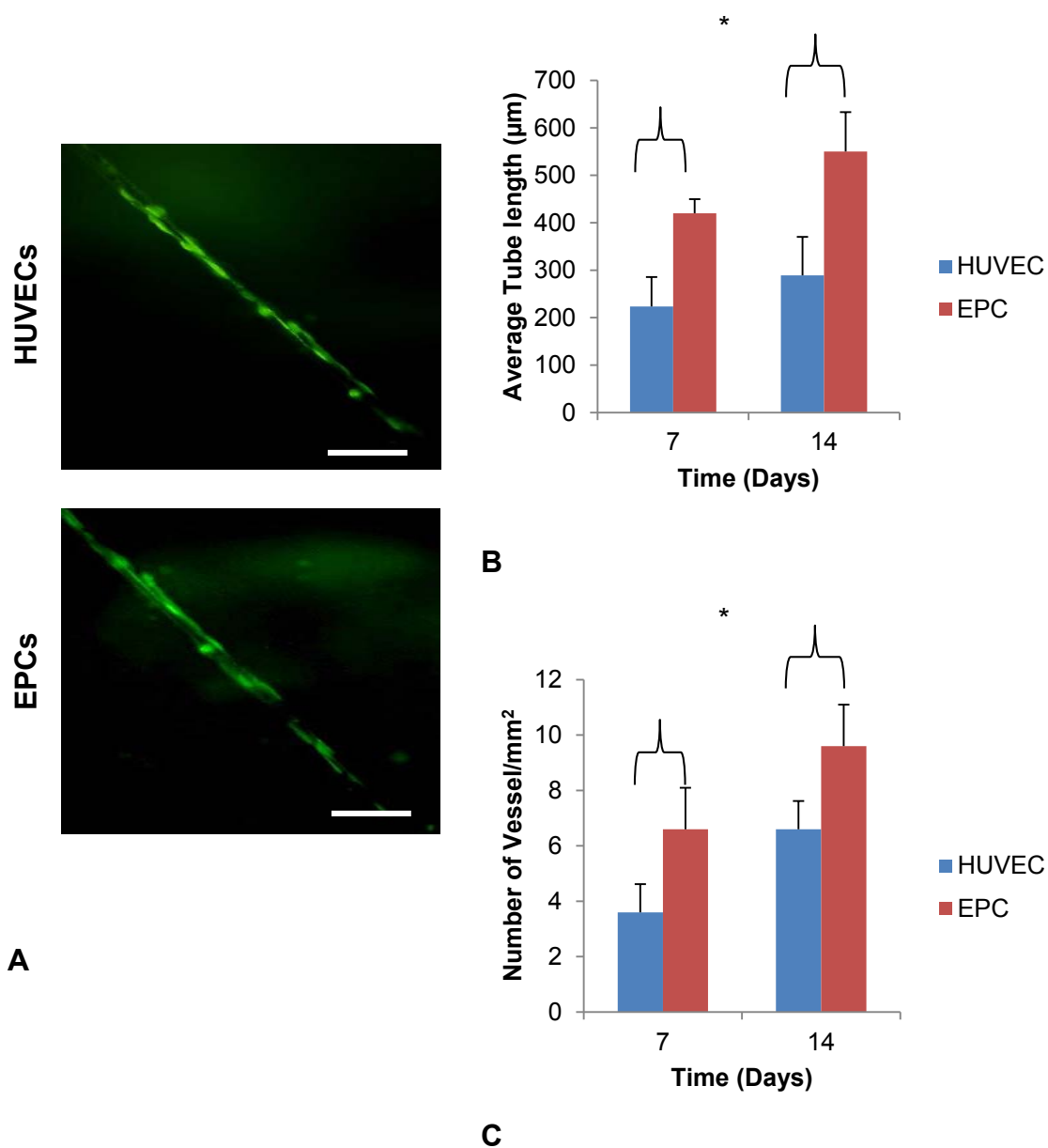
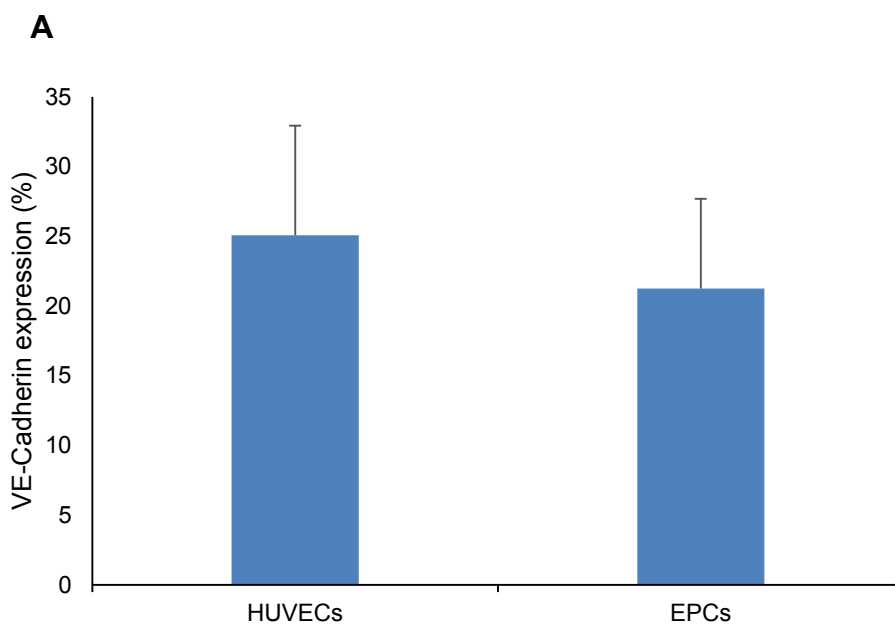
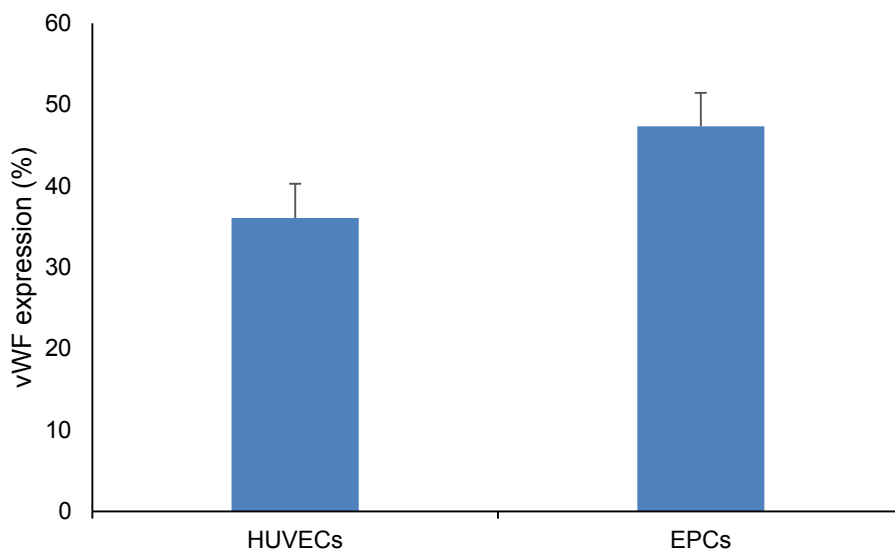


Figure 3.11: Effect of VEGF gradient and scaffold nanotopography on tubular formation. Tubular development was observed only in cells seeded on aligned fiber scaffolds (A). Vessel elongation differences were observed between cell types (B). HUVECs were found to develop shorter vessels compared to EPCs over a period of 14 days ($*p < 0.05$). Number of vessels per unit area were significantly different between cell types (C). HUVECs developed less number of tubules per unit area compared to EPCs. Bar = $20\mu\text{m}$.



B

Figure 3.12: EPC and HUVEC immunohistochemistry evaluating expression of von Willebrand factor and VE-Cadherin as a function of VEGF gradients and scaffold topography. Tubular formation was observed only in cells cultured on aligned fiber scaffolds. The level of vWF (A) and VE-Cadherin (B) expression was found to be similar in tubules developed from HUVECs and EPCs at day 14. Corrected total cell fluorescence (CTCF) shows tubules are positive for vWF and VECadherin staining in both groups. There were no significant differences in staining intensity when comparing groups. CTCF is expressed and percentage of protein expression per group.

Studies have shown that both spatial presentation of cytokines [69,91,92] and scaffold topography [85,93,94] dictate a plethora of cell responses and play a major roles in neovascularization.

This study focused on the effects of nanotopographical cues and VEGF gradients immobilized onto gelatin nanofibrous scaffolds on EPC and HUVEC proliferation, migration, displacement, alignment and tubular formation. Results demonstrated that scaffold morphology and VEGF gradients influenced cell behavior and tubular formation over a period of 14 days. The observed cellular response of EPCs and HUVECs to aligned or random fibers is in concord with our previous studies [102] and several others [100,104-108]. Nanoscopic topography is known to influence cell behavior and morphology via contact guidance [83,84,109,110]. We found EPCs and HUVECs responded to aligned scaffold morphology through elongation and organization parallel to the nanofibers, increase in proliferation rates, enhanced migration and tubular formation. Conversely, cells seeded on random fiber scaffolds exhibited a rounded morphology, lower proliferation rates and reduced migration. This difference in cellular response could be a result of gap size between fibers; the larger the gaps between fibers the less cell-cell interactions will occur, hindering cellular processes [85]. Aligned fibers presented cells with smaller gaps between fibers and increased surface area which allowed for EPCs and HUVECs to attach and spread more easily compared to random fibers.

Moreover, cells migrating up the VEGF concentration gradient, yielding to higher cell densities, and changes in cellular morphology, proliferation rates and tubular

formation. EPCs and HUVECs seeded on aligned fiber scaffolds modified with VEGF gradients developed capillaries parallel to the fibers. In contrast, cells seeded on random fiber scaffolds did not have apparent tubular growth. Studies have demonstrated migration of endothelial cells and sprouting vessels are dependent on VEGF gradient shape [100] and cell migration pathways [91,104,111,112]. Cells cultured on exponential gradients show increased chemotactic response and directed capillary growth [86,100] compared to linear gradients [87]. This cellular behavior towards gradients in combination with spatially constraining cells to follow specific paths, leads to an increase of coupling of cells via cell-cell interactions, which have been found to govern directionality. Cell migration has been often classified as a persistent random-walk and it is characterized by cell velocity and directional persistence (i.e. how long the cells tend to move linearly before changing direction). If directional persistence is high, groups of cells are more likely to move in a correlated manner. This collective migration is further enhanced by adhesive bonds between individual cells [113-115]. This could explain why the combination of aligned fiber scaffolds and VEGF gradients enhanced the formation of tube-like structures along the fibers. Conclusively, an increase in migration velocity of both EPCs and HUVECs resulted in higher cell densities and cellular elongation, which lead to higher cell-cell interactions and contact guidance.

Another aspect that we investigated was whether EPCs behaved differently from mature endothelial cells (i.e. HUVECs) when cultured on nanofibrous scaffolds modified with VEGF gradients. Results demonstrated EPCs had increased

elongation, proliferation, migration and tubular formation compared to HUVECs. Studies have found EPCs are more sensitive to VEGF than HUVECs, due their higher VEGF receptor (i.e. KDR) expression [95,96]. Thus, functions such as migration and proliferation are increased in EPCs compared to HUVECs, which would likely explain the differences in cellular behavior.

3.3 Conclusions

In this study, EPC and HUVEC behavior was influenced by nanotopographical changes and VEGF gradients. Cells cultured on aligned fiber scaffolds in combination with VEGF gradients displayed significant changes and differences in proliferation, cell displacement and morphology compared to cells seeded on random fiber constructs. Furthermore, HUVEC and EPC behavior was found to be similar however, EPCs seeded on aligned fibers constructs modified with VEGF gradients displayed longer tubules, higher migration velocities and increased elongation on compared to HUVECs. These results suggest the combinatory effect of electrospun aligned fiber scaffolds, VEGF gradients and EPCs could be a potential tissue engineering approach to direct vascular patterning.

CHAPTER 4: DEVELOP EPC-SEEDED VASCULAR SHEETS AND DETERMINE CAPILLARY FORMATION AND DIRECTIONALITY AS A FUNCTION OF CONSTRUCT PARAMETERS AND CO-ADMINISTRATION OF VEGF AND SDF-1A

In angiogenesis, activated endothelial cells degrade the basement membrane, followed by migration, proliferation, alignment, tubular formation, and branching creating anastomoses with neighboring vessels. Several cytokines are involved in post ischemic angiogenesis, among these are VEGF and stromal cell-derived factor-1 (SDF-1) [97,98]. Both SDF-1 α and VEGF have been considered crucial in EPC differentiation and migration [116]. Recent studies have shown SDF-1 α has the characteristic of binding specifically to only one type of receptor – CXCR4, resulting in a potent chemokine that plays a role in targeted biological processes [99] such as (a) migration, (b) chemotactic responses, (c) adhesion and (d) secretion of MMPs and angiopoietic factors (e.g., VEGF) (115). Furthermore, SDF-1 α has been found to increase the adhesion of CD34⁺ haematopoietic cells and endothelial progenitor cells to VCAM-1, ICAM-1, fibronectin, collagen and fibrinogen by activating cell surface integrins [117-120]. The contribution of SDF-1 α to cellular migration and adhesion has prompted investigators to study how SDF-1 α regulates the dynamics of angiogenesis and its potential therapeutic applications. SDF-1 α delivered locally as a free protein enhances EPC recruitment into ischemic tissue resulting in increased angiogenesis [119,121]. Moreover, SDF-1 α expression is up-regulated in ischemic tissues, suggesting an SDF-1 α gradient is established thus facilitating progenitor cell mobilization and homing [121]. Although studies utilizing SDF-1 α alone have yielded promising results [122], capillary formation has not been significant compared to combination

therapies. Studies have demonstrated the co-administration of angiogenic growth factors (i.e., VEGF, IGF, SDF-1 α and Ang-1) significantly increase the size and number of capillaries compared to the delivery of a single cytokine [31,123,124]. Sun et al. found that immobilizing a combination of VEGF, IGF, Ang-1 and SDF-1 α within a Dex/PEGDA hydrogel increased the size and number of vessels compared to the delivery of a single cytokine (e.g. SDF-1 α , VEGF). They also demonstrated this synergistic effect between biomolecules was only present when VEGF was delivered [123].

VEGF is a unique potent angiogenic factor that has a direct mitogenic actions specific to endothelial cells, and is responsible for neoangiogenesis [46,100,125]. Although several cytokines work in conjunction to entice neovascularization, VEGF and SDF-1 α have been found to be key mediators of interactions between angiogenic growth factors and chemokine-induced angiogenesis. There is extensive evidence that demonstrates SDF-1 α upregulates VEGF synthesis during angiogenic processes [116,124,126], thus regulating migration, survival, proliferation, and differentiation of endothelial cells.

The goal of this aim is to determine if the co-delivery of SDF-1 α and VEGF in combination with aligned electrospun scaffolds will provide the necessary cues to entice EPC attachment, proliferation and migration within nanofibrous scaffolds and promote vessel development and directionality.

4.1 Experimental Approach

4.1.1 EPC cell culture

EPCs (Promocell, Germany) were processed according to manufacturer specifications, followed by seeding on type I collagen-coated plates. Cells were expanded in Endothelial Progenitor Medium - Ready to use - (Promocell, Germany) and maintained at 37°C and 5% CO₂. At day 4 cells were passaged, seeded on type I collagen coated plates and cultured in EBM-2 (Lonza AG, Rockland, ME) supplemented with SingleQuotes growth factors. Passages 2-4 were utilized for all experiments.

4.1.2 Cell density and proliferation as a function of VEGF and SDF-1 α delivery

To assess cellular density and proliferation as a function VEGF and SDF-1 α the following groups were evaluated (A) Scaffold alone (B) Scaffold with VEGF gradient (C) Scaffold supplemented with SDF-1 α (D) Scaffold with VEGF gradient in combination with SDF-1 α supplementation and (E) Bare well supplemented with VEGF and SDF-1 α (Figure 4.1).

Scaffolds were synthesized as previously described [102]. Briefly, aligned scaffolds were adhered to the bottom of a 12- well plate utilizing fibrin glue and VEGF (10ng/ml) was physically entrapped on the right side of the scaffold for 20 min (Groups B and D). EPCs were then seeded (50,000 cells/scaffold) on the left side and allowed to attach for 20 min at 37 °C (All groups). Subsequently, groups C and D were supplemented with a 10ng/ml solution of SDF-1 α (Invitrogen,

Carlsbad, CA). All groups were cultured in EBM-2 and maintained at 37°C and 5% CO₂.

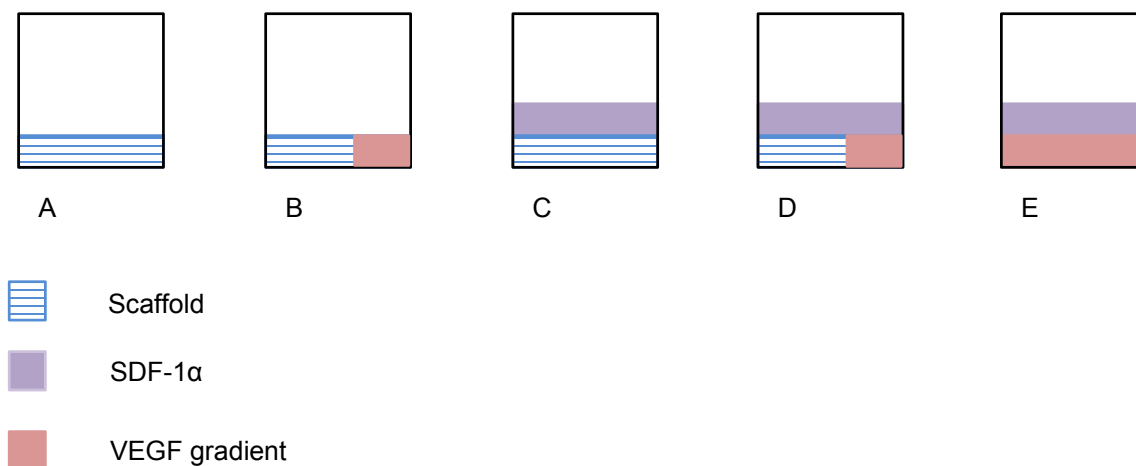


Figure 4.1: Diagrammatic representation of scaffold preparation and cell seeding. (A) Bare scaffold (B) VEGF gradient (C) SDF-1α (D) VEGF gradient/SDF-1α (E) Bare well supplemented with VEGF and SDF-1α.

At day 7 and 14 scaffolds were stained with CalceinAm (Invitrogen, Carlsbad, CA) to assess cell density per unit area. Subsequently, images of each scaffold were captured utilizing a Motic AE 20/21 microscope (VWR, Radnor, PA) with a 4X-10X objective. To ensure each scaffold was observed in its entirety 15 images were taken per construct. The number of images per scaffold was defined as a function of total scaffold area (2 cm²) and microscope field of view (diameter 0.26 cm). To measure cell density per unit area we uploaded the images to ImageJ (NIH, Bethesda, MD) and utilizing particle analysis we determined the number of cells.

EPC proliferation on aligned nanofiber scaffolds was evaluated utilizing a Click-iT® EdU Alexa Fluor® 488 Imaging Kit (Invitrogen, Carlsbad, CA). EPCs were incubated with 10µl of EdU for 48 hrs subsequent to seeding on nanofibrous

constructs. Cells were then fixed and permeabilized followed by the addition of the Click-iT® reaction cocktail. Images were taken to evaluate cell proliferation as a function VEGF and SDF-1 α delivery.

4.1.3 Capillary formation as a function of VEGF and SDF-1 α activity

At day 7 and 14 scaffolds were stained with CalceinAm (Invitrogen, Carlsbad, CA) to assess capillary number per unit area and length. Images of each group were captured utilizing a Motic AE 20/21 microscope (VWR, Radnor, PA) with a 4X-10X objective. To ensure each scaffold was observed in its entirety 15 images were taken per construct. The number of images per scaffold was defined as a function of total scaffold area (2 cm²) and microscope field of view (diameter 0.26 cm). To assess tubule length and number we identified and selected 5 cell clusters from where tubule growth was apparent and took measurements utilizing the measurement analysis tool from Image J. (NIH, Bethesda, MD). The total number of measurements was averaged to determine the overall tubular number and length per scaffold.

4.1.4 Cell Migration Evaluation

Prior to cell seeding onto scaffolds, EPCS were transfected with CellLight® Reagent *BacMam 2.0* (Baculovirus) following manufacturer's (Invitrogen, Carlsbad, CA) protocol. Subsequently, aligned scaffolds were placed on glass bottom dishes, Briefly, aligned scaffolds were adhered to the bottom of a 12- well plate utilizing fibrin glue and VEGF (10ng/ml) was physically entrapped on the right side of the scaffold for 20 min (Groups B and D). Transfected EPCs were then

seeded (50,000 cells/scaffold) on the left side and allowed to attach for 20 min @ 37 °C (All groups). Subsequently, groups C and D were supplemented with a 10ng/ml solution of SDF-1 α (Invitrogen, Carlsbad, CA). All groups were cultured in EBM-2 and maintained at 37°C and 5% CO₂.

Cells were incubated for 24 hrs before beginning time lapse imaging. Images were collected at 10min intervals for 24 hrs utilizing a Motic AE 20/21 microscope equipped with a stage incubator (OKO labs, Warner instruments, Hamden, CT). Cell migration was quantified manually by tracking the coordinates of 25 migrating cells using Motic Plus 2.0 software. Average migration velocity (V_{mig}) was calculated equation (a) The effective displacement (D_{migeff}) due to migration was calculated using equation (b). Additionally, using Image J plugin chemotaxis and migration tool (NIH- IBIDI, Bethesda, MD) cellular migration paths were delineated and animated by manually tracking 3 cells per group over 25 successional coordinates.

(a) Average migration velocity (V_m)

$$V_m = \frac{\sum_{i=1}^n \sqrt{(x_i - x_{i-1})^2 + (y_i - y_{i-1})^2}}{\sum_{i=1}^n t_i}$$

(b) Displacement due to migration

$$D_{mig.eff} = \sqrt{(x_{fin} - x_o)^2 + (y_{fin} - y_o)^2}$$

4.1.5 Cell morphology

Images of cells were taken at 10X magnification to evaluate circularity at day 7 and 14. Perimeter and area measurements were calculated utilizing ImageJ software. Circularity was evaluated using formula below (c).

(c) Circularity

$$C = \frac{4\pi A}{P^2}$$

A is the approximate area of the cell and P is the perimeter of the cell. Circularity is described as a measurement that ranges between 0 and 1, where $0 < C \leq 1$ (In an elongated shape $C \rightarrow 0$ and in a circle $C \rightarrow 1$).

4.1.6 Immunohistochemistry

Cells were fixed in 4% paraformaldehyde, permeabilized with 0.1% Triton X-100 in PBS and stained for endothelial cell markers and cytoskeleton structure. Primary antibodies utilized were: anti-von Willenbrand Factor (Sigma) and anti-vascular endothelial cadherin (Chemicon). Subsequently cells were viewed using a Motic AE 20/21 microscope equipped with Motic Plus 2.0 software. Fluorescence intensity was determined by using ImageJ (NIH, Bethesda, MD). Photos were converted to grey scale and in each picture five representative vessels were selected. The integrated density (product of area and mean grey value) was calculated for each selected area. Additionally, the mean average value was subtracted from five background intensities per image (mean grey value_{background}). The average fluorescence intensity (mean grey value_{vessels}) was calculated

(CFCT: integrated fluorescence density) whereby the total vessel area multiplied with mean grey value _{background} was subtracted from the average fluorescence intensity and summarized as the corrected total cell fluorescence.

4.2 Results and Discussion

In this study, we evaluated if the co-administration of VEGF gradients and SDF-1 α in combination with aligned nanofibrous scaffolds influenced EPC behavior and their angiogenic potential. Results demonstrated EPC behavior (adhesion, proliferation and migration) was highly dependent on the co-delivery of VEGF gradients and SDF-1 α . After a 14 day period, average circularity showed EPCs cultured with VEGF gradients and SDF-1 α had increased alignment and elongation (0.28 ± 0.012) compared to cells incubated with a single cytokine (VEGF or SDF-1 α) and to the control ($p < 0.05$) (Figure 4.2). There was no statistical significance when comparing single cytokine delivery, the average circularity for EPCs cultured on VEGF gradients was of 0.36 ± 0.11 and of 0.33 ± 0.07 when cultured with SDF-1 α .

Furthermore, the over a 24 hour period the rate of cell migration of EPCs was significantly higher ($0.49 \pm 0.083 \mu\text{m}/\text{min}$) when VEGF gradients and SDF-1 α were co-delivered ($p < 0.05$) (Figure 4.3). There were no significant differences in cell migration when EPCs were incubated with a single growth factor. The average velocity of EPCs cultured on VEGF gradients was $0.43 \pm 0.08 \mu\text{m}/\text{min}$, while for EPCs supplemented with SDF-1 only it was estimated at $0.46 \pm 0.069 \mu\text{m}/\text{min}$.

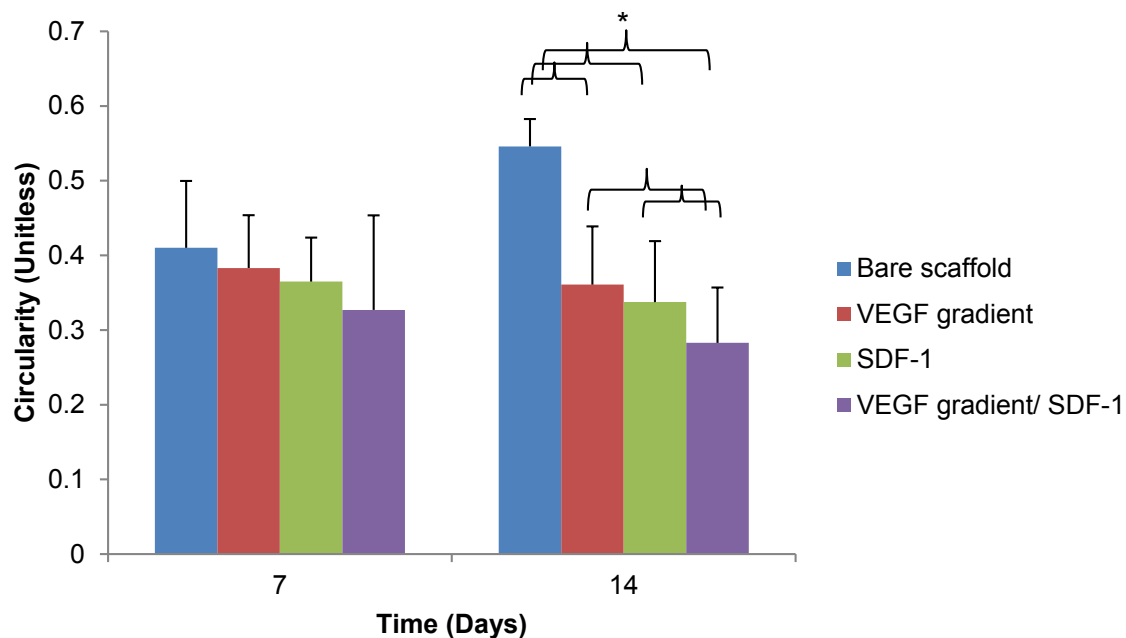


Figure 4.2: EPC response to the co-administration of VEGF gradients and SDF-1 α (Circularity) EPCs cultured with VEGF and SDF-1 α had reduced circularity compared to cells incubated with a single cytokine (VEGF or SDF-1 α) (* $p < 0.05$). There were no significant differences in groups incubated with a

This migratory behavior was not constant in all groups over the 24 hour period. Initially, at 8 hours there was a velocity peak in all groups, this was particularly evident in EPCs treated with SDF-1 α only ($0.53 \pm 0.07 \mu\text{m}/\text{min}$) ($p < 0.05$). However, this rate was not maintained; after 24 hours, migration velocity in SDF-1 α treated groups decreased significantly ($0.42 \pm 0.06 \mu\text{m}/\text{min}$) compared to groups cultured with VEGF gradients (alone or in combination with SDF-1 α).

Results of effective displacement evaluation (Figure 4.4) demonstrated EPCs travelled further when VEGF gradient was delivered alone or co-delivered with SDF-1 α ($2135 \pm 118 \mu\text{m}$) ($p < 0.05$). The effective migration distance was of $1727 \pm 132 \mu\text{m}$ when EPCs were incubated on VEGF gradients and $1947 \pm 134 \mu\text{m}$

when cells were supplemented with SDF-1 α . As mentioned in chapter 3, these results could indicate EPCs migrate in a linear fashion when seeded on aligned substrates, however cellular migration path tracking demonstrated cells in all groups migrated based on random walk (Figure 4.5). Results show the angle of cell path dispersion is smaller (12 °) when VEGF gradients and SDF-1 α are co-administered (Figure 4.5 C) compared to single cytokine delivery (Figure 4.5 A and B). Briefly, the random walk dispersion angle of was of 15° when EPCs were seeded on VEGF gradients and of 20° when supplemented with SDF-1 α .

In all groups, cell proliferation rate and cell density (Figures 4.6 and 4.7) were a function of co-administration of VEGF gradients and SDF-1 α . After a 14 days of incubation, the number of EPCs that migrated towards the right side of the scaffold was higher in groups treated with VEGF gradients and SDF-1 α (407 \pm 28 cells/mm²) compared to cells incubated with a single cytokine (VEGF or SDF-1 α) and to the control (p<0.05) (Figure 4.6).

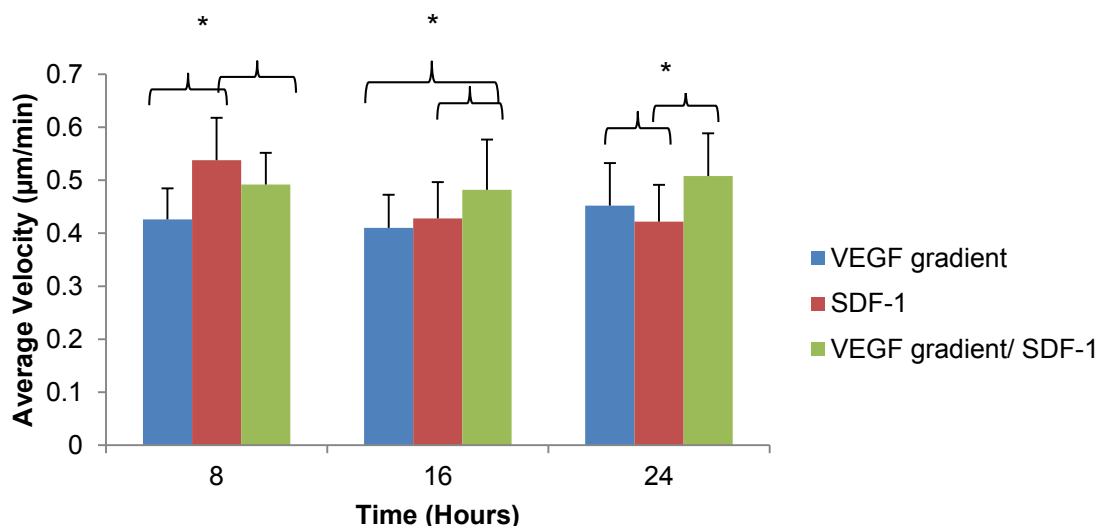


Figure 4.3: Migration velocity as a function of the co-delivery of VEGF gradients and SDF-1 α . Cell migration velocity was found to be higher when VEGF and SDF-1 α was co-administered compared to single cytokine delivery (* $p < 0.05$). Migration velocity was not constant in all groups over a 24 hour period, migration velocity of EPCs treated with SDF-1 α only increased significantly after 8 hours (* $p < 0.05$) compared to the other groups. After 16 hours migration velocity of SDF-1 α supplemented groups decreased significantly

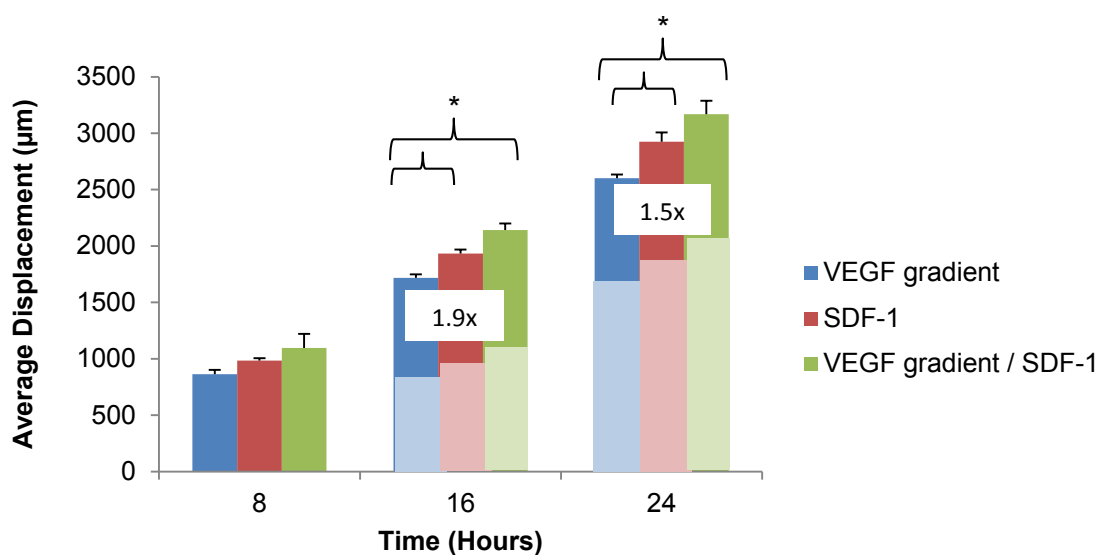


Figure 4.4: Effective displacement as a function of the co-delivery of VEGF gradients and SDF-1 α . EPC migration distance was found to be higher when VEGF gradient was delivered alone and when VEGF gradient was co-delivered with SDF-1 α (* $p < 0.05$). The increase in effective displacement was similar in all groups. After 16 hours there was a 1.9 fold increase and after 24 hours the fold increase was of 1.5.

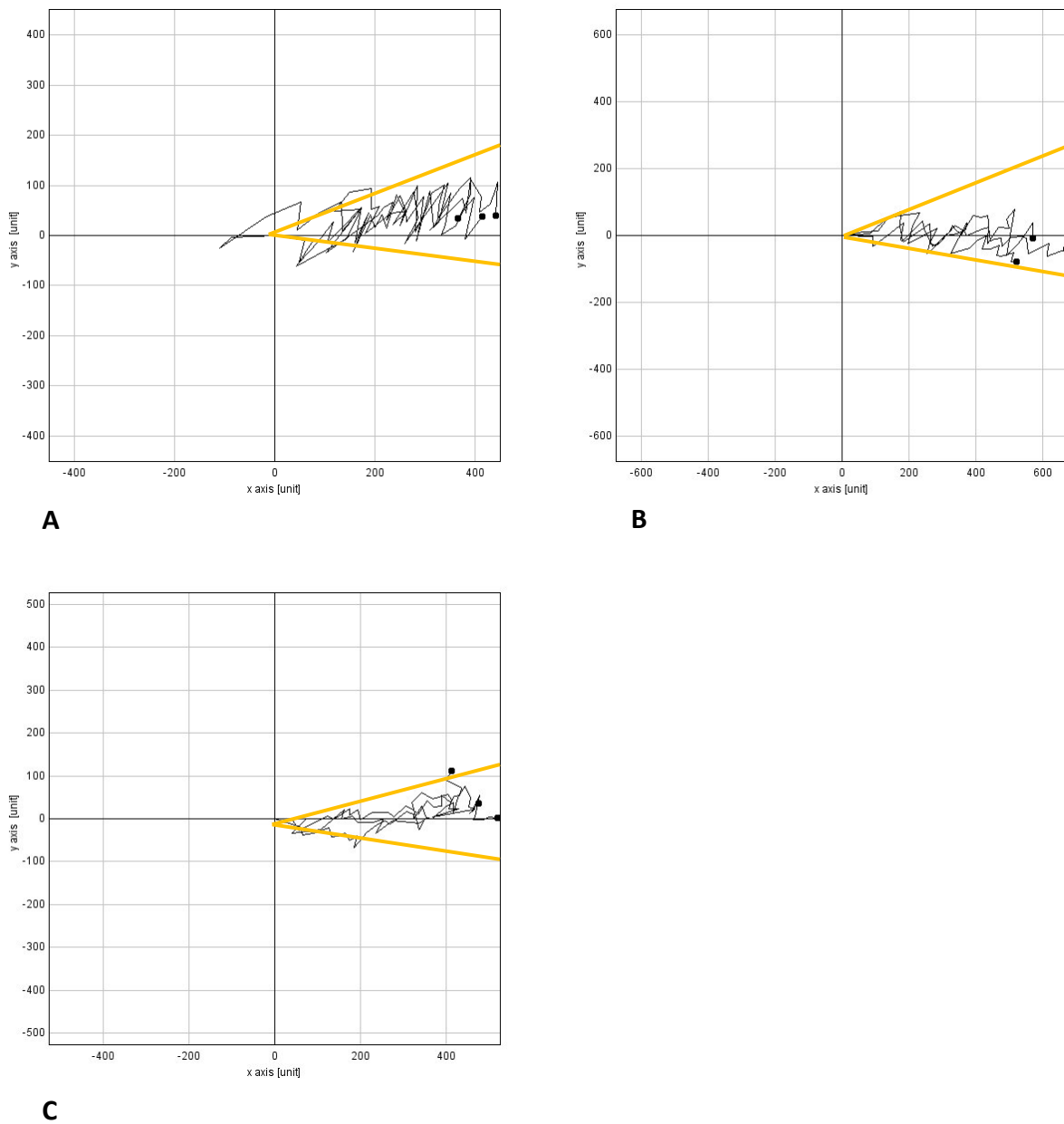


Figure 4.5: Cellular migration paths as a function of co-administration of VEGF gradients and SDF-1 α . EPC migration distance was found to be to be higher when VEGF and SDF-1 α was co-administered compared to single cytokine delivery ($*p < 0.05$), despite cell movement was in a random walk fashion. Yellow lines show the angle of cellular path dispersion of each group-- (A) VEGF gradient only -- 15 $^{\circ}$ (B) SDF-1 α only -- 20 $^{\circ}$ and (C) VEGF gradient and SDF-1 α --12 $^{\circ}$.

There was no statistical significance when comparing single cytokine delivery, the average number of EPCs per mm² was of 298 ± 13.4 cells/mm² when cultured on VEGF gradients only and of 326 ± 37 cells/mm² when supplemented with SDF-1 α only. Cell proliferation rates (Figure 4.7) of EPCs were increased in all groups compared to the control (Bare scaffold) ($p < 0.05$). EPC proliferation rates were not significantly different among groups treated with cytokines.

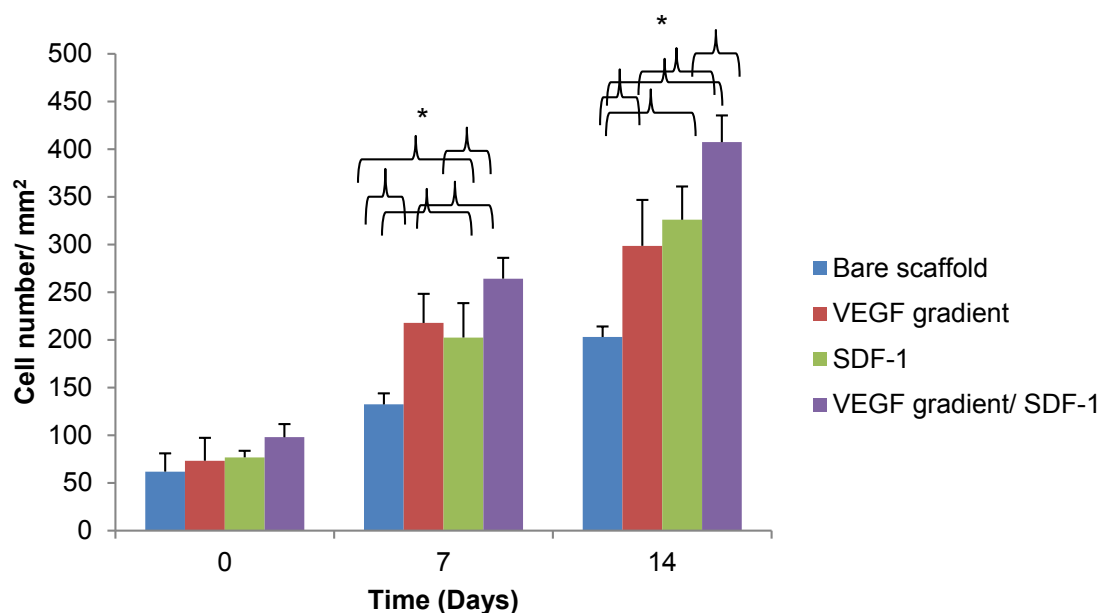


Figure 4.6: Cell density as a function of co-delivery of VEGF gradients and SDF-1 α . The number of EPCs that migrated towards the right side of the scaffold was higher in groups treated with VEGF gradients and SDF-1 α compared to cells incubated with a single cytokine (VEGF or SDF-1 α) ($*p < 0.05$).

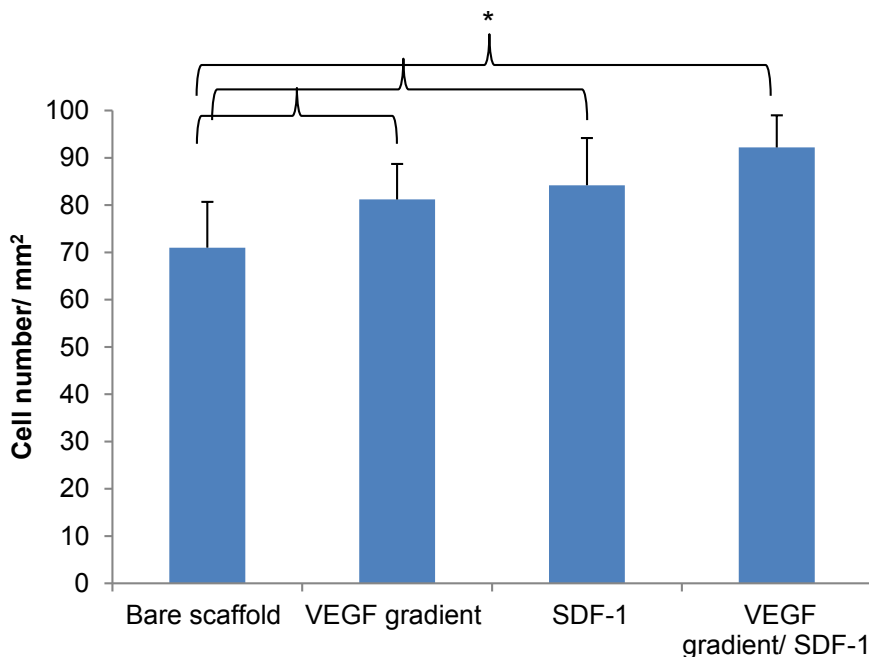
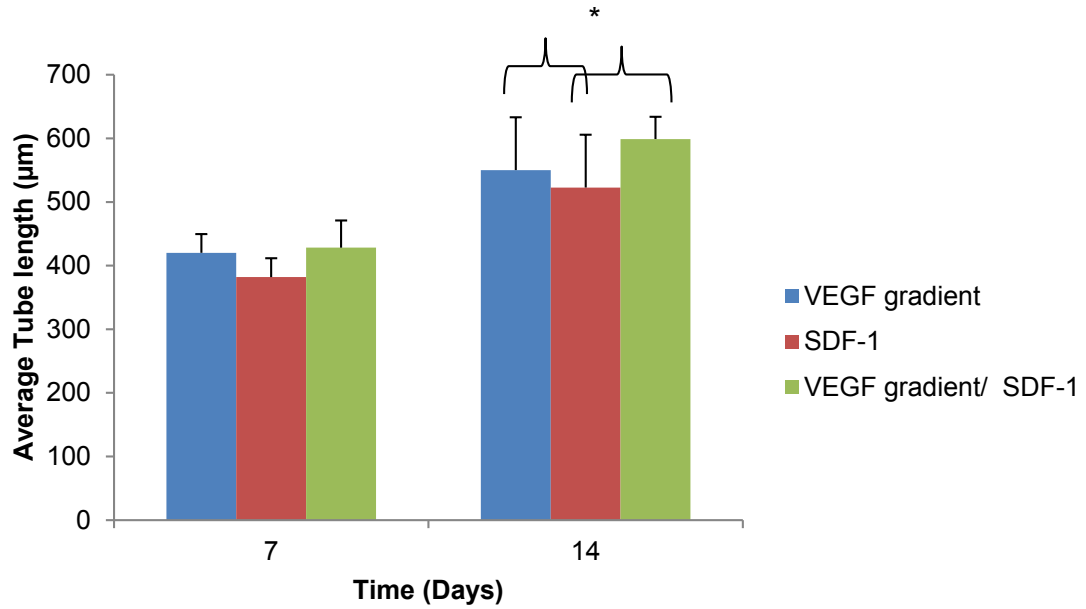
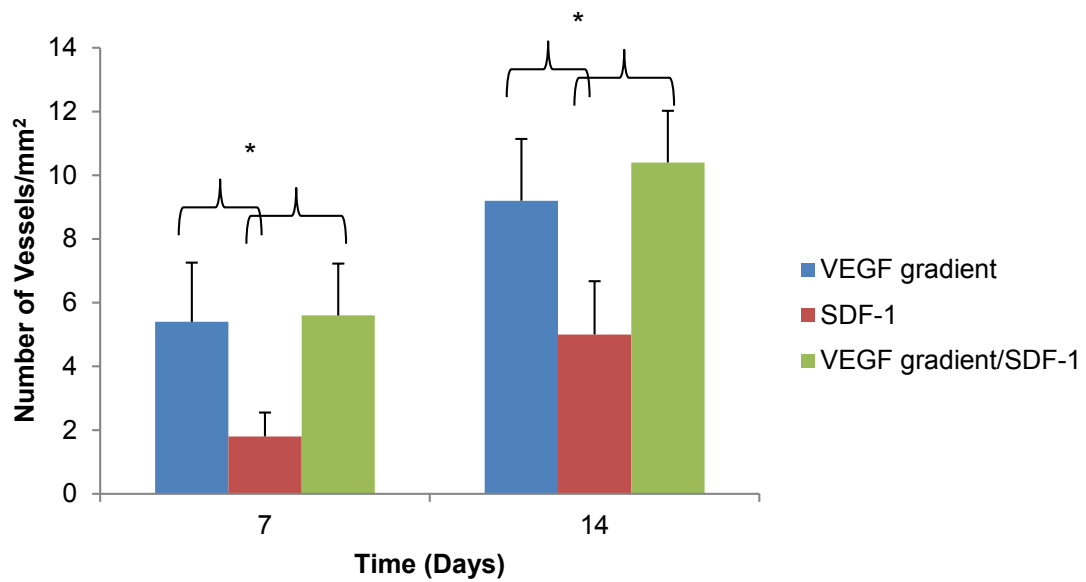


Figure 4.7: EPC proliferation as a function of co-administration of VEGF gradients and SDF-1 α . EPC proliferation was reduced when incubated without cytokine supplementation ($p > *0.05$). Proliferation rates were not statistically significant among groups treated with cytokines (single or co-delivered) ($*p < 0.05$).

Tubular growth was apparent among all groups evaluated (Figure 4.8). At day 7 tubules began to elongate and align themselves parallel to the nanofibers, however, at day 14 groups incubated with VEGF gradients alone ($550 \pm 84 \mu\text{m}$) or combined with SDF-1 α ($589 \pm 94 \mu\text{m}$) had increased elongation compared to groups treated with SDF-1 α alone ($522 \pm 55 \mu\text{m}$). Average number of tubules per unit area was significantly increased in groups treated with VEGF gradients alone ($7.3 \pm 1.9 \text{ vessels/mm}^2$) or combined with SDF-1 α ($8.0 \pm 1.6 \text{ vessels/mm}^2$) compared to groups treated with SDF-1 α alone ($7.3 \pm 1.9 \text{ vessels/mm}^2$). Immunohistochemistry showed vWF expression was similar among

all groups. Conversely, VE-Cadherin expression was higher when VEGF gradient was delivered alone and when VEGF gradient was co-delivered with SDF-1 α (* $p < 0.05$). (Figure 4.9).

**A****B**

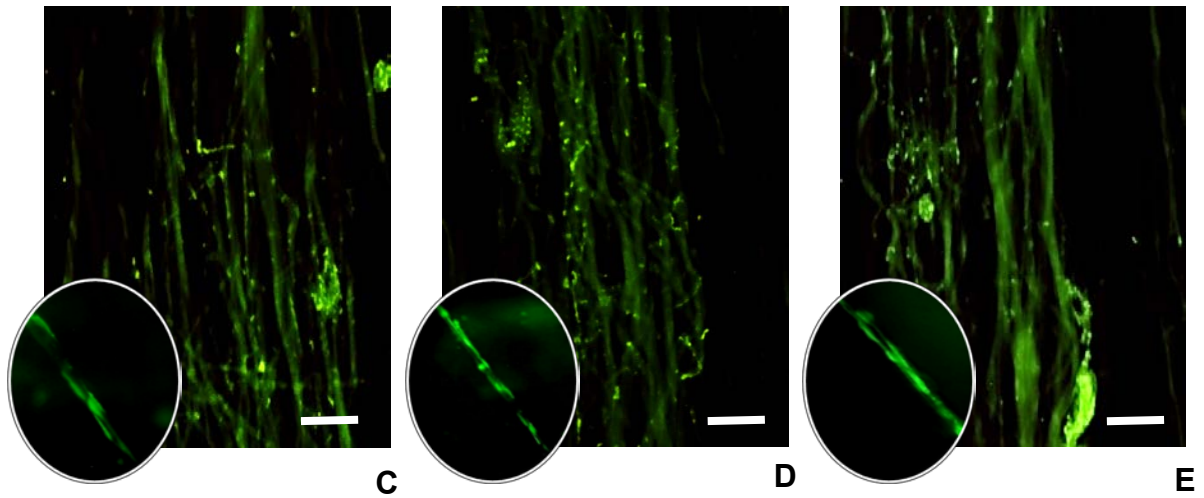


Figure 4.8: Tubular formation as a function of co-administration of VEGF gradients and SDF-1 α . Tubular development was similar in all groups. At day 14 significant differences in elongation were observed in groups incubated with VEGF gradients alone and with VEGF gradients co-delivered with SDF-1 α compared to these cultured with SDF-1 α alone (A) (* $p < 0.05$). Tubule number per unit area was significant in groups treated with VEGF gradients alone and with VEGF gradients co-delivered with SDF-1 α compared to groups cultured with SDF-1 α alone (B). Images show examples of tubules in each group (C) SDF-1 α (D) VEGF gradient (E) VEGF gradients and SDF-1 α . Bar = 20 μ m.

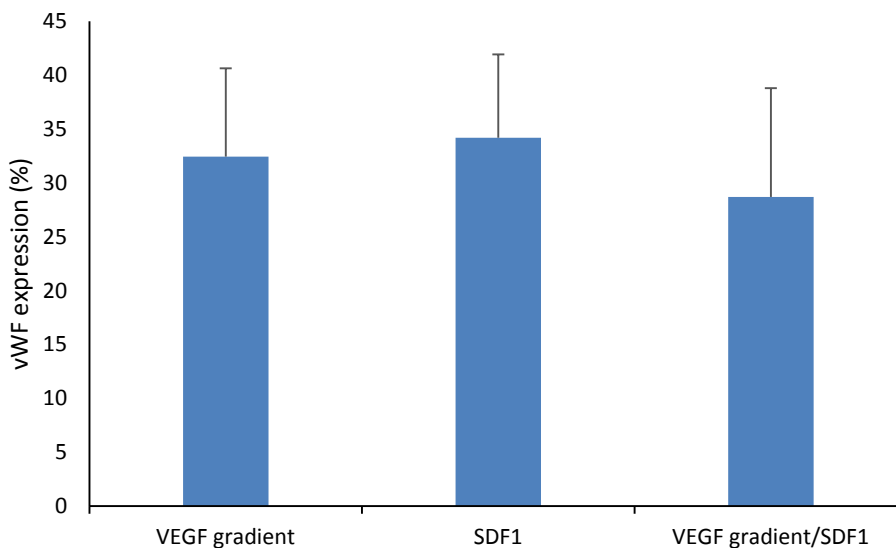
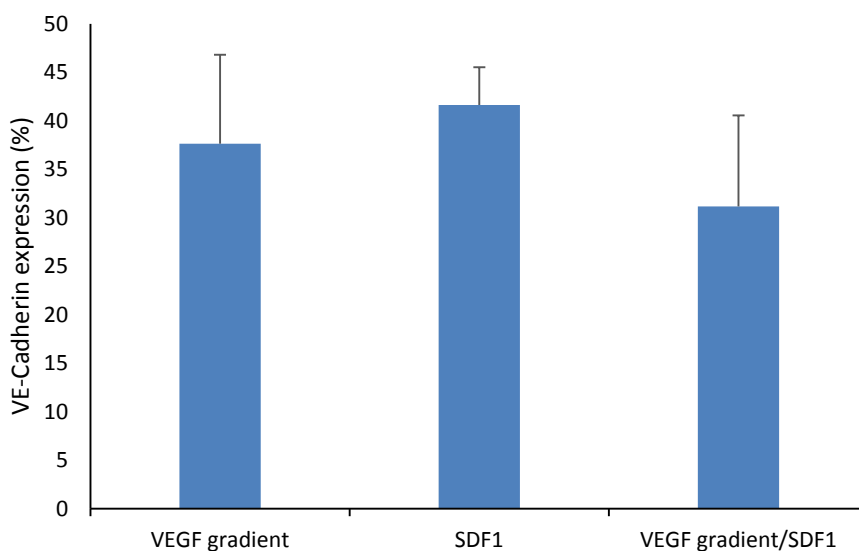
**A****B**

Figure 4.9: EPC and HUVEC immunohistochemistry evaluating expression of von Willebrand factor and VE-Cadherin as a function of VEGF gradients and scaffold topography. Tubular formation was observed only in cells cultured on aligned fiber scaffolds. The level of vWF (A) and VE-Cadherin (B) expression was found to be similar in tubules developed from HUVECs and EPCs at day 14. Corrected total cell fluorescence (CTCF) shows tubules are positive for vWF and VECadherin staining in both groups. There were no significant differences in staining intensity when comparing groups. CTCF is expressed and percentage of protein expression per group.

The co-delivery of SDF-1 α and VEGF gradients immobilized on nanofibrous scaffolds were investigated for their effects on EPC behavior and angiogenic potential. Because angiogenic growth factors are the main driving force of neoangiogenesis, tuning and directing these cytokines have become critically important [17,101,127,128]. Among these different cytokines, VEGF, which regulates the migration, survival, proliferation, and differentiation of EPCs [28,29,129,130] plays a key role in new blood vessel formation [44,47,68,101,130]. Additionally, SDF-1 α further increases EPC mobilization and stimulates angiogenesis [122,126,131]. Current applications have focused on the delivery of a single growth factor [121,122]; however, blood vessel development requires a finely tuned interplay between multiple signaling cues. This has lead studies to evaluate the synergistic effect of co-delivering two or more growth factors on vascular regeneration. The use of VEGF in combination with different cytokines, especially SDF-1 α has been shown to have potent chemotactic effects on EPCs [106], not only by orchestrating migratory responses, but also play a significant role in trafficking.

This study focused on the effects of SDF-1 α and VEGF gradients immobilized onto gelatin nanofibrous scaffolds on EPC proliferation, migration, displacement, alignment and tubular formation. Results demonstrated that the co-delivery of SDF-1 α and VEGF gradients significantly influenced cell behavior and tubular formation over a period of 14 days. The observed cellular response of EPCs was found to be in agreement with previous studies [116,119,124]. We found EPCs responded to the co-administration of VEGF and SDF-1 α through elongation and

organization parallel to the nanofibers, increase in cell densities, enhanced migration and tubular formation. Conversely, cells cultured with a single cytokine (VEGF or SDF-1 α) exhibited a rounded morphology, lower cell densities and reduced migration. This difference in cellular response could be a result of the additive effect SDF-1 has on VEGF. Studies have found that EPCs after being stimulated by SDF-1 secrete more angiogenic factors, especially VEGF [17,116,124,131]. This crosstalk between EPCs, SDF-1 α and VEGF contribute in cell adhesion, migration through vascular basement membranes and vasculogenesis.

Moreover, cells migrated successfully through the aligned fiber scaffolds however, cell densities, migration velocities, displacement and tubular length were found to be increased when SDF-1 α and VEGF gradients were combined. Studies have demonstrated migration of endothelial cells is dependent on cytokine type and delivery profiles [87,91,104,132]. Kucia et al found that due to their synergistic and additive effect, SDF-1 α and VEGF yield to higher EPC migration and homing in areas where both cytokines are being delivered [122,126]. This EPC response towards VEGF gradients and SDF-1 α delivery in combination with aligned fiber scaffolds could have led to an increase in cell migration velocities, thus enhancing cell-cell interactions, increasing cell densities and effective displacement. As mentioned in chapter 3, cell migration is described as a persistent random-walk and it is characterized by how cells tend to move linearly before changing direction. When groups were cultured either with VEGF gradients alone or with SDF-1 α and VEGF gradients, directional persistence was high leading to increased cell-cell

interactions. VE-Cadherin (CD144) staining further confirmed the increase in cell-cell interactions in all groups. Studies have shown positive VE-Cadherin staining can be correlated to the presence of cell-cell junctions. VE- Cadherin is an adhesion molecule that helps maintain and control endothelial cell contacts, in addition to modulating VEGF functions [100,133,134]. This could explain why there was enhanced formation of tube-like structures along the fibers. Conclusively, an increase in migration velocity of EPCs as a result of the co-delivery of SDF-1 α and VEGF gradients yielded in higher cell densities and cellular elongation, which lead to higher cell-cell interactions and contact guidance.

4.3 Conclusions

In this study, EPC was influenced by the co-delivery of SDF-1 α and VEGF gradients. Cells cultured with SDF-1 α and VEGF gradients displayed significant differences in cell migration velocities, displacement and morphology compared to cells incubated with a single cytokine. These results suggest the combinatory effect of electrospun aligned fiber scaffolds, SDF-1 α , VEGF gradients and EPCs could be utilized to direct neoangiogenesis and vascular patterning.

CHAPTER 5: CONCLUSIONS AND FUTURE DIRECTIONS

In this study, we described a novel electrospinning approach to fabricate VEGF-loaded nanofibrous scaffolds with patterned fiber architecture and assessed their ability to direct cellular behavior. Electrospun gelatin scaffolds with variable fiber orientation, dimensions and rate of degradation were produced by controlling the fabrication parameters (i.e. needle-to-collector distance, electric field, electrode polarity, glutaraldehyde crosslinking, etc.). To determine the angiogenic potential of the nanofibrous scaffolds we evaluated parameters such as cell proliferation, migration velocity, effective displacement, etc. Results from this assessment helped us define the proper balance between physical (i.e. electrospun scaffold fiber architecture) and chemical (i.e. VEGF) cues in order to achieve optimum EPC or HUVEC attachment, proliferation and migration within electrospun scaffolds. Results demonstrated, HUVEC and EPC behavior was influenced by nanotopographical changes and VEGF gradients. Cells cultured on aligned fiber scaffolds in combination with VEGF gradients displayed significant changes and differences in proliferation, cell displacement and morphology compared to cells seeded on random fiber constructs. Furthermore, we found EPCs seeded on aligned fibers constructs modified with VEGF gradients displayed longer tubules, higher migration velocities and increased elongation on compared to HUVECs. Although results from the previous study were promising we decided to evaluate if the combination of EPCs seeded on aligned nanofibrous scaffolds and the co-administration of VEGF gradients and SDF-1 α would provide the necessary cues to entice EPC attachment, proliferation and migration within nanofibrous scaffolds and promote vessel development and directionality. Studies have shown several

cytokines work in conjunction to entice neovascularization, VEGF and SDF-1 α have been found to be key mediators of interactions between angiogenic growth factors and chemokine-induced angiogenesis. There is extensive evidence that demonstrates SDF-1 α upregulates VEGF synthesis during angiogenic processes [116,124,126], thus regulating migration, survival, proliferation, and differentiation of endothelial cells. Results demonstrated EPCs were influenced by the co-delivery of SDF-1 α and VEGF gradients. Cells cultured with SDF-1 α and VEGF gradients displayed significant differences in cell migration velocities, displacement and morphology compared to cells incubated with a single cytokine.

These results suggest the combinatory effect of electrospun aligned fiber scaffolds, VEGF gradients, SDF-1 α and EPCs could be a potential tissue engineering approach to direct vascular patterning. This is particularly important since the formation of new vessels in response to pro-angiogenic growth factor stimulation or matrix rearrangement is associated with the activation of quiescent endothelial cells which in part involves changes in cell morphology (i.e. elongation) and the formation of new contacts with the underlying substrate [39]. To further understand this synergistic effect between aligned nanofibrous scaffold, VEGF gradients, SDF-1 α and EPCs in vivo evaluations were initially planned, however, we were not able to complete animal studies because of funding issues.

This study can be further expanded by varying the different parameters utilized and evaluating them as a function of angiogenic development. For example, different VEGF and SDF-1 α patterns can be immobilized on the nanofibrous

scaffolds, cytokine immobilization methods (physical or covalent) can be tailored to finely tuned biomolecule release and growth factor concentration can be increased or decreased. This could provide us with additional understanding angiogenic processes and help us develop tailored approaches for specific pathophysiologies.

REFERENCES

1. Loscalzo J, Libby P, Braunwald E. Chapter 217. Basic biology of the cardiovascular system. In: Fauci AS, Braunwald E, Kasper DL, Hauser SL, Longo DL, Jameson JL, et al, editors. Harrison's Principles of Internal Medicine. 17th ed.
2. Creager MA, Loscalzo J. Chapter 243. Vascular diseases of the extremities. In: Fauci AS, Braunwald E, Kasper DL, Hauser SL, Longo DL, Jameson JL, et al, editors. Harrison's Principles of Internal Medicine. 17th ed.
3. Libby P. Chapter 235. The pathogenesis, prevention, and treatment of atherosclerosis. In: Fauci AS, Braunwald E, Kasper DL, Hauser SL, Longo DL, Jameson JL, Loscalzo J, editor. . Harrison's Principles of Internal Medicine ed.
4. Brevetti G, Giugliano G, Brevetti L, Hiatt WR. Inflammation in Peripheral Artery Disease [Contemporary Reviews in Cardiovascular Medicine] *Circulation* 2010;122:1862-1875.
5. Syed IS, Sanborn TA, Rosengart TK. Therapeutic angiogenesis: a biologic bypass *Cardiology* 2004;101:131-143.
6. Zhang G, Suggs LJ. Matrices and scaffolds for drug delivery in vascular tissue engineering *Adv Drug Deliv Rev* 2007;59:360-373.
7. Phelps EA, Garcia AJ. Update on therapeutic vascularization strategies *Regen Med* 2009;4:65-80.
8. Jain RK. Molecular regulation of vessel maturation *Nat Med* 2003;9:685-693.
9. Zisch AH, Lutolf MP, Hubbell JA. Biopolymeric delivery matrices for angiogenic growth factors. *Cardiovascular Pathology* 2003;12:295-310.
10. Yancopoulos GD, Davis S, Gale NW, Rudge JS, Wiegand SJ, Holash J. Vascular-specific growth factors and blood vessel formation *Nature* 2000;407:242-248.
11. Freedman SB, Isner JM. Therapeutic angiogenesis for ischemic cardiovascular disease *J Mol Cell Cardiol* 2001;33:379-393.
12. Carmeliet P. Mechanisms of angiogenesis and arteriogenesis *Nat Med* 2000;6:389-395.
13. Buschmann I, Schaper W. Arteriogenesis versus angiogenesis: two mechanisms of vessel growth *News Physiol Sci* 1999;14:121-125.

14. Semenza GL. Vasculogenesis, angiogenesis, and arteriogenesis: mechanisms of blood vessel formation and remodeling *J Cell Biochem* 2007;102:840-847.
15. Heissig B, Hattori K, Friedrich M, Rafii S, Werb Z. Angiogenesis: vascular remodeling of the extracellular matrix involves metalloproteinases *Curr Opin Hematol* 2003;10:136-141.
16. Sato TN. Vascular development: molecular logic for defining arteries and veins *Curr Opin Hematol* 2003;10:131-135.
17. Pandya NM, Dhalla NS, Santani DD. Angiogenesis--a new target for future therapy *Vascul Pharmacol* 2006;44:265-274.
18. Cao Y, Hong A, Schulten H, Post MJ. Update on therapeutic neovascularization *Cardiovasc Res* 2005;65:639-648.
19. Cao R, Brakenhielm E, Pawliuk R, Wariaro D, Post MJ, Wahlberg E, Leboulch P, Cao Y. Angiogenic synergism, vascular stability and improvement of hind-limb ischemia by a combination of PDGF-BB and FGF-2 *Nat Med* 2003;9:604-613.
20. Pepper MS, Mandriota SJ, Jeltsch M, Kumar V, Alitalo K. Vascular endothelial growth factor (VEGF)-C synergizes with basic fibroblast growth factor and VEGF in the induction of angiogenesis in vitro and alters endothelial cell extracellular proteolytic activity. *J Cell Physiol* 1998;177:439-452.
21. Hattori K, Dias S, Heissig B, Hackett NR, Lyden D, Tateno M, Hicklin DJ, Zhu Z, Witte L, Crystal RG, Moore MAS, Rafii S. Vascular endothelial growth factor and angiopoietin-1 stimulate postnatal hematopoiesis by recruitment of vasculogenic and hematopoietic stem cells. *The Journal of Experimental Medicine* 2001;193:1005-1014.
22. Yla-Herttuala S, Alitalo K. Gene transfer as a tool to induce therapeutic vascular growth *Nat Med* 2003;9:694-701.
23. Freedman SB, Isner JM. Therapeutic angiogenesis for coronary artery disease *Ann Intern Med* 2002;136:54-71.
24. Lawall H, Bramlage P, Amann B. Stem cell and progenitor cell therapy in peripheral artery disease. A critical appraisal *Thromb Haemost* 2010;103:696-709.
25. Aicher A. Mobilizing endothelial progenitor cells *Hypertension* 2005;45:321-325.

26. Minamino K, Adachi Y, Okigaki M, Ito H, Togawa Y, Fujita K, Tomita M, Suzuki Y, Zhang Y, Iwasaki M, Nakano K, Koike Y, Matsubara H, Iwasaka T, Matsumura M, Ikehara S. Macrophage colony-stimulating factor (M-CSF), as well as granulocyte colony-stimulating factor (G-CSF), accelerates neovascularization *Stem Cells* 2005;23:347-354.
27. Gonçalves L. Angiogenic growth factors potential new treatment for acute myocardial infarction? *Cardiovasc Res* 2000;45:294-302.
28. Losordo DW, Dimmeler S. Therapeutic angiogenesis and vasculogenesis for ischemic disease. Part I: angiogenic cytokines *Circulation* 2004;109:2487-2491.
29. Losordo DW, Dimmeler S. Therapeutic angiogenesis and vasculogenesis for ischemic disease: part II: cell-based therapies *Circulation* 2004;109:2692-2697.
30. Spadaccio C, Chello M, Trombetta M, Rainer A, Toyoda Y, Genovese JA. Drug releasing systems in cardiovascular tissue engineering *J Cell Mol Med* 2009;13:422-439.
31. Chen FM, Zhang M, Wu ZF. Toward delivery of multiple growth factors in tissue engineering *Biomaterials* 2010;31:6279-6308.
32. Williams DF. To engineer is to create: the link between engineering and regeneration *Trends Biotechnol* 2006;24:4-8.
33. Vasita R, Katti DS. Growth factor-delivery systems for tissue engineering: a materials perspective *Expert Rev Med Devices* 2006;3:29-47.
34. Kobsa S, Saltzman WM. Bioengineering approaches to controlled protein delivery *Pediatr Res* 2008;63:513-519.
35. Tabata Y. Significance of release technology in tissue engineering *Drug Discov Today* 2005;10:1639-1646.
36. Tabata Y. Tissue regeneration based on growth factor release *Tissue Eng* 2003;9 Suppl 1:S5-15.
37. Guldberg RE. Spatiotemporal delivery strategies for promoting musculoskeletal tissue regeneration *Journal of bone and mineral research* 2009;24:1507-1511.
38. Chen RR, Silva EA, Yuen WW, Mooney DJ. Spatio-temporal VEGF and PDGF delivery patterns blood vessel formation and maturation *Pharm Res* 2007;24:258-264.

39. Tabata Y. Biomaterial technology for tissue engineering applications J R Soc Interface 2009;6 Suppl 3:S311-24.
40. Biondi M, Ungaro F, Quaglia F, Netti PA. Controlled drug delivery in tissue engineering Adv Drug Deliv Rev 2008;60:229-242.
41. Sokolsky-Papkov M, Agashi K, Olaye A, Shakesheff K, Domb AJ. Polymer carriers for drug delivery in tissue engineering Adv Drug Deliv Rev 2007;59:187-206.
42. Mikos AG, Herring SW, Ochareon P, Elisseeff J, Lu HH, Kandel R, Schoen FJ, Toner M, Mooney D, Atala A, Van Dyke ME, Kaplan D, Vunjak-Novakovic G. Engineering complex tissues. Tissue Eng 2006;12:3307-3339.
43. Ferrara N, Alitalo K. Clinical applications of angiogenic growth factors and their inhibitors Nat Med 1999;5:1359-1364.
44. Carmeliet P, Collen D. Role of vascular endothelial growth factor and vascular endothelial growth factor receptors in vascular development Curr Top Microbiol Immunol 1999;237:133-158.
45. Risau W. Angiogenic growth factors Prog Growth Factor Res 1990;2:71-79.
46. Neufeld G, Cohen T, Gengrinovitch S, Poltorak Z. Vascular endothelial growth factor (VEGF) and its receptors. The FASEB Journal 1999;13:9-22.
47. Carmeliet P. Manipulating angiogenesis in medicine J Intern Med 2004;255:538-561.
48. Lovett M, Lee K, Edwards A, Kaplan DL. Vascularization strategies for tissue engineering Tissue Eng Part B Rev 2009;15:353-370.
49. Royce PM, Kato T, Ohsaki K, Miura A. The enhancement of cellular infiltration and vascularisation of a collagenous dermal implant in the rat by platelet-derived growth factor BB J Dermatol Sci 1995;10:42-52.
50. Friess W. Collagen--biomaterial for drug delivery Eur J Pharm Biopharm 1998;45:113-136.
51. Tabata Y, Ikada Y. Vascularization effect of basic fibroblast growth factor released from gelatin hydrogels with different biodegradabilities Biomaterials 1999;20:2169-2175.
52. Kaigler D, Wang Z, Horger K, Mooney DJ, Krebsbach PH. VEGF scaffolds enhance angiogenesis and bone regeneration in irradiated osseous defects J Bone Miner Res 2006;21:735-744.

53. Zisch AH, Schenk U, Schense JC, Sakiyama-Elbert SE, Hubbell JA. Covalently conjugated VEGF–fibrin matrices for endothelialization J Controlled Release 2001;72:101-113.
54. Lin H, Chen B, Sun W, Zhao W, Zhao Y, Dai J. The effect of collagen-targeting platelet-derived growth factor on cellularization and vascularization of collagen scaffolds Biomaterials 2006;27:5708-5714.
55. Zhao W, Han Q, Lin H, Gao Y, Sun W, Zhao Y, Wang B, Chen B, Xiao Z, Dai J. Improved neovascularization and wound repair by targeting human basic fibroblast growth factor (bFGF) to fibrin J Mol Med 2008;86:1127-1138.
56. Steffens GC, Yao C, Prevel P, Markowicz M, Schenck P, Noah EM, Pallua N. Modulation of angiogenic potential of collagen matrices by covalent incorporation of heparin and loading with vascular endothelial growth factor Tissue Eng 2004;10:1502-1509.
57. Yao C, Prevel P, Koch S, Schenck P, Noah EM, Pallua N, Steffens G. Modification of collagen matrices for enhancing angiogenesis Cells Tissues Organs 2004;178:189-196.
58. Markowicz M, Heitland A, Steffens GC, Pallua N. Effects of modified collagen matrices on human umbilical vein endothelial cells Int J Artif Organs 2005;28:1251-1258.
59. Perets A, Baruch Y, Weisbuch F, Shoshany G, Neufeld G, Cohen S. Enhancing the vascularization of three-dimensional porous alginate scaffolds by incorporating controlled release basic fibroblast growth factor microspheres J Biomed Mater Res A 2003;65:489-497.
60. Richardson TP, Peters MC, Ennett AB, Mooney DJ. Polymeric system for dual growth factor delivery. Nat Biotechnol 2001;19:1029-1034.
61. Nillesen ST, Geutjes PJ, Wismans R, Schalkwijk J, Daamen WF, van Kuppevelt TH. Increased angiogenesis and blood vessel maturation in acellular collagen-heparin scaffolds containing both FGF2 and VEGF Biomaterials 2007;28:1123-1131.
62. Peattie RA, Rieke ER, Hewett EM, Fisher RJ, Shu XZ, Prestwich GD. Dual growth factor-induced angiogenesis in vivo using hyaluronan hydrogel implants Biomaterials 2006;27:1868-1875.
63. Dogan AK, Gumusderelioglu M, Aksoz E. Controlled release of EGF and bFGF from dextran hydrogels in vitro and in vivo J Biomed Mater Res B Appl Biomater 2005;74:504-510.

64. Riley CM, Fuegy PW, Firpo MA, Shu XZ, Prestwich GD, Peattie RA. Stimulation of in vivo angiogenesis using dual growth factor-loaded crosslinked glycosaminoglycan hydrogels *Biomaterials* 2006;27:5935-5943.
65. Dor Y. Making vascular networks in the adult: branching morphogenesis without a roadmap *Trends Cell Biol* 2003;13:131-136.
66. Campbell PG, Miller ED, Fisher GW, Walker LM, Weiss LE. Engineered spatial patterns of FGF-2 immobilized on fibrin direct cell organization *Biomaterials* 2005;26:6762-6770.
67. Luong LN, Hong SI, Patel RJ, Outslay ME, Kohn DH. Spatial control of protein within biomimetically nucleated mineral *Biomaterials* 2006;27:1175-1186.
68. Rieux AD, Ucakar B, Mupendwa BP, Colau D, Feron O, Carmeliet P, Preat V. 3D systems delivering VEGF to promote angiogenesis for tissue engineering *J Control Release* 2010.
69. Peirce SM, Price RJ, Skalak TC. Spatial and temporal control of angiogenesis and arterialization using focal applications of VEGF164 and Ang-1 *Am J Physiol Heart Circ Physiol* 2004;286:H918-25.
70. Quaglia F. Bioinspired tissue engineering: the great promise of protein delivery technologies *Int J Pharm* 2008;364:281-297.
71. Miller ED, Fisher GW, Weiss LE, Walker LM, Campbell PG. Dose-dependent cell growth in response to concentration modulated patterns of FGF-2 printed on fibrin *Biomaterials* 2006;27:2213-2221.
72. Mironov V, Kasyanov V, Markwald RR. Nanotechnology in vascular tissue engineering: from nanoscaffolding towards rapid vessel biofabrication *Trends Biotechnol* 2008;26:338-344.
73. Laham RJ, Garcia L, Baim DS, Post M, Simons M. Therapeutic angiogenesis using basic fibroblast growth factor and vascular endothelial growth factor using various delivery strategies *Curr Interv Cardiol Rep* 1999;1:228-233.
74. Layman H, Sacasa M, Murphy AE, Murphy AM, Pham SM, Andreopoulos FM. Co-delivery of FGF-2 and G-CSF from gelatin-based hydrogels as angiogenic therapy in a murine critical limb ischemic model *Acta Biomater* 2009;5:230-239.
75. Silva EA, Mooney DJ. Spatiotemporal control of vascular endothelial growth factor delivery from injectable hydrogels enhances angiogenesis *Journal of Thrombosis and Haemostasis* 2007;5:590-598.

76. DeLong SA, Moon JJ, West JL. Covalently immobilized gradients of bFGF on hydrogel scaffolds for directed cell migration. *Biomaterials* 2005;26:3227-3234.
77. Hockel M, Schlenger K, Doctrow S, Kissel T, Vaupel P. Therapeutic angiogenesis *Arch Surg* 1993;128:423-429.
78. Liu Y, Ji Y, Ghosh K, Clark RA, Huang L, Rafailovich MH. Effects of fiber orientation and diameter on the behavior of human dermal fibroblasts on electrospun PMMA scaffolds. *J Biomed Mater Res A* 2009;90:1092-1106.
79. Qian T, Wang Y. Micro/nano-fabrication technologies for cell biology *Med Biol Eng Comput* 2010.
80. Bhardwaj N, Kundu SC. Electrospinning: a fascinating fiber fabrication technique. *Biotechnol Adv* 2010;28:325-347.
81. Lowery JL, Datta N, Rutledge GC. Effect of fiber diameter, pore size and seeding method on growth of human dermal fibroblasts in electrospun poly(epsilon-caprolactone) fibrous mats. *Biomaterials* 2010;31:491-504.
82. DeLong SA, Moon JJ, West JL. Covalently immobilized gradients of bFGF on hydrogel scaffolds for directed cell migration. *Biomaterials* 2005;26:3227-3234.
83. Sarkar S, Dadhania M, Rourke P, Desai TA, Wong JY. Vascular tissue engineering: microtextured scaffold templates to control organization of vascular smooth muscle cells and extracellular matrix. *Acta Biomater* 2005;1:93-100.
84. Bettinger CJ, Zhang Z, Gerecht S, Borenstein JT, Langer R. Enhancement of in vitro capillary tube formation by substrate nanotopography. *Adv Mater* 2008;20:99-103.
85. Heath DE, Lannutti JJ, Cooper SL. Electrospun scaffold topography affects endothelial cell proliferation, metabolic activity, and morphology *Journal of Biomedical Materials Research Part A* 2010.
86. Helm CL, Fleury ME, Zisch AH, Boschetti F, Swartz MA. Synergy between interstitial flow and VEGF directs capillary morphogenesis in vitro through a gradient amplification mechanism. *Proc Natl Acad Sci U S A* 2005;102:15779-15784.
87. Barkefors I, Le Jan S, Jakobsson L, Hejll E, Carlson G, Johansson H, Jarvius J, Park JW, Li Jeon N, Kreuger J. Endothelial cell migration in stable gradients of vascular endothelial growth factor A and fibroblast growth factor 2: effects on chemotaxis and chemokinesis. *J Biol Chem* 2008;283:13905-13912.

88. Finkenzeller G, Torio-Padron N, Momeni A, Mehlhorn AT, Stark GB. In vitro angiogenesis properties of endothelial progenitor cells: a promising tool for vascularization of ex vivo engineered tissues. *Tissue Eng* 2007;13:1413-1420.
89. Finkenzeller G, Graner S, Kirkpatrick CJ, Fuchs S, Stark GB. Impaired in vivo vasculogenic potential of endothelial progenitor cells in comparison to human umbilical vein endothelial cells in a spheroid-based implantation model. *Cell Prolif* 2009;42:498-505.
90. Mukai N, Akahori T, Komaki M, Li Q, Kanayasu-Toyoda T, Ishii-Watabe A, Kobayashi A, Yamaguchi T, Abe M, Amagasa T, Morita I. A comparison of the tube forming potentials of early and late endothelial progenitor cells. *Exp Cell Res* 2008;314:430-440.
91. Miller ED, Li K, Kanade T, Weiss LE, Walker LM, Campbell PG. Spatially directed guidance of stem cell population migration by immobilized patterns of growth factors. *Biomaterials* 2011;32:2775-2785.
92. des Rieux A, Ucakar B, Mupendwa BP, Colau D, Feron O, Carmeliet P, Preat V. 3D systems delivering VEGF to promote angiogenesis for tissue engineering. *J Control Release* 2011;150:272-278.
93. Nisbet DR, Forsythe JS, Shen W, Finkelstein DI, Horne MK. Review paper: a review of the cellular response on electrospun nanofibers for tissue engineering. *J Biomater Appl* 2009;24:7-29.
94. Brandl F, Sommer F, Goepferich A. Rational design of hydrogels for tissue engineering: impact of physical factors on cell behavior. *Biomaterials* 2007;28:134-146.
95. Bompais H, Chagraoui J, Canron X, Crisan M, Liu XH, Anjo A, Tolla-Le Port C, Leboeuf M, Charbord P, Bikfalvi A, Uzan G. Human endothelial cells derived from circulating progenitors display specific functional properties compared with mature vessel wall endothelial cells. *Blood* 2004;103:2577-2584.
96. Smadja DM, Bieche I, Helley D, Laurendeau I, Simonin G, Muller L, Aiach M, Gaussem P. Increased VEGFR2 expression during human late endothelial progenitor cells expansion enhances in vitro angiogenesis with up-regulation of integrin alpha(6). *J Cell Mol Med* 2007;11:1149-1161.
97. Murphy PM. Chemokines and the molecular basis of cancer metastasis. *N Engl J Med* 2001;345:833-835.
98. Unoki N, Murakami T, Nishijima K, Ogino K, van Rooijen N, Yoshimura N. SDF-1/CXCR4 contributes to the activation of tip cells and microglia in retinal angiogenesis. *Invest Ophthalmol Vis Sci* 2010;51:3362-3371.

99. Haas P, Gilmour D. Chemokine signaling mediates self-organizing tissue migration in the zebrafish lateral line. *Dev Cell* 2006;10:673-680.
100. Gerhardt H, Golding M, Fruttiger M, Ruhrberg C, Lundkvist A, Abramsson A, Jeltsch M, Mitchell C, Alitalo K, Shima D, Betsholtz C. VEGF guides angiogenic sprouting utilizing endothelial tip cell filopodia. *J Cell Biol* 2003;161:1163-1177.
101. Shamloo A, Xu H, Heilshorn S. Mechanisms of vascular endothelial growth factor-induced pathfinding by endothelial sprouts in biomaterials. *Tissue Eng Part A* 2012;18:320-330.
102. Montero RB, Vial X, Nguyen DT, Farhand S, Reardon M, Pham SM, Tsechpenakis G, Andreopoulos FM. bFGF-containing electrospun gelatin scaffolds with controlled nano-architectural features for directed angiogenesis. *Acta Biomater* 2012;8:1778-1791.
103. Helm CL, Zisch A, Swartz MA. Engineered blood and lymphatic capillaries in 3-D VEGF-fibrin-collagen matrices with interstitial flow. *Biotechnol Bioeng* 2007;96:167-176.
104. Hadjizadeh A, Doillon CJ. Directional migration of endothelial cells towards angiogenesis using polymer fibres in a 3D co-culture system. *J Tissue Eng Regen Med* 2010;4:524-531.
105. Nehls V, Herrmann R, Hühnken M. Guided migration as a novel mechanism of capillary network remodeling is regulated by basic fibroblast growth factor *Histochem Cell Biol* 1998;109:319-329.
106. Papavasiliou G, Cheng MH, Brey EM. Strategies for vascularization of polymer scaffolds. *J Investig Med* 2010;58:838-844.
107. Dikovsky D, Bianco-Peled H, Seliktar D. The effect of structural alterations of PEG-fibrinogen hydrogel scaffolds on 3-D cellular morphology and cellular migration. *Biomaterials* 2006;27:1496-1506.
108. Ruhrberg C, Gerhardt H, Golding M, Watson R, Ioannidou S, Fujisawa H, Betsholtz C, Shima DT. Spatially restricted patterning cues provided by heparin-binding VEGF-A control blood vessel branching morphogenesis. *Genes Dev* 2002;16:2684-2698.
109. Uttayarat P, Toworfe GK, Dietrich F, Lelkes PI, Composto RJ. Topographic guidance of endothelial cells on silicone surfaces with micro- to nanogrooves: orientation of actin filaments and focal adhesions. *J Biomed Mater Res A* 2005;75:668-680.

110. Teixeira AI, Abrams GA, Bertics PJ, Murphy CJ, Nealey PF. Epithelial contact guidance on well-defined micro- and nanostructured substrates. *J Cell Sci* 2003;116:1881-1892.
111. Mehes E, Mones E, Nemeth V, Vicsek T. Collective motion of cells mediates segregation and pattern formation in co-cultures. *PLoS One* 2012;7:e31711.
112. Cai K, Kong T, Wang L, Liu P, Yang W, Chen C. Regulation of endothelial cells migration on poly(D, L-lactic acid) films immobilized with collagen gradients. *Colloids Surf B Biointerfaces* 2010;79:291-297.
113. Friedl P, Gilmour D. Collective cell migration in morphogenesis, regeneration and cancer. *Nat Rev Mol Cell Biol* 2009;10:445-457.
114. Gov NS. Collective cell migration patterns: follow the leader. *Proc Natl Acad Sci U S A* 2007;104:15970-15971.
115. Friedl P. Prespecification and plasticity: shifting mechanisms of cell migration. *Curr Opin Cell Biol* 2004;16:14-23.
116. Claes F, Vandeveldel W, Moons L, Tjwa M. Another angiogenesis-independent role for VEGF: SDF1-dependent cardiac repair via cardiac stem cells. *Cardiovasc Res* 2011;91:369-370.
117. Jo DY, Rafii S, Hamada T, Moore MA. Chemotaxis of primitive hematopoietic cells in response to stromal cell-derived factor-1. *J Clin Invest* 2000;105:101-111.
118. Urbich C, Dimmeler S. Endothelial progenitor cells: characterization and role in vascular biology. *Circ Res* 2004;95:343-353.
119. De Falco E, Porcelli D, Torella AR, Straino S, Iachininoto MG, Orlandi A, Truffa S, Biglioli P, Napolitano M, Capogrossi MC, Pesce M. SDF-1 involvement in endothelial phenotype and ischemia-induced recruitment of bone marrow progenitor cells. *Blood* 2004;104:3472-3482.
120. Urbich C, Aicher A, Heeschen C, Dernbach E, Hofmann WK, Zeiher AM, Dimmeler S. Soluble factors released by endothelial progenitor cells promote migration of endothelial cells and cardiac resident progenitor cells. *J Mol Cell Cardiol* 2005;39:733-742.
121. Yamaguchi J, Kusano KF, Masuo O, Kawamoto A, Silver M, Murasawa S, Bosch-Marce M, Masuda H, Losordo DW, Isner JM, Asahara T. Stromal cell-derived factor-1 effects on ex vivo expanded endothelial progenitor cell recruitment for ischemic neovascularization. *Circulation* 2003;107:1322-1328.

122. Prokoph S, Chavakis E, Levental KR, Zieris A, Freudenberg U, Dimmeler S, Werner C. Sustained delivery of SDF-1alpha from heparin-based hydrogels to attract circulating pro-angiogenic cells. *Biomaterials* 2012;33:4792-4800.

123. Sun G, Shen YI, Kusuma S, Fox-Talbot K, Steenbergen CJ, Gerecht S. Functional neovascularization of biodegradable dextran hydrogels with multiple angiogenic growth factors. *Biomaterials* 2011;32:95-106.

124. Jin F, Hagemann N, Schafer ST, Brockmeier U, Zechariah A, Hermann DM. SDF-1 restores angiogenesis synergistically with VEGF upon LDL exposure despite CXCR4 internalization and degradation. *Cardiovasc Res* 2013;100:481-491.

125. Ruhrberg C. Growing and shaping the vascular tree: multiple roles for VEGF. *Bioessays* 2003;25:1052-1060.

126. Kucia M, Jankowski K, Reza R, Wysoczynski M, Bandura L, Allendorf DJ, Zhang J, Ratajczak J, Ratajczak MZ. CXCR4-SDF-1 signalling, locomotion, chemotaxis and adhesion. *J Mol Histol* 2004;35:233-245.

127. Dietrich F, Lelkes PI. Fine-tuning of a three-dimensional microcarrier-based angiogenesis assay for the analysis of endothelial-mesenchymal cell co-cultures in fibrin and collagen gels *Angiogenesis* 2006;9:111-125.

128. Nagy JA, Benjamin L, Zeng H, Dvorak AM, Dvorak HF. Vascular permeability, vascular hyperpermeability and angiogenesis *Angiogenesis* 2008;11:109-119.

129. Madeddu P. Therapeutic angiogenesis and vasculogenesis for tissue regeneration. *Exp Physiol* 2005;90:315-326.

130. Hanjaya-Putra D, Yee J, Ceci D, Truitt R, Yee D, Gerecht S. Vascular endothelial growth factor and substrate mechanics regulate in vitro tubulogenesis of endothelial progenitor cells. *J Cell Mol Med* 2010;14:2436-2447.

131. Petit I, Jin D, Rafii S. The SDF-1-CXCR4 signaling pathway: a molecular hub modulating neo-angiogenesis. *Trends Immunol* 2007;28:299-307.

132. Chung S, Sudo R, Mack PJ, Wan CR, Vickerman V, Kamm RD. Cell migration into scaffolds under co-culture conditions in a microfluidic platform. *Lab Chip* 2009;9:269-275.

133. Wu X, Rabkin-Aikawa E, Guleserian KJ, Perry TE, Masuda Y, Sutherland FW, Schoen FJ, Mayer JE, Jr, Bischoff J. Tissue-engineered microvessels on three-dimensional biodegradable scaffolds using human endothelial progenitor cells. *Am J Physiol Heart Circ Physiol* 2004;287:H480-7.

134. Yang J, li M, Kamei N, Alev C, Kwon SM, Kawamoto A, Akimaru H, Masuda H, Sawa Y, Asahara T. CD34+ cells represent highly functional endothelial progenitor cells in murine bone marrow. PLoS One 2011;6

Appendices

Appendix I

Stage Incubator Protocol







The last review of this protocol was performed on: **11/13/2012 by Miguel Quevedo and Ximena Vial**

General Guidelines:

A. System setup:



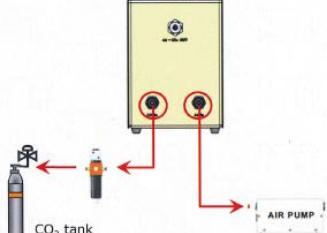

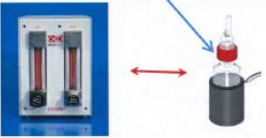
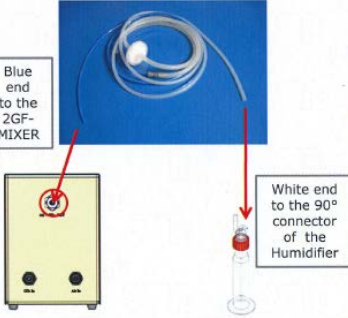
1. Before anything read the entire protocol and acquire permission from the graduate student that you have been working with.
2. When planning to use the stage incubator the first thing that should be done is to sign up online in the calendar (google calendar- When you start a project that requires the use of the stage incubator you will be granted access).
3. Come in to the lab at your assigned time and prepare the experiment that is going to be put in the incubator.
4. Be CAREFUL with each component of the incubator...Parts are very delicate and expensive...Remember that you are not the only person utilizing the system. If you do not take care of the stage incubator and damage it you may affect not only your work but the work of others. Failure to take care of the system will result in loss of privileges.
5. Make sure you have the following units as well as the CO₂ tank, O₂ tank, with their safety valves and pressure gauges (if something is missing immediately notify Ximena Vial or the graduate student that you have been working with so that the parts may be ordered):



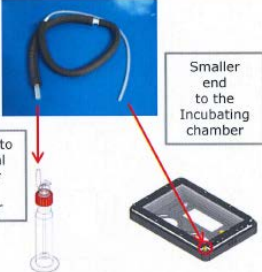




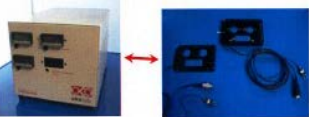

1) UNITS

<p>Electric incubating chamber plus the plate adapter mounted on</p>  <p>Code: H301-EC, H301-EC-HG-LID and H301-EC-[57mm]GS3BASE</p>	<p>Chamber temperature controller</p>  <p>Code: H301-TC1</p>	<p>Manual 2 Gas Mixer</p>  <p>Code: 2GF-MIXER</p>
<p>Humidifying module Temperature Controller</p>  <p>Code: H301-HMTC</p>	<p>Humidifying module</p>  <p>Code: H301-BC</p>	<p>Air pump</p>  <p>Code: OKO-AP</p> <p>Plate adapters</p> <ul style="list-style-type: none"> ✓ H301-EC-12MWBASE ✓ H301-EC-24MWBASE

6. Connect the tubes and cables in the following manner:

2) Tubes and cables connection

This cable/tube	Connects the following devices	In this way
 <p>Tubes D</p>		 <p>CO₂ tank</p> <p>AIR PUMP</p>
 <p>Tube E</p>	<p>Remember to place the Glass Bottle into H301-HMTC and to fill it in with distilled water. Check water level from time to time.</p> 	 <p>Blue end to the 2GF-MIXER</p> <p>White end to the 90° connector of the Humidifier</p>

This cable/tube	Connects the following devices	In this way
 <p data-bbox="488 499 537 516">Tube H</p>		 <p data-bbox="997 411 1094 495">Bigger end to the vertical connector of the Humidifier</p> <p data-bbox="1256 331 1338 415">Smaller end to the Incubating chamber</p>
 <p data-bbox="396 842 639 873">Cables from the Humidifying module Temperature Controller</p>		
This cable/tube	Connects the following devices	In this way
 <p data-bbox="347 1314 659 1335">Cables from the Electric I incubating chamber</p>		 <p data-bbox="997 1010 1138 1041">Cover cables to T2/Heater 2</p> <p data-bbox="1256 1010 1354 1041">Base cables to T1/Heater 1</p>

3) Usage of the Incubating chamber

IMPORTANT:

When you exchange plate adapters on the incubating chamber few parameters have to be changed in the thermal controller H301-TC1. Instructions to quickly do this are listed in the operating manual, for further support please feel free to contact us.



The chamber riser is needed only when using plates higher than 17mm. It can be removed if you use petri-dishes for instance, or if you need to reduce the chamber's height to work with High numerical aperture condensers

7. If your experiment requires control of gas conditions at specific parameters please read the following:

CO₂ is mixed with air in the control unit and is continuously fed into the incubating chamber to control medium pH. Upon request, a third gas can be fed into the incubating chamber.

Open the gas valves about 15 minutes before inserting the specimen in the Micro Environmental Chamber.

Two Flow Meters:

Target Gas Percentage [%]		Gas flow rate values to set [Nl/min]		
Air	CO ₂	Air	CO ₂	Total
95.00	5.00	0.80	0.04	0.84
95.00	5.00	1.00	0.05	1.05
95.00	5.00	1.20	0.06	1.26

Three Flow Meters:

	Target Gas Percentage [%]			Gas flow rate values to set [Nl/min]			Total
	Air/N ₂	CO ₂	O ₂ /Other	Air/N ₂	CO ₂	O ₂ /Other	
1	95.00	5.00	0.00	0.80	0.04	0.00	0.84
2	95.00	5.00	0.00	1.00	0.05	0.00	1.05
3	95.00	5.00	0.00	1.20	0.06	0.00	1.26
4	94.00	5.00	1.00	1.70	0.09	0.02	1.81
5	93.00	5.00	2.00	0.90	0.05	0.02	0.97
6	93.00	5.00	2.00	1.30	0.07	0.03	1.40
7	92.00	5.00	3.00	0.90	0.05	0.03	0.98
8	92.00	5.00	3.00	1.30	0.07	0.04	1.41
9	91.00	5.00	4.00	0.90	0.05	0.04	0.99
10	91.00	5.00	4.00	1.10	0.06	0.05	1.21
11	90.00	5.00	5.00	0.70	0.04	0.04	0.78
12	90.00	5.00	5.00	0.90	0.05	0.05	1.00
13	90.00	5.00	5.00	1.10	0.06	0.06	1.22
14	89.00	5.00	6.00	0.90	0.05	0.06	1.01
15	88.00	5.00	7.00	0.90	0.05	0.07	1.02
16	87.00	5.00	8.00	0.90	0.05	0.08	1.03
17	86.00	5.00	9.00	0.70	0.04	0.07	0.81
18	86.00	5.00	9.00	1.00	0.06	0.11	1.17
19	85.00	5.00	10.00	0.70	0.04	0.08	0.82
20	85.00	5.00	10.00	1.00	0.06	0.12	1.18
21	84.00	5.00	11.00	0.80	0.05	0.11	0.96
22	83.00	5.00	12.00	0.80	0.05	0.12	0.97
23	82.00	5.00	13.00	0.70	0.04	0.10	0.84
24	82.00	5.00	13.00	0.80	0.05	0.13	0.98
25	81.00	5.00	14.00	0.60	0.04	0.11	0.75
26	80.00	5.00	15.00	0.60	0.04	0.12	0.76
27	79.00	5.00	16.00	0.60	0.04	0.13	0.77
28	78.00	5.00	17.00	0.50	0.03	0.10	0.63

4) Setting Gas Flowmeters

Open the valve of the CO₂ tank and turn the Air pump on. Pressure after gas tanks has to be around 30 psi (2 bar). Pressure after the pressure gauge regulator has to be about 15 psi (1 bar).

Regulate the flowmeters to obtain the desired relative quantity of Air and CO₂. Suggested flowrates to obtain a gas stream of Air+5%CO₂: 0.80 l/min for air and 0.04 l/min for CO₂. If you use a single premixed tank of Air+5% CO₂ (to be connected to the Air flowmeter) suggested flowrate is 0.8 l/min.

Air flow rate, l/mn	Carbon dioxide flow rate, l/min	Total gas stream flow rate, l/min	Carbon dioxide percentage	
0.6	0.03	0.63	5	
0.8	0.04	0.84	5	Optimal flow
1	0.05	1.05	5	
1.2	0.06	1.26	5	

8. Ask about the last time the stage incubator was calibrated for temperature control and read the following:

The Okolab electrical stage incubation chamber is heated by miniaturized DC electrical resistances at low voltage (24V). The specimen, contained in plastic or glass support for cells culture, is maintained at 37.0°C thanks to a constant metal warming up ensured by controllers designed. To ensure a specimen temperature of 37.0°C both lid and base are maintained at a temperature that depends on the ambient temperature and the cells culture support used (Multi-well plate ore Petri dish). The chamber control temperature can work in two different modalities:

a) Chamber temperature feedback:

In this configuration, the thermocouple reads the temperature of the incubating chamber. A careful calibration performed in our laboratories guarantees that specimen temperature is maintained at the desired value. The advantage of this solution is that the thermocouple is not visible since it is embedded into the chamber.

b) Specimen temperature feedback:

In this configuration, the thermocouple is a thin flexible green wire that reads the temperature of a reference well placed in the incubating chamber, very close to the specimen. The advantage of this configuration is in the accuracy of the temperature control. Simple manipulation is required to stick the thermocouple into the reference well with some adhesive tape.

Calibration:

The calibration was performed, the first time, in the Okolab lab. The calibration document shows the 'calibration offset values' (red) for every controller (see Figure 18).

Once two years, it is suitable to perform the calibration. Use the fine thermocouple sensor provided by Okolab, connected to T1 thermocouple connectors as sensor. Use an accurate thermostatic water bath, set to 37°C , as reference temperature.

- Set the Offset temperature to 0.
- Please, disconnect the cables.
- Insert the fine thermocouple sensor (this calibration sensor can be provided by Okolab) into T1 connector
- Put the free end of the fine calibration sensor in the water bath (in steady state and set at 37.0°C).
- Please, fix the thermocouple to a support in order to maintain a constant position of the sensor in the warm water.
- Wait about 30 min to reach a stable temperature
- Register the temperature difference between the water bath temperature (37.0°C) and the displayed "Temperature 1".
- Calibration Offset 1 (@ T=37.0°C) = (T(water bath set to T=37.0°C) – Temperature 1) for Temperature 1 > T (water bath)
or
Calibration Offset 1 (@ T=37.0°C) = - (T(water bath set to T=37.0°C) + Temperature 1) for Temperature 1 < T (water bath)
- Repeat the sequence for 30°C, 35°C, 40°C
- Calibration Offset 1 AVG = Average (Calibration offset 1 ((@ T=37.0°C),(@ T=30.0°C), (@ T=35.0°C), (@ T=40.0°C))
- Insert this calibration value as COSTANT offset (PV BIAS) to add (or subtract) in 'Temperature 1' PID.
- Please, after meter calibration, compare the temperature difference between the water bath set point temperature (37.0°C) and the displayed temperature 1.
- Substitute the new calibration value to the offset 1 AVG (then offset 2 AVG) reported in the Calibration document
- Repeat for T2, H.M. and alarm controller

Calibration document Cod-CD-E-MSI 001.08

Order number: _____
 Control unit serial number: _____
 Calibration date: _____

PID T1		
Water bath temperature (°C)	Measured temperature T1 (°C)	Calibration Offset 1 (AVG)
30		
35		
37		
40		
PID T2		
Water bath temperature (°C)	Measured temperature T2 (°C)	Calibration Offset 2 (AVG)
30		
35		
37		
40		
PID U.M.		
Water bath temperature (°C)	Measured temperature T U.M. (°C)	Calibration Offset H.M. (AVG)
30		
35		
37		
40		
PID Alarm		
Water bath temperature (°C)	Measured temperature T Alarm (°C)	Calibration Offset Alarm (AVG)
30		
35		
37		
40		

The offset 1 is: _____
 The offset 2 is: _____
 The offset U.M. is: _____
 The offset Alarm is: _____

Calibrated Signature: _____

Checker Signature: _____

Figure 18: Calibration document, facsimile

In this configuration, the thermocouple reads the temperature of the incubating chamber. If ambient temperature differs from 23°C more than 2°C or the support plate changes, consider to modify the parameters of the controllers T1 and T2 (**'Secondary Offset'**), in order to have the specimen at the correct temperature. Notice that the parameters for the Humidifying Module heater (PID H.M.) are constant. The calibration has been performed in the Okolab lab. Notice the factory parameters depend on the plate adapter you order. The default values are optimized for $T_{Ambient} 23.0 \pm 1.0^{\circ}\text{C}$ and active Humidifying Module heater. Anyway, the controllers PID T1 and PID T2 parameters do not depend on Humidifying Module presence.

'Secondary offset' values are calculated with the following targets:

1. Specimen temperature $37 \pm 0.3^{\circ}\text{C}$
2. Avoid condensation on the lid glass
3. Improve the gas stream humidity level

In case you use 'Specimen temperature feedback' configuration, you need to insert the following set of parameters in the controllers. Remember the controllers parameters depend on cells culture support.

Standard 6 Well Plate			
	PID T1	PID T2	PID H.M.
Set Point (SV)	37.0	37.0	37.0
'Total Offset' = 'Secondary Offset' + 'Calibration Offset'			
Total Offset (PV)	-4.2+ Calibration Offset 1 (AVG)	-8.2+ Calibration Offset 2 (AVG)	-3.0+ Calibration Offset H.M. (AVG)
controllers parameters			
P	010.0	010.0	010.0
I	0240	0240	0240
d	0120	0120	0120
Ar	0060	0060	0060
t	0002	0002	0002
df	16	16	16

Table 1: $T_{Ambient}$ $23.0 \pm 1.0^{\circ}\text{C}$, standard 6 Well plate, with Humidifying Module heater.

Standard 96 Well Plate			
	PID T1	PID T2	PID H.M.
Set Point (SV)	37.0	37.0	37.0
'Total Offset' = 'Secondary Offset' + 'Calibration Offset'			
Total Offset (PV)	-1.9+ Calibration Offset 1 (AVG)	-5.9+ Calibration Offset 2 (AVG)	-3.0+ Calibration Offset H.M. (AVG)
controllers parameters			
P	020.0	020.0	020.0
I	0240	0240	0240
d	0120	0120	0120
Ar	0060	0060	0060
t	0002	0002	0002
df	16	16	16

Table 2: $T_{Ambient}$ $23.0 \pm 1.0^{\circ}\text{C}$, standard 96 Well plate, with Humidifying Module heater.

#2 35mm petri dish and #1 glass slide			
	PID T1	PID T2	PID H.M.
Set Point (SV)	37.0	37.0	37.0
'Total Offset' = 'Secondary Offset' + 'Calibration Offset'			
Total Offset (PV)	-2.0+ Calibration Offset 1 (AVG)	-6.0+ Calibration Offset 2 (AVG)	-3.0+ Calibration Offset H.M. (AVG)
controllers parameters			
P	010.0	010.0	010.0
I	0240	0240	0240
d	0120	0120	0120
Ar	0060	0060	0060
t	0002	0002	0002
df	16	16	16

Table 3: $T_{Ambient}$ $23.0 \pm 1.0^{\circ}\text{C}$, #2 35mm petri dish and #1 glass slide, with Humidifying Module heater.

Standard 6 Well Plate

	PID T1 = Specimen Temp.	PID T2	PID H.M.	PID Alarm
Set Point (SV)	37.0	37.0	37.0	
<i>'Total Offset' = 'Secondary Offset' + 'Calibration Offset'</i>				
Total Offset (PV)	Calibration Offset 1 (AVG) (Secondary Offset=0)	-5.5+ Calibration Offset 2 (AVG)	-3.0+ Calibration Offset H.M. (AVG)	
<i>controllers parameters</i>				
P	005.0	010.0	010.0	
I	0720	0240	0240	
d	0300	0260	0120	
Ar	0060	0060	0060	
t	0010	0002	0002	
df	08	08	16	

Table 5: $T_{Ambient}$ $23.0 \pm 1.0^{\circ}\text{C}$, standard 6 Well plate, with Humidifying Module heater.

Standard 96 Well Plate

	PID T1 = Specimen Temp.	PID T2	PID H.M.	PID Alarm
Set Point (SV)	37.0	37.0	37.0	
<i>'Total Offset' = 'Secondary Offset' + 'Calibration Offset'</i>				
Total Offset (PV)	Calibration Offset 1 (AVG) (Secondary Offset=0)	-4.0+ Calibration Offset 2 (AVG)	-3.0+ Calibration Offset H.M. (AVG)	
<i>controllers parameters</i>				
P	005.0	010.0	020.0	
I	0720	0240	0240	
d	0300	0260	0120	
Ar	0050	0050	0060	
t	0005	0002	0002	
df	08	08	16	

Table 6: $T_{Ambient}$ $23.0 \pm 1.0^{\circ}\text{C}$, standard 96 Well plate, with Humidifying Module heater.

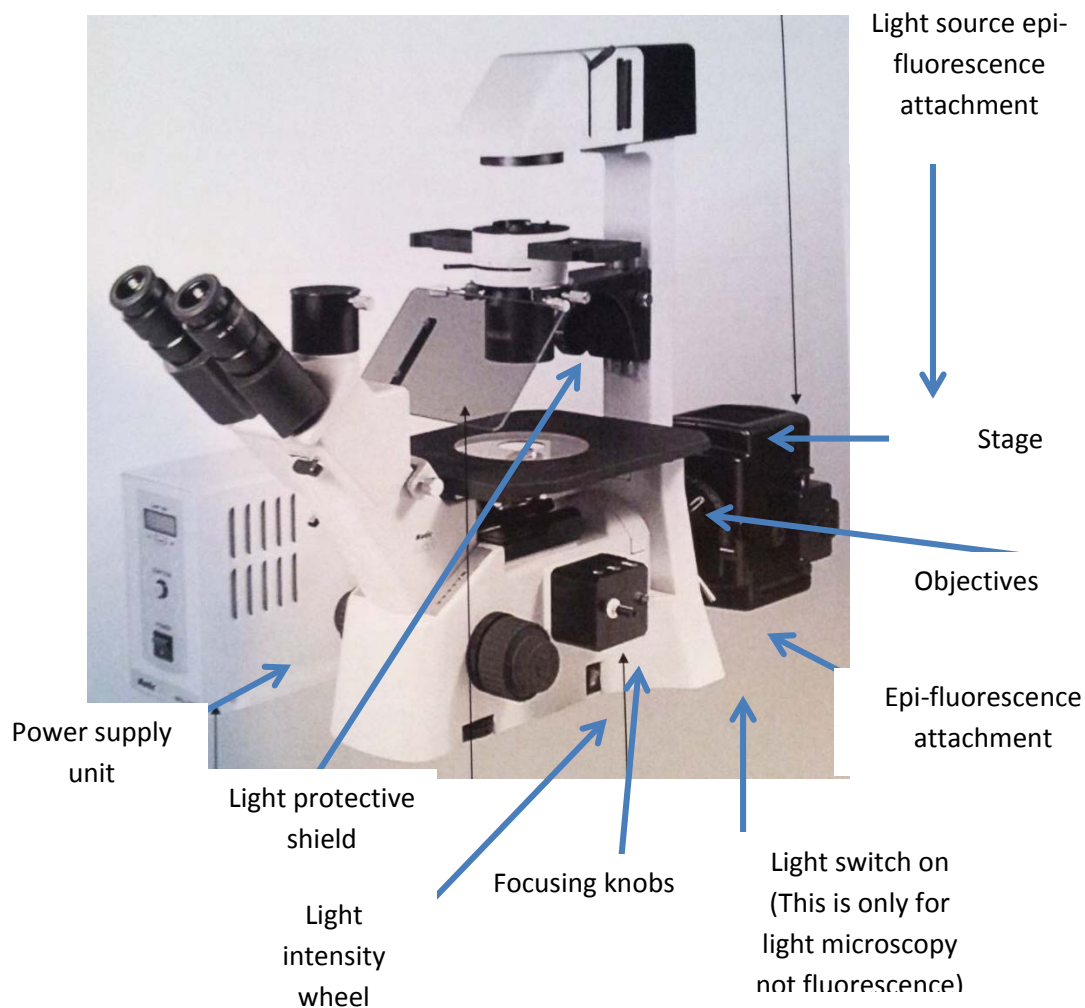
#2 35mm petri dish and #1 glass slide

	PID T1 = Specimen Temp.	PID T2	PID H.M.	PID Alarm
Set Point (SV)	37.0	37.0	37.0	
<i>'Total Offset' = 'Secondary Offset' + 'Calibration Offset'</i>				
Total Offset (PV)	Calibration Offset 1 (AVG) (Secondary Offset=0)	-5.5+ Calibration Offset 2 (AVG)	-3.0+ Calibration Offset H.M. (AVG)	
<i>controllers parameters</i>				
P	005.0	010.0	010.0	
I	0720	0240	0240	
d	0300	0260	0120	
Ar	0060	0060	0060	
t	0010	0002	0002	
df	08	08	16	

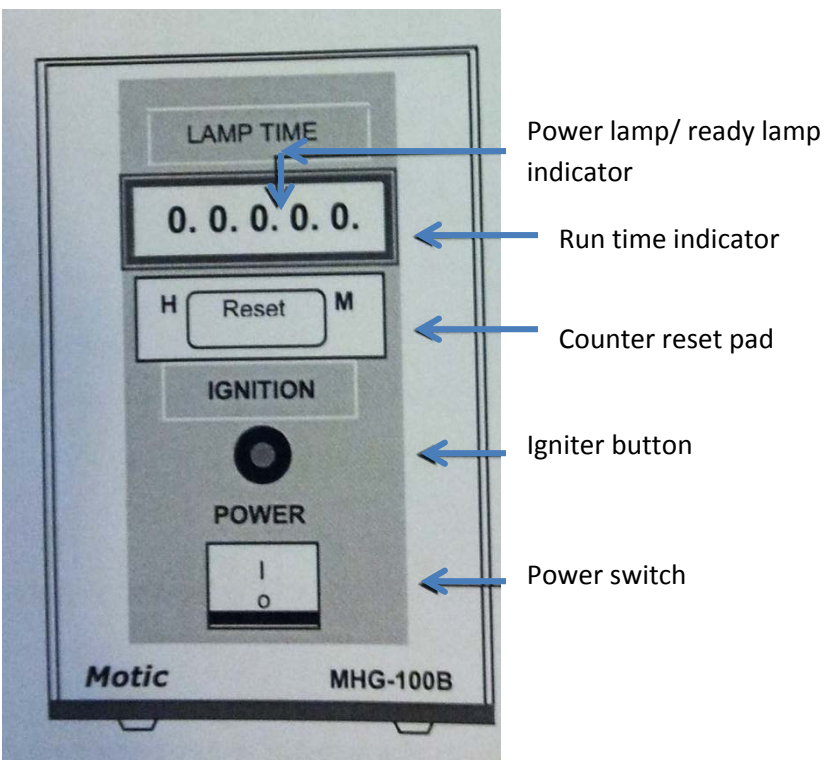
Table 7: $T_{Ambient}$ $23.0 \pm 1.0^{\circ}\text{C}$, #2 35mm petri dish and #1 glass slide, with Humidifying Module heater.

B. MICROSCOPE SETUP:

1. Our lab has a Motic inverted microscope equipped with epi-fluorescence. It is placed next to the stage incubator components and to the computer you will be utilizing to capture images and for time-lapse video. The microscope has several objectives (4x, 10x, 20x and 40x).



2. Once you have the stage incubator system connected place the incubator chamber on the stage of the microscope. Once you have the chamber in place place your sample inside and close the top lid (Be careful with the screw that keeps the lid in place). Make sure your sample is aligned with the objective you are going to utilize.
3. Switch on your microscope's light source (if you are going to utilize fluorescence you will have to turn on the power supply and not the light switch- below is a diagram of the power supply) and then adjust the diaphragm to the largest hole diameter, allowing the greatest amount of light through.



To turn on the lamp for fluorescence microscopy:

- Set the power supply switch to “I”
 - Press the ignition button on the power supply unit for 5-10 seconds
 - The power lamp/ ready lamp will light up to indicate that the power is turned on
 - The power lamp/ ready lamp indicator lamp will start flashing briefly to indicate that the lamp is stabilized
 - Press the rest pad below the run time counter on the power supply
 - The “run time” counter displays the elapsed time
4. Rotate the nosepiece to the lowest-power objective 4x. It is easiest to scan a sample at a low setting, since you have a wider field of view at low power.
 5. Adjust the large coarse focus knob until the specimen is in focus. Slowly move the sample to center the specimen under the lens, if necessary. Do this by nudging the chamber gently with your fingers.
 6. Adjust the small fine focus knob until the specimen is clearly in focus. Then adjust the diaphragm to get the best lighting. Start with the most light and gradually lessen it until the specimen image has clear, sharp contrast.

7. Rotate the nosepiece to the 10x objective. Refocus and view your specimen carefully. Adjust the lighting again until the image is most clear (you will need more light for higher power). Repeat this process if you want to utilize a higher magnification.
8. Once your sample is situated and focused turn on the stage incubator system.
9. Turn on the computer and open MoticPlus 2.0 program. The manual for the program is attached to this document. Set the parameters necessary for imaging project (i.e. exposure, timelines, brightness, contrast, etc.)
10. Let you experiment run...once the experiment is done make sure to turn EVERYTHING off, clean each component and place it where it belongs. Cover the microscope.

Appendix II



Electric CO₂ Microscope Stage Incubator

Manual

Ver 03/2008

Preface

The Electric CO₂ Microscope Stage Incubator (MSI) is the latest release in the family of our Top Stage Incubators. It represents a one-button solution for long term experiments. The same model fits all the XY stages on the market, and it is suitable at the same time for high magnification microscopy and multipoint experiments.

The Electric CO₂ MSI is designed to maintain the desired temperature for cell cultures right on the inverted or upright microscope stage. Digital thermo-regulators ensure high reading and control accuracy. The heating systems are powered at 24V DC. That improves the thermal stability, avoids electro-magnetic interference with microscope or other devices electronic and ensures the safety. In addition, an alarm warns if the temperature limit is reached.

The read temperatures and the set temperatures are at the same time displayed. It is possible to change the set temperatures and the offset temperatures values.

A spacer adapter allows you to load higher Multi Well into the chamber. Different Multi Well adapters are available, from 6 well to 96 well. Special design adapters support different configuration as 35 mm Petri dish, 60 mm Petri dish, Labtek and any flat support. Incubating chamber and adapter can be customized upon request.

Contents

1. DEVICE DESCRIPTION	5
1.1. OVERVIEW	5
1.1.1. <i>Temperature Regulation</i>	5
1.1.2. <i>CO₂ Regulation</i>	6
1.1.3. <i>Humidity Regulation</i>	6
1.1.4. <i>Software</i>	6
1.2. HARDWARE DETAILS	6
1.3. TUBING DETAILS	6
1.4. CABLES DETAILS	6
1.5. ACCESSORIES	6
1.6. EQUIPMENT REQUIRED (<i>NOT SUPPLIED</i>)	7
2. CONNECTIONS	8
2.1. TUBINGS CONNECTION (<i>AIR/O₂ AND CO₂</i>)	8
2.1.1. <i>Gas reservoirs to Control Unit</i>	9
2.1.2. <i>Control Unit to Humidifying module</i>	10
2.1.3. <i>Humidifying module-Micro to Environmental Chamber</i>	10
2.2. HEATING AND TEMPERATURE CABLES CONNECTIONS	10
2.2.1. <i>Control Unit front panel</i>	10
2.2.2. <i>Control Unit rear panel</i>	11
2.2.3. <i>Standard configuration (Chamber temperature feedback)</i>	12

3.	ELECTRIC CHAMBER.....	13
3.1.	ELECTRIC CHAMBER PARTS DESCRIPTION	15
3.2.	ADD-REMOVE INSERTS	16
4.	TEMPERATURE CONTROL MECHANISM	17
4.1.	PID CONTROLLERS CALIBRATION (CALIBRATION OFFSET).....	18
4.2.	CHAMBER TEMPERATURE FEEDBACK	19
4.2.1.	<i>Chamber configurations and controllers parameters</i>	19
4.2.2.	<i>Secondary offset calibration with 6 well Plate configuration</i>	20
4.3.	SPECIMEN TEMPERATURE FEEDBACK.....	23
5.	CONTROLLER DESCRIPTION	24
5.1.	DISPLAY FUNCTIONS	24
5.2.	SET POINT TEMPERATURE AND OFFSET TEMPERATURE RANGE.....	25
5.3.	CHANGE THE SET POINT TEMPERATURE.....	25
5.4.	CHANGE THE OFFSET TEMPERATURE	26
5.5.	STOP THE CONTROLLER.....	26
6.	FLOW METERS REGULATION	27
6.1.	TWO FLOW METERS CONTROL UNIT	27
6.2.	THREE FLOW METERS CONTROL UNIT	29
7.	ELECTRICAL MICROSCOPE STAGE INCUBATOR USE.....	30
7.1.	CHAMBER TEMPERATURE FEEDBACK	30
7.1.1.	<i>Multi well adapters</i>	30
7.1.2.	<i>Petri dish adapter (technically qualified personnel)</i>	31
7.2.	SPECIMEN TEMPERATURE FEEDBACK.....	31
7.2.1.	<i>Multi well adapter</i>	32
7.2.2.	<i>Petri dish adapter</i>	35
8.	SUPPORT.....	37
8.1.	WEB CONFERENCE FOR ASSISTANCE AND TRAINING	37
8.2.	TECHNICAL SUPPORT	37
8.3.	TECHNICAL SPECIFICATIONS	37
8.4.	TROUBLESHOOTING.....	38
9.	APPENDIX: CONTROLLER MANUAL.....	39

Safety Notes

In order to achieve maximum performance and to ensure proper operation of your new equipment, carefully read the following safety notes and the instructions. If you have any questions, please contact Okolab.

- The equipment must only be used as intended and as described in this Manual.
- Equipment should only be operated by technically qualified personnel.
- Equipment and its internal parts can be damaged by dropping and by shock.
- Do not start up the equipment if the supply cable is damaged.
- Connect the equipment only to grounded mains power socket.
- Some equipment parts may reach temperatures above 50°C. Take care when touching it.
- This instrument is not intended for use in locations subject to flammable or explosive gases.
- Prevent throttling and kinking of cables.
- Check cables time to time for possible material usage.
- This device is not designed for use under medical conditions.
- Prevent metal fragments or lead wire scraps from falling inside instrument case to avoid electric shock, fire or malfunction.
- Do not use a volatile solvent such as paint thinner to clean the instrument. Deformation or discoloration will occur. Use a soft, dry cloth to remove stains from the instrument.
- To avoid damage to instrument display, do not rub with an abrasive material or push front panel with a hard object.
- Avoid rapid changes in ambient temperature which may cause condensation, avoid direct air flow from air conditioner, exposure to direct sunlight, excessive heat accumulation; do not close the air intake.
- Avoid water, oil, chemicals, vapor or steam splashes, excessive dust, salt or iron particles.
- Avoid excessive induction noise, static electricity, magnetic fields.
- Do not hold the plate by lead wires.
- Do not disassemble the plate.
- Do not machine or hole the plate.
- Do not disconnect the cables while in operation.
- We reserve the right to make technical variations.



International caution symbol marks this device. It is important to read the 'Safety Notes' before installing, using and commissioning this device, as the notes contain important information relating to safety and EMC.

IN NO EVENT OKOLAB S.R.L. SHALL BE LIABLE FOR ANY DIRECT, INCIDENTAL OR CONSEQUENTIAL DAMAGES OF ANY NATURE, OR LOSSES OR EXPENSES RESULTING FROM ANY DEFECTIVE PRODUCT OR THE USE OF ANY PRODUCT.

CAUTION- Risk of electric shock! Do not open the 'Control Unit'. To prevent the risk of electric shock, do not remove cover or back. No user serviceable parts inside.

1. Device description

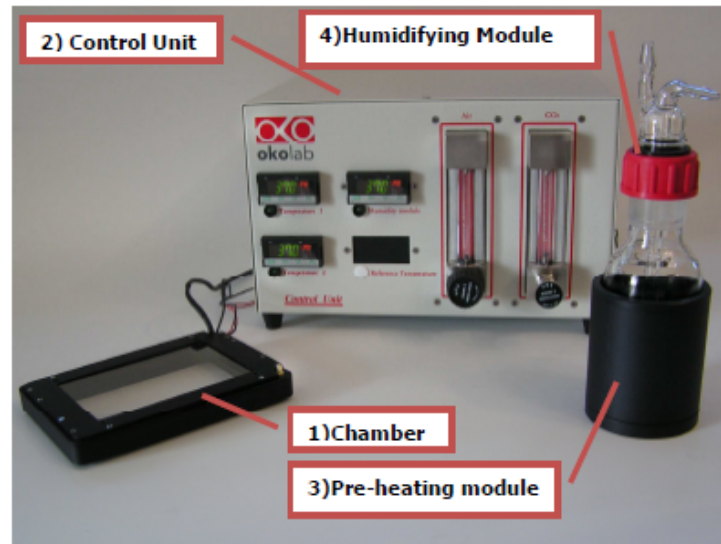


Figure 1. System Overview

1.1. Overview

1.1.1. Temperature Regulation

The CO₂ Electric MSI regulates the specimen temperature by the combined action of two controllers acting on the power dissipated by the electric resistances, embedded both in the base and in the lid of the incubating chamber. Two temperature feedback mechanisms are available:

Chamber temperature feedback

In this configuration, the thermocouple reads the temperature of the incubating chamber. A careful calibration performed in our laboratories guarantees that specimen temperature is maintained at the desired value. The advantage of this solution is that the thermocouple is not visible since it is embedded into the chamber.

Specimen temperature feedback

In this configuration, the thermocouple is a thin flexible green wire reads the temperature of a reference well placed in the incubating chamber, very close to the specimen. The advantage of this configuration is in the accuracy of the temperature control. Simple manipulation is required to stick the thermocouple into the reference well with some adhesive tape.

1.1.2. CO₂ Regulation

CO₂ is mixed with air in the control unit and is continuously fed into the incubating chamber to control medium pH. Upon request, a third gas can be fed into the incubating chamber.

1.1.3. Humidity Regulation

Humidifying and pre-heating module (on request) prevent medium evaporation and avoid water condensation on glass and plastic surfaces

1.1.4. Software

Read Temperature Software is available on request to read incubator temperature and store the data in computer memory.

1.2. Hardware details

1. Electrical Micro-Environmental Chamber + cover and plate adapter (it depends on request)
2. Control Unit. It contains two (or more, it depends on Control Unit model) Temperature Controller and, from zero to three (it depends on Control Unit model) Gas Flow meters
3. Humidifying Module Heater (on request).
4. Humidifying Module (pay attention: FRAGILE)

1.3. Tubing details

1. #1 TUBE A: 4mm ID silicon transparent tube mounting a Swift-Fit connector at one end, 1.3 m long
2. #1 TUBE B: It is composed of 2mm ID silicon transparent tube (0.5 m long) connected to 4mm ID silicon transparent tube (0.5 m long) then connected to 8mm ID silicon transparent tube, 0.2 m long.
3. #2 (or more depending on model) white rigid tubes of 6mm OD, 3 m long
4. #1 blue rigid tube of 6mm OD, 2 m long
5. Pressure Gauge for CO₂ + regulator + assembly stirrup

1.4. Cables details

1. #1 power supply cable

1.5. Accessories

1. Pressure Gauge for CO₂ with regulator, degree of filtration 20µm and condensate drain (supplied)
2. Pressure Gauge for Air with regulator, degree of filtration 20µm and condensate drain (supplied on request)
3. Pressure Gauge for O₂ with regulator, degree of filtration 20µm and condensate drain (supplied on request: third gas Control Unit)
4. Free Fine Gauge Thermocouple (sensor, supplied with Specimen Temperature Feedback configuration)

5. 1mm thickness glass (for Multi Well plate configuration)
6. Screwdriver 325 0.5x3x75

1.6. Equipment Required (*Not supplied*)

1. CO₂ reservoir
2. Air reservoir (It can be substituted by a compressed air line)
3. O₂ reservoir
4. Pressure reduction gears for O₂, CO₂ reservoir and Air reservoir (or compressed Air line) exit to be ready for rigid tubes of 6mm OD
5. Pressure Gauge for Air with regulator, degree of filtration 20µm and condensate drain (provided by Okolab on request)

2. Connections

2.1. Tubings connection (air/O₂ and CO₂)

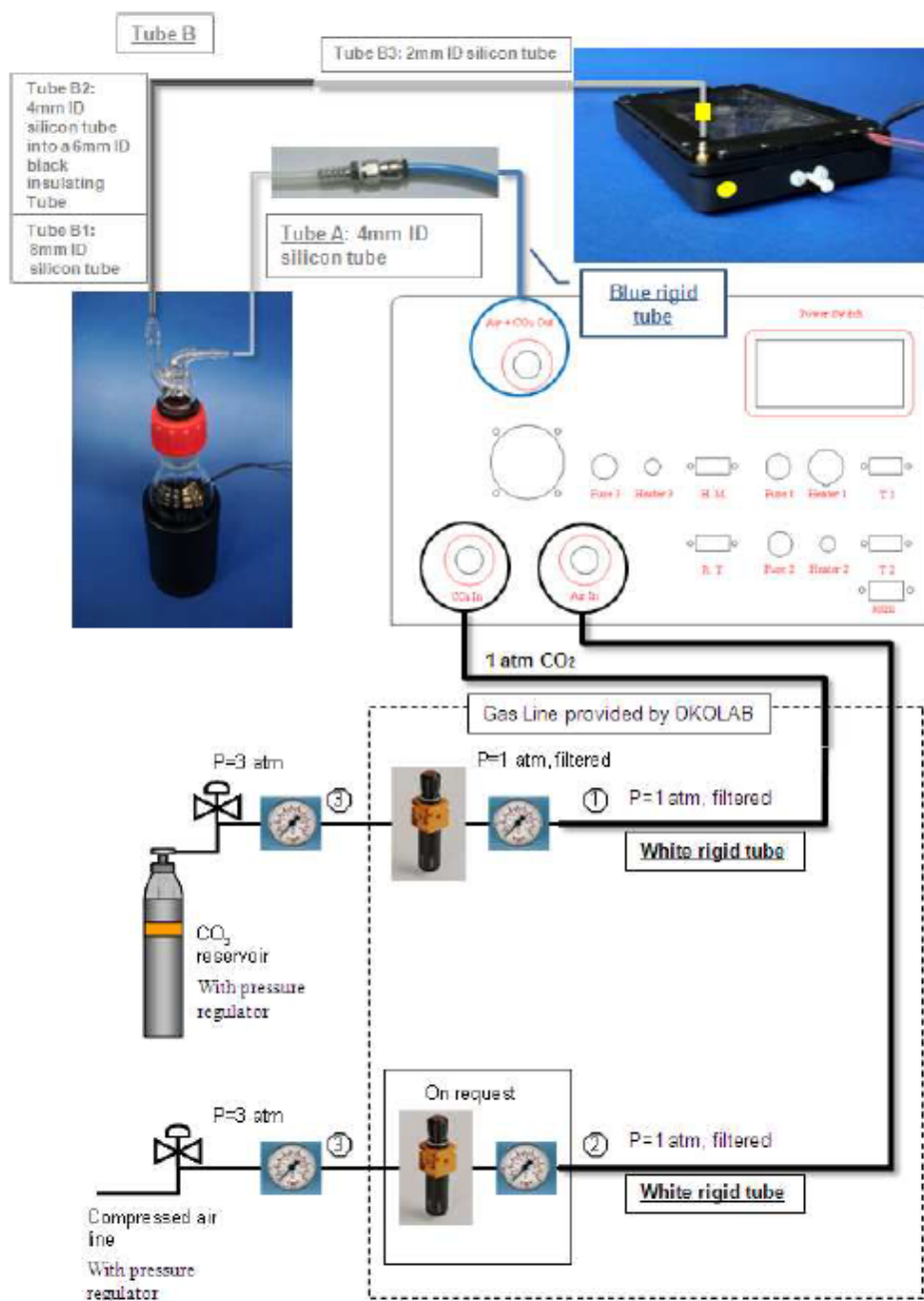


Figure 2: Complete gas lines scheme.

2.1.1. Gas reservoirs to Control Unit

Provide your system of CO₂ reservoir with safety valve and pressure gauge with pressure rigid tubes 6 mm OD exiting (for further details, please contact Okolab hardware support)

Provide your system of Air reservoir (Okolab suggests to use a compressed Air line) with safety valve and pressure gauge with pressure rigid tubes 6 mm OD exiting

Provide your system of O₂ (optional configuration) reservoir, or compressed line, with safety valve and pressure gauge with pressure rigid tubes 6 mm OD exiting

Mount the Pressure Gauge for CO₂ with regulator, degree of filtration 20µm and condensate drain (supplied)

Be sure that Air stream is FILTERED and with a STABLE Pressure Gauge otherwise mount another Pressure Gauge for air with regulator, degree of filtration 20µm and condensate drain (non supplied, if you need ask to Okolab for a prompt shipping)

Please use the white rigid tubes, 6mm OD 3 m long, (1, 2) to connect the controlled (filtered and at P=1 atm) flows of air and CO₂ (O₂ optional configuration) from Pressure Gauges to the Control Unit. Simply push in (until the end of run) the tubes into the Swift-Fit connectors (Air IN and CO₂ IN on the rear of the Control Unit. If you want to remove the tube, please, pull the tube while pushing the black ring on the Swift-Fit connector. If you have other filters or devices (i.e. filters for bacterial) insert them before final Pressure Gauges

Follow the arrow on the Pressure Gauge for the correct gas In-Out.

In order to avoid gas leak and correctly insert the tube, please, strongly push the tube into the Swift-Fit connector. (See Figure 4)

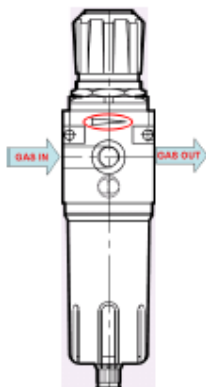


Figure 3: Pressure Gauge (provided by Okolab): Correct Gas Input – Output.



Figure 4: Avoid gas leak: strongly push the tube into the Swift-Fit connector

2.1.2. Control Unit to Humidifying module

Please connect the blue rigid tube, 6mm OD, 2 m long, to the 'Air + CO₂ Outlet', from one side, and to the Swift-Fit connector of the TUBE A (4mm ID silicon transparent tube) on the other side.



Figure 5: Connecting the blue rigid plastic tube

Please, connect the free end of the TUBE A (4mm ID silicon transparent tube) to the humidifying module 90° glass connector.

2.1.3. Humidifying module-Micro to Environmental Chamber

Tube B is the connection of:

- a. 8mm ID silicon tube (0.2m) to connect to the 180° glass connector of the Humidifying module +
- b. 4mm ID silicon tube into a 6 ID black insulating Tube (0.5m) +
- c. 2mm ID silicon tube (0.5m), yellow marked to connect to the aluminum barb connector placed on the Micro-Environmental Chamber.

IMPORTANT

Avoid narrowing of the tubes and formation of condensation inside them. Please, periodically check gas are correctly flowing and tubes are properly connected.

2.2. Heating and temperature cables connections

2.2.1. Control Unit front panel

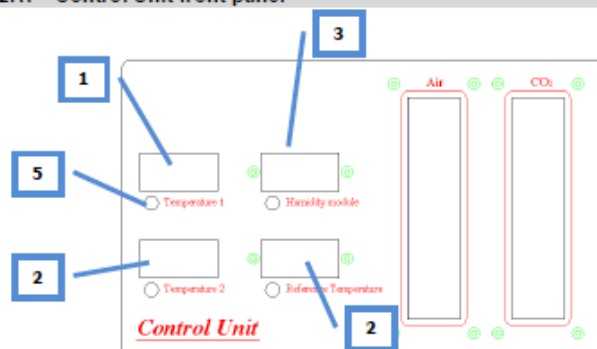


Figure 6. Front panel

1. Display of Temperature 1.
 - Chamber temperature feedback: it displays base chamber temperature and its set point temperature.
 - Specimen temperature feedback: it displays specimen temperature and its set point temperature.

2. Display of Temperature 2. It displays temperature of the chamber lid and its set point temperature.
3. Display of Humidity module temperature. Optional, provided with the Humidifying module Heater. It displays Humidity module temperature and its set point temperature.
4. Display of Reference Temperature (Alarm). In case of Specimen temperature feedback mechanism it controls the maximum temperature allowed.
5. 'Heater on' led: it lights when the heater is powered.

2.2.2. Control Unit rear panel

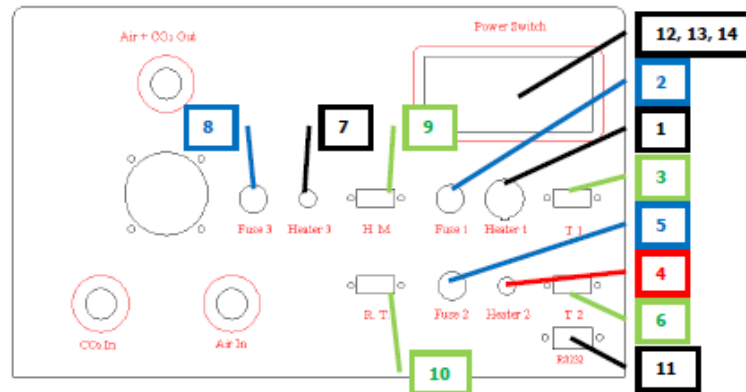

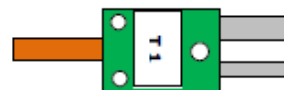


Figure 7. Back panel

1. Heater 1 connection: for Base chamber heating
2. Fuse 1 box: # 1, 2.50 A Fast Fuse.
3. Thermocouple connector T1
 - Chamber temperature feedback: for Base chamber temperature measuring and heating, OR
 - Specimen temperature feedback: for Specimen temperature measuring and chamber heating.
4. Heater 2 connection: for Lid plate heating
5. Fuse 2 box: # 1, 1.60 A Fast Fuse.
6. Thermocouple connector T2 for Lid plate temperature measuring and heating
7. Heater 3 connection: for humidifying module-heating (optional).
8. Fuse 3 box: # 1, 1.60 A Fast Fuse.
9. Thermocouple connector H.M. for humidifying module temperature measuring and heating
10. Thermocouple connector R.T. (Alarm)
 - Specimen temperature feedback: for temperature Base chamber temperature alarm function.
11. Serial port: (Supplied with Software Read Temperature, optional) to read incubator temperature and store the data in computer memory.
12. Power fuse: # 2, 1 A Time Lag Fuse, 100-240 V AC.

13. Power Supply connection.
14. Power Switch.

 Tip: Notice the correspondence between the thermocouple connector (T1, T2, and H.M.) on the rear of the control unit and the labels on the male thermocouple connectors.



2.2.3. Standard configuration (Chamber temperature feedback)

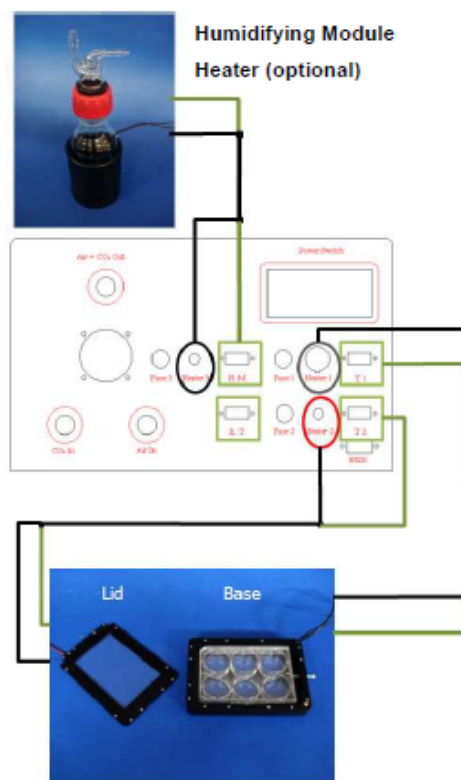


Figure 8: Complete cables scheme for Chamber control feedback configuration

- 1) Base plate to Control Unit
 - Connect the cables coming from the base to 'Heater 1' and 'T1' connectors on the rear of the control unit.
- 2) Lid plate to Control Unit
 - Connect the cables coming from the Lid to 'Heater 2' and 'T2' connectors on the rear of the control unit.
- 3) Humidifying module heater to Control Unit (Optional)

-
- Connect the cables coming from the humidifying module heater to 'Heater 3' and 'H.M.' connectors on the rear of the control unit.

3. Electric Chamber

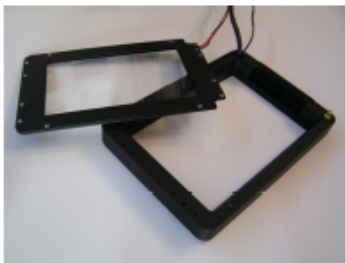


Figure 9. Electric MSI overview, base plate and lid without adapters

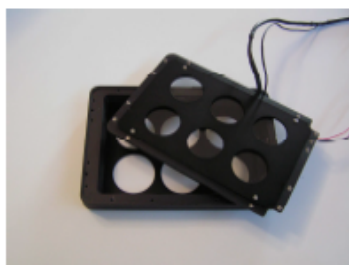


Figure 10: Electric MSI overview, base plate and lid with 6 Well adapter

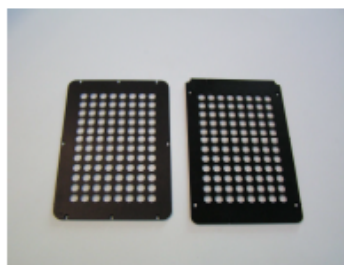


Figure 11: Interchangeable plate adapters for 2 well, glass slides and 96 multiwell

The standard equipments are:

1. Base
2. Lid
3. One couple base and lid adapters for Multi well plates, Petri dishes or glass slides.

The optional equipments are:

1. Additional Body for standard base. It converts the standard base for short multi well plate into the base for shallow multi well plates (22 mm). See Figure 13
2. Base and lid adapters for 12, 24, 48, 96 well plate.
3. Base and lid adapters for 35 mm Petri dish, 60 mm Petri dish, Labtek and any flat support
4. Customized adapters upon request: please ask to Okolab for further details about accessories and news.

3.1. Electric chamber parts description

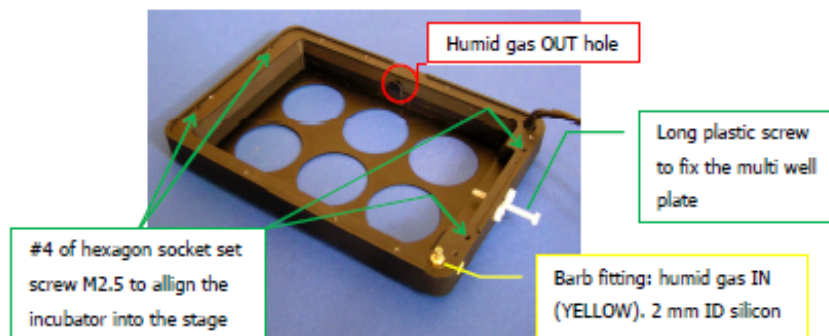


Figure 12. Standard base

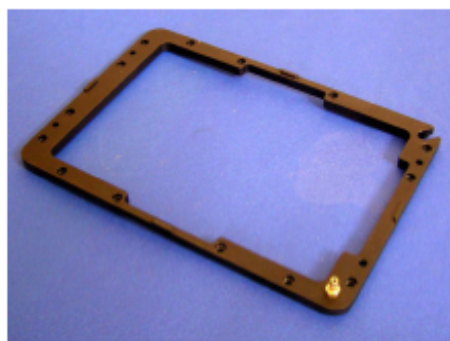


Figure 13. Additional body for standard base. Spacer to increment the base vertical height

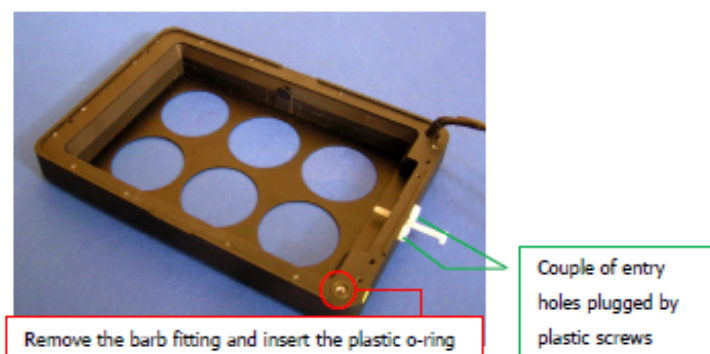


Figure 14, Standard base without barb fitting

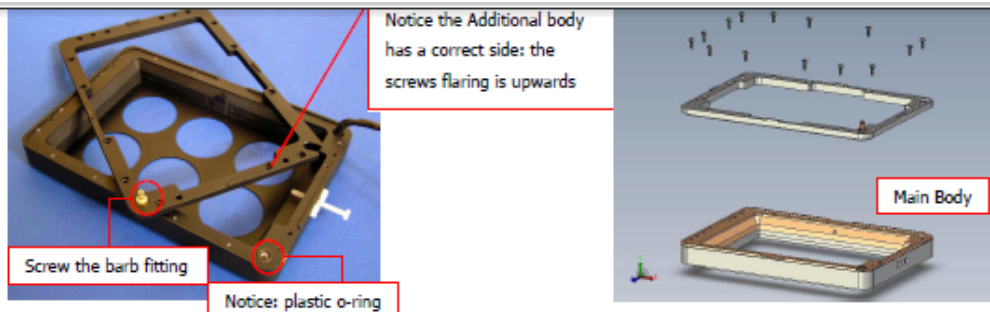


Figure 15, Put the Additional body on the Standard base

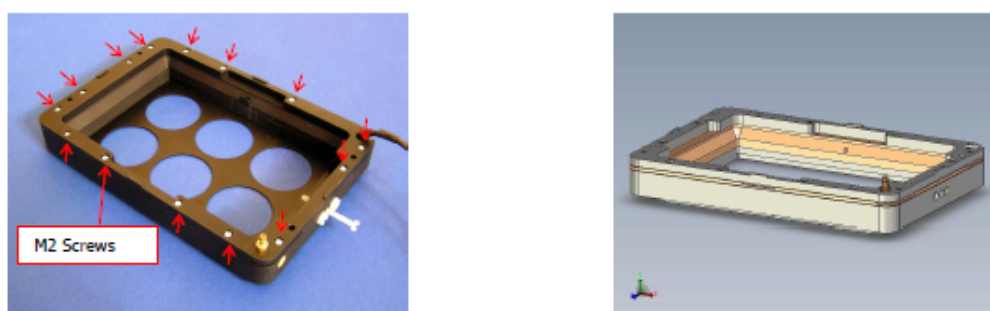


Figure 16, Tighten the M2 screws

3.2. Add-Remove inserts

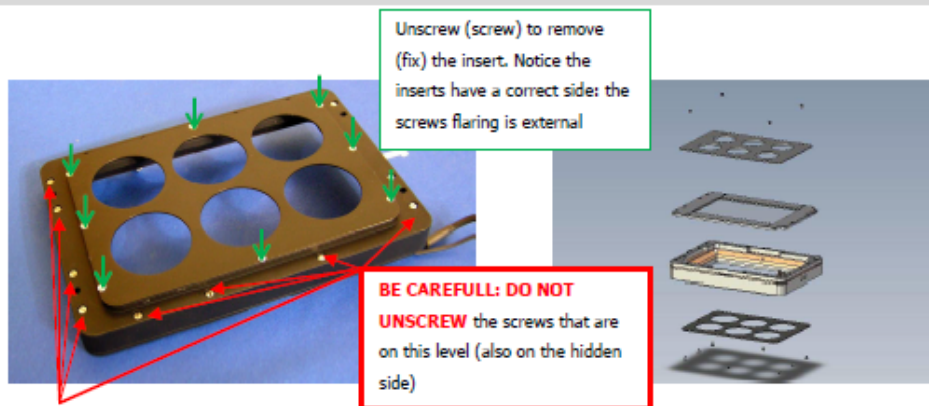


Figure 17, Stage incubator base and lid inserts

You can easily change chamber configuration from Multi Well to Petri dish version by substituting base and lid inserts. Please, in Multi-well configuration once fixed the multi well adapter (see Figure 17), to reduce thermal gradient inside the chamber, put the 1mm thickness glass inside the chamber, from the top, on the insert.

4. Temperature control mechanism



The Okolab electrical stage incubation chamber is heated by miniaturized DC electrical resistances at low voltage (24V). The specimen, contained in plastic or glass support for cells culture, is maintained at 37.0°C thanks to a constant metal warming up ensured by controllers designed. To ensure a specimen temperature of 37.0°C both lid and base are maintained at a temperature that depends on the ambient temperature and the cells culture support used (Multi-well plate or Petri dish).

The chamber control temperature can work in two different modalities:

1) Chamber temperature feedback:

In this configuration, the thermocouple reads the temperature of the incubating chamber. A careful calibration performed in our laboratories guarantees that specimen temperature is maintained at the desired value. The advantage of this solution is that the thermocouple is not visible since it is embedded into the chamber.

a. Advantages:

- Easier than "Specimen temperature feedback" configuration to use
- Fast experiment start up 
- Well suited for multi user task 


b. Disadvantage:

- It needs of calibration in case of ambient temperature or incubation temperature (set point temperature) variations


2) Specimen temperature feedback:

In this configuration, the thermocouple is a thin flexible green wire that reads the temperature of a reference well placed in the incubating chamber, very close to the specimen. The advantage of this configuration is in the accuracy of the temperature control. Simple manipulation is required to stick the thermocouple into the reference well with some adhesive tape.

a. Advantages:

- Direct control of the specimen temperature 
- Independence from ambient temperature

b. Disadvantage:

- It needs to set the controllers parameters by changing supports to optimized thermal control (the parameter are provided by Okolab)
- Require skilled operator 

4.1. PID controllers calibration (Calibration Offset)

The calibration was performed, the first time, in the Okolab lab. The calibration document shows the 'calibration offset values' (red) for every controller (see Figure 18).

Once two years, it is suitable to perform the calibration. Use the fine thermocouple sensor provided by Okolab, connected to T1 thermocouple connectors (see Figure 8) as sensor. Use an accurate thermostatic water bath, set to 37°C, as reference temperature.

- Set the Offset temperature to 0, please see paragraph 5.3.
- Please, disconnect the cables shown in Figure 8
- Insert the fine thermocouple sensor (this calibration sensor can be provided by Okolab) into T1 connector (Figure 8)
- Put the free end of the fine calibration sensor in the water bath (in steady state and set at 37.0°C). Please, fix the thermocouple to a support in order to maintain a constant position of the sensor in the warm water.
- Wait about 30 min to reach a stable temperature
- Register the temperature difference between the water bath temperature (37.0°C) and the displayed 'Temperature 1'.
- Calibration Offset 1 (@ T=37.0°C) = (T(water bath set to T=37.0°C) – Temperature 1) for Temperature 1 > T (water bath) or
Calibration Offset 1 (@ T=37.0°C) = - (T(water bath set to T=37.0°C) + Temperature 1) for Temperature 1 < T (water bath)
- Repeat the sequence for 30°C, 35°C, 40°C
- Calibration Offset 1 AVG = Average (Calibration offset 1 (@ T=37.0°C), (@ T=30.0°C), (@ T=35.0°C), (@ T=40.0°C))
- Insert this calibration value as COSTANT offset (PV BIAS) to add (or subtract) in 'Temperature 1' PID. See paragraph 5.3.
- Please, after meter calibration, compare the temperature difference between the water bath set point temperature (37.0°C) and the displayed temperature 1.
- Substitute the new calibration value to the offset 1 AVG (then offset 2 AVG) reported in the Calibration document (see
- Repeat for T2, H.M. and alarm controller

Okolab S.p.A.
Via Garibaldi 41, Pinerolo, Italy
0110-0291001 fax: 0291-0291002
phone: +39 011 229 4600-08 001 876 4102
E-Mail: info@okolab.it
www.okolab.com

Calibration document Cod-CD-E-MSI 001.08

Order number: _____
Control unit serial number: _____
Calibration date: _____

PID T1		
Water bath temperature T°C	Measured temperature T1 (°C)	Calibration Offset 1 (AVG)
30		
35		
37		
40		

PID T2		
Water bath temperature T°C	Measured temperature T2 (°C)	Calibration Offset 2 (AVG)
30		
35		
37		
40		

PID U.M.		
Water bath temperature T°C	Measured temperature T U.M. (°C)	Calibration Offset U.M. (AVG)
30		
35		
37		
40		

PID Alarm		
Water bath temperature T°C	Measured temperature T Alarm (°C)	Calibration Offset Alarm (AVG)
30		
35		
37		
40		

The offset 1 is: _____
The offset 2 is: _____
The offset U.M. is: _____
The offset Alarm is: _____

Calibrated Signature: _____
Checker Signature: _____

Figure 18: Calibration document, facsimile

4.2. Chamber temperature feedback

In this configuration, the thermocouple reads the temperature of the incubating chamber. If ambient temperature differs from 23°C more than 2°C or the support plate changes, consider to modify the parameters of the controllers T1 and T2 ('Secondary Offset'), in order to have the specimen at the correct temperature. Notice that the parameters for the Humidifying Module heater (PID H.M.) are constant. The calibration has been performed in the Okolab lab.

4.2.1. Chamber configurations and controllers parameters

Notice the factory parameters depend on the plate adapter you order.

The default values are optimized for $T_{Ambient} 23.0 \pm 1.0^\circ\text{C}$ and active Humidifying Module heater. Anyway, the controllers PID T1 and PID T2 parameters do not depend on Humidifying Module presence.

'Secondary offset' values are calculated with the following targets:

1. Specimen temperature $37 \pm 0.3^\circ\text{C}$
2. Avoid condensation on the lid glass
3. Improve the gas stream humidity level

Thanks to a new calibration (see 4.2.2), the customer can find new Secondary offset, at different set point value and/or at different ambient temperature. Please, do not insert control parameters different from the values reported in this manual for each configuration.

Standard 6 Well Plate			
	PID T1	PID T2	PID H.M.
Set Point (SV)	37.0	37.0	37.0
'Total Offset' = 'Secondary Offset' + 'Calibration Offset'			
Total Offset (PV)	-4.2+Calibration Offset 1 (AVG)	-8.2+ Calibration Offset 2 (AVG)	-3.0+ Calibration Offset H.M. (AVG)
controllers parameters			
P	010.0	010.0	010.0
I	0240	0240	0240
d	0120	0120	0120
Ar	0060	0060	0060
t	0002	0002	0002
df	16	16	16

Table 1: $T_{Ambient} 23.0 \pm 1.0^\circ\text{C}$, standard 6 Well plate, with Humidifying Module heater.

	PID T1	PID T2	PID H.M.
Set Point (SV)	37.0	37.0	37.0
'Total Offset' = 'Secondary Offset' + 'Calibration Offset'			
Total Offset (PV)	-1.9+Calibration Offset 1 (AVG)	-5.9+ Calibration Offset 2 (AVG)	-3.0+ Calibration Offset H.M. (AVG)
'controllers parameters'			
P	020.0	020.0	020.0
I	0240	0240	0240
d	0120	0120	0120
Ar	0060	0060	0060
t	0002	0002	0002
df	16	16	16

Table 2: $T_{Ambient} 23.0 \pm 1.0^{\circ}\text{C}$, standard 96 Well plate, with Humidifying Module heater.

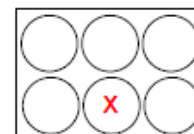
#2 35mm petri dish and #1 glass slide

	PID T1	PID T2	PID H.M.
Set Point (SV)	37.0	37.0	37.0
'Total Offset' = 'Secondary Offset' + 'Calibration Offset'			
Total Offset (PV)	-2.0+Calibration Offset 1 (AVG)	-6.0+ Calibration Offset 2 (AVG)	-3.0+ Calibration Offset H.M. (AVG)
'controllers parameters'			
P	010.0	010.0	010.0
I	0240	0240	0240
d	0120	0120	0120
Ar	0060	0060	0060
t	0002	0002	0002
df	16	16	16

Table 3: $T_{Ambient} 23.0 \pm 1.0^{\circ}\text{C}$, #2 35mm petri dish and #1 glass slide, with Humidifying Module heater.

4.2.2. Secondary offset calibration with 6 well Plate configuration

The goal is to increase or decrease the controlled metal cover and lid temperature so that the specimen is at the wished temperature (37.0°C). By measuring the specimen temperature, during steady state experimental condition, the offset value can be estimated. We use one sensor to check the temperature, e.g., of the well 'X' in a 6 well plate, as shown in the scheme. We fix the end of the fine sensor on the internal base of the well using scotch tapes. Then, in order to simulate a standard experiment we fill the wells with water, instead of the culture medium.



Please,

- 1) Perform the calibration in steady state conditions. Please, monitor the room temperature and reduce airstream to reduce the forced convection. Please, pay attention to the airstream coming out from air conditioner.
- 2) By using a temperature meter, provided of fine sensor (ask Okolab for further support), you have to monitor:
 - a. The temperatures in one well of the multi plate

In Figure 19 a plot, temperature vs. time, shows how to realize the temperature calibration. The ambient temperature is about $23 \pm 1^{\circ}\text{C}$.

Let us define:

- 1) Base Temperature = Temperature 1 (37.0°C) + 'secondary offset 1'
- 2) Lid Temperature = Temperature 2 (37.0°C) + 'secondary offset 2'
- 3) 'Secondary offset 2' = 'Secondary offset 1' + 4°C , to avoid lid condensation

With these assumptions the ONLY parameters to find is 'Secondary offset 1' by making some trials.

FIRST TRIAL

As first trial, we set 'Secondary offset 1' -2.0°C (then 'Secondary offset 2' -6.0°C). In order modify the offset temperature (PV bias), please, follow the paragraph 5.4.

The system response involves the well, after a transient; reaches about 34.1°C , in steady state. See Figure 19.

- Set point 1 = Set point 2 = Set point value (SV): 37.0°C .
- Secondary Offset 1: -2.0°C , which corresponds to a base temperature of 39.5°C .
- Secondary Offset 2: -6.0°C , which corresponds to a base temperature of 42.5°C .
- Then, the 'Total Offset 1' (PV Bias) = 'Calibration Offset 1 (AVG)' + 'Secondary Offset 1' and,
- The 'Total Offset 2' (PV Bias) = 'Calibration Offset 2 (AVG)' + 'Secondary Offset 2'
- Response: well temperature 34.1°C at Ambient temperature 23.0°C .

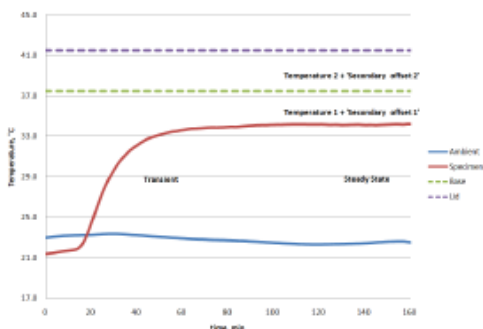


Figure 19. Temperature profiles, Ambient 23.0°C , Set point 37.0°C and 'Secondary offset 1' -2.0°C .

SECOND TRIAL

Next step will be to increase the 'Secondary offset 1' (then, the Secondary offset 2 = Secondary offset 1 + 4°C) so that the specimen temperature is 37°C .

We set 'Secondary offset 1' -4.2°C (then 'Secondary offset 2' -8.2°C). In order modify the offset temperature (PV bias), please, follow the paragraph 5.4.

The system response involves the well, after a transient; reaches $37.0 \pm 0.3^{\circ}\text{C}$, in steady state. See Figure 20.

- Set point 1 = Set point 2 = Set point value (SV): 37.0°C .
- Secondary Offset 1: -4.2°C , which corresponds to a base temperature of 41.5°C .
- Secondary Offset 2: -8.2°C , which corresponds to a base temperature of 45.5°C .
- Then, the 'Total Offset 1' (PV Bias) = 'Calibration Offset 1 (AVG)' + 'Secondary Offset 1' and,
- The 'Total Offset 2' (PV Bias) = 'Calibration Offset 2 (AVG)' + 'Secondary Offset 2'
- Response: well temperature $37.0 \pm 0.3^{\circ}\text{C}$ at Ambient temperature 23.0°C .

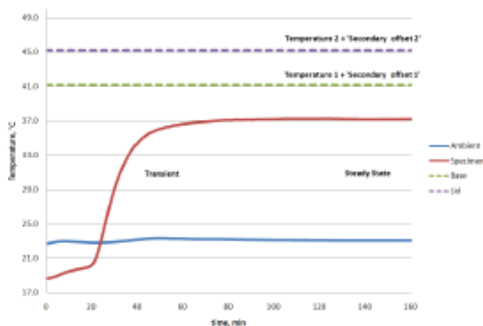


Figure 20. Temperature profiles, Ambient 23.0°C , Set point 37.0°C and 'Secondary offset 1' -4.2°C .

It is possible to list the 'Secondary offset' for different specimen temperature, at different ambient temperature, as shown in Table 4.

Ambient temperature [°C]	Desired well temperature [°C]	Secondary Offset 1 [°C]	Secondary Offset 2 [°C]
23.0 ± 1.0 (Suggested ambient temperature)	32.0	2.0	-2.0
	33.0	0.8	-3.2
	34.0	-0.5	-4.5
	35.0	-1.7	-5.7
	36.0	-3.0	-7.0
	37.0 (Default)	-4.2 (Default)	-8.2 (Default)
	38.0	-5.5	-9.5
	39.0	-6.7	-10.7
19.0 ± 1.0	32.0	1.4	-2.6
	33.0	0.0	-4.0
	34.0	-1.4	-5.4
	35.0	-2.9	-6.9
	36.0	-4.3	-8.3
	37.0	-5.7	-9.7
	38.0	-7.1	-11.1
	39.0	-8.6	-12.6

Table 4: Secondary offset estimated value: extrapolated values from trend lines equations. Configuration; standard 6 Well adapter, with Humidifying Module heater.

Standard values are pointed out (specimen temperature 37°C).

Please, ask to Okolab for further info or visit www.oko-lab.com.

4.3. Specimen temperature feedback

In case you use 'Specimen temperature feedback' configuration (please see paragraph 7.2 for connections), you need to insert the following set of parameters in the controllers. Remember the controllers parameters depend on cells culture support.

Standard 6 Well Plate				
	PID T1 = Specimen Temp.	PID T2	PID H.M.	PID Alarm
Set Point (SV)	37.0	37.0	37.0	
Total Offset' = 'Secondary Offset' + 'Calibration Offset'				
Total Offset (PV)	Calibration Offset 1 (AVG) (Secondary Offset=0)	-5.5+ Calibration Offset 2 (AVG)	-3.0+ Calibration Offset H.M. (AVG)	
controllers parameters				
P	005.0	010.0	010.0	
I	0720	0240	0240	
d	0300	0260	0120	
Ar	0060	0060	0060	
t	0010	0002	0002	
df	08	08	16	

Table 5: $T_{Ambient} 23.0 \pm 1.0^{\circ}\text{C}$, standard 6 Well plate, with Humidifying Module heater.

Standard 96 Well Plate				
	PID T1 = Specimen Temp.	PID T2	PID H.M.	PID Alarm
Set Point (SV)	37.0	37.0	37.0	
Total Offset' = 'Secondary Offset' + 'Calibration Offset'				
Total Offset (PV)	Calibration Offset 1 (AVG) (Secondary Offset=0)	-4.0+ Calibration Offset 2 (AVG)	-3.0+ Calibration Offset H.M. (AVG)	
controllers parameters				
P	005.0	010.0	020.0	
I	0720	0240	0240	
d	0300	0260	0120	
Ar	0050	0050	0060	
t	0005	0002	0002	
df	08	08	16	

Table 6: $T_{Ambient} 23.0 \pm 1.0^{\circ}\text{C}$, standard 96 Well plate, with Humidifying Module heater.

#2 35mm petri dish and #1 glass slide				
	PID T1 = Specimen Temp.	PID T2	PID H.M.	PID Alarm
Set Point (SV)	37.0	37.0	37.0	
Total Offset' = 'Secondary Offset' + 'Calibration Offset'				
Total Offset (PV)	Calibration Offset 1 (AVG) (Secondary Offset=0)	-5.5+ Calibration Offset 2 (AVG)	-3.0+ Calibration Offset H.M. (AVG)	
controllers parameters				
P	005.0	010.0	010.0	
I	0720	0240	0240	
d	0300	0260	0120	
Ar	0060	0060	0060	
t	0010	0002	0002	
df	08	08	16	

Table 7: $T_{Ambient} 23.0 \pm 1.0^{\circ}\text{C}$, #2 35mm petri dish and #1 glass slide, with Humidifying Module heater.

5. Controller description

5.1. Display functions

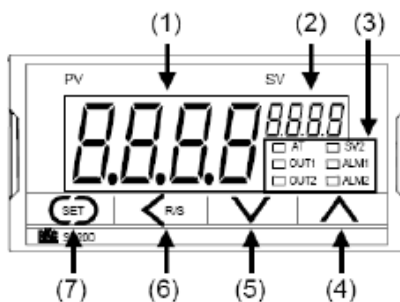


Figure 21. Display description

The gray background indicates previously set parameter or unnecessary function. For further information see the digital controller manual (see Appendix). The following steps show all the necessary function for a correct use of the instrument.

1. Measured value (PV) display [Green]
 - Displays PV or various parameter symbols.
2. Set point value (SV) display [Orange]
 - Displays SV or STEP Set point value (SV1, SV2).
 - Displays various parameter Set point values.
3. Indication lamps
 - Auto tuning (AT) lamp [Green]
 - Flashes during auto tuning activated.
 - (After autotuning is completed: AT lamp will become OFF)
 - Output lamps (OUT1, OUT2) [Green]
 - OUT1: Lights when output 1 is turned on.
 - OUT2: Lights when output 2 is turned on.
 - STEP set value (SV2) lamp [Orange]
 - Lights when the SV2 of STEP function is selected.
 - Alarm lamps (ALM1, ALM2) [Orange]
 - ALM1: Lights when alarm 1 is turned on.
 - ALM2: Lights when alarm 2 is turned on.
4. UP key
 - Increase numerals.

5. DOWN key
 - Decrease numerals.
6. Shift & R/S key
 - Shift digits when settings are changed. Selects the RUN/STOP function.
7. Set key
 - Used for parameter calling up and Set point value registration.

Please, before modifying the PID parameters, carefully read the following instruction and/or the linked Digital Controller SA200 Instruction Manual

5.2. Set point temperature and Offset temperature range

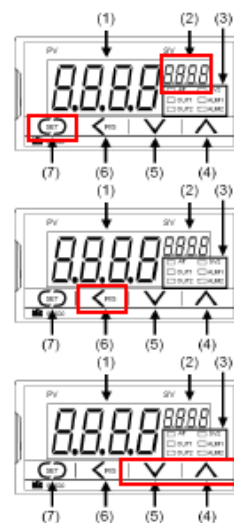
The offset is a calibrated deviation that forces the read temperature of the meter in order to calibrate the instrument.

Set point temperature range	30÷45
Offset temperature range	-15÷5
$T_{\text{controlled}} = (\text{Set point temp}) - (\text{Offset temp})$	

5.3. Change the Set point temperature

The default set point value is 37.0°C.

1. Select the SV setting mode
Press the SET key (7) at PV/SV monitor screen until SV setting screen is displayed.
2. Shift the blinking digit
Press the <R/S key (6) to blink the digit to change. The blinking digit indicates which digit can be set.
3. Change the Set point value
Press the UP key (4 and 5) to change the number.
4. Store the Set point value
Press the SET key (7) to store the new Set point value.
5. Come back to PV/SV display mode
Press SET key (7) for few seconds or leave it and the display automatically returns to the PV/SV display mode.



5.4. Change the offset temperature

The value set in the PV bias is added to the input value (actual measured value) to correct the input value. Default parameters are at paragraph 4.2.1.

Pressing the SET key after the setting end shifts to the next parameter.

1. Select the Parameters setting mode

Press the SET key (7) at PV/SV monitor screen for 2 seconds.

2. Shift to the next parameter.

Press the SET key (7) until Pb (PV bias).

3. Change the offset value

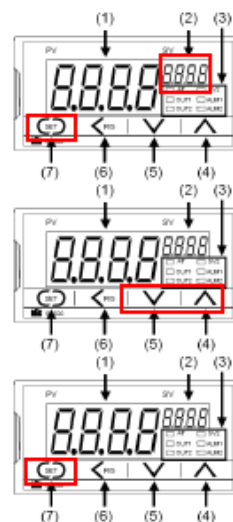
Press the UP key (4 and 5) to change the number.

4. Store the Set point value

Press the SET key (7) to store the new Set point value.

5. Come back to PV/SV display mode

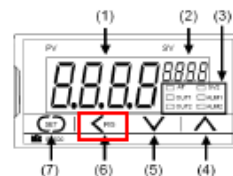
Press SET key (7) for few seconds or leave it and the display automatically returns to the PV/SV display mode.



5.5. Stop the controller

1. Shift & R/S key (6 in Figure 21. Display description)

- Click 2 seconds to selects the RUN/STOP function.



6. Flow Meters regulation

6.1. Two Flow meters Control Unit


IMPORTANT


Do not use the flow meters as closing-opening valves. Once regulated the flow rate (at P=1bar, see Error! Reference source not found.), use the flow meters carefully only for fine regulations.

Open the gas valves about 15 minutes before inserting the specimen in the Micro Environmental Chamber. Please, follow carefully scheme in Figure 2: Complete gas lines scheme.


Target Gas Percentage [%]		Gas flow rate values to set [NL/min]		
Air	CO ₂	Air	CO ₂	Total
95.00	5.00	0.80	0.04	0.84
95.00	5.00	1.00	0.05	1.05
95.00	5.00	1.20	0.06	1.26

Table 8. Flow meter regulation, two flow meters control unit. [NL = normal liter]

 **Tip** ► If you need, ask Okolab for personalized Gas Percentage Tables. ◀

 **Tip** ► Same color is equivalent to same gas percentage. ◀

- 'Target Gas Percentage' indicates the stream gas percentage that the operator wants during the experiment.
- 'Gas flow rate values to set', in Normal liter per minute [NL/min], are the values of gas flow rate to set on the graduated scale (see Figure 22).
- 'Total' indicates the measured total gas stream flow rate.

 **Example** ► The target Air percentage is 95.00%, the target CO₂ percentage is 5.00%. In Table 8, three possibilities that realize the required gas percentage are. Notice that the values are a compromise between CO₂ consumption, condensation (normally it decreases if Total gas stream flow rate increases), medium evaporation (normally it decreases if Total gas stream flow rate decreases). We could consider the second line in Table 8. So, we regulate the two flow meters to obtain the desired relative quantity of air and CO₂, as shown in Figure 22. Notice that the correct position of the indicator (ball) is about in its middle. The gas stream mix contains, now, 95.00% of Air and 5.00% of CO₂. ◀

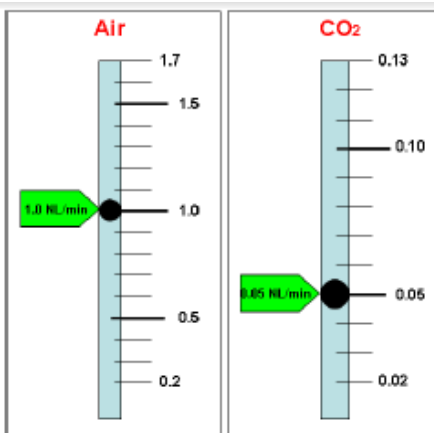


Figure 22. Flow meters graduated scales, example for two gas lines.

If you use a single reservoir of air+5% CO₂ the total gas steam flow rate suggested is 0.8 l/min.

6.2. Three Flow meters Control Unit

IMPORTANT

Do not use the flow meters as closing-opening valves. Once regulated the flow rate (at P=1bar, see Error! Reference source not found.), use the flow meters carefully only for fine regulations.

Open the gas valves about 15 minutes before inserting the specimen in the Micro Environmental Chamber. Please follow carefully scheme in Figure 2: Complete gas lines scheme.

	Target Gas Percentage [%]			Gas flow rate values to set [NL/min]			
	Air/N ₂	CO ₂	O ₂ /Other	Air/N ₂	CO ₂	O ₂ /Other	Total
1	95.00	5.00	0.00	0.80	0.04	0.00	0.84
2	95.00	5.00	0.00	1.00	0.05	0.00	1.05
3	95.00	5.00	0.00	1.20	0.06	0.00	1.26
4	94.00	5.00	1.00	1.70	0.09	0.02	1.81
5	93.00	5.00	2.00	0.90	0.05	0.02	0.97
6	93.00	5.00	2.00	1.30	0.07	0.03	1.40
7	92.00	5.00	3.00	0.90	0.05	0.03	0.98
8	92.00	5.00	3.00	1.30	0.07	0.04	1.41
9	91.00	5.00	4.00	0.90	0.05	0.04	0.99
10	91.00	5.00	4.00	1.10	0.06	0.05	1.21
11	90.00	5.00	5.00	0.70	0.04	0.04	0.78
12	90.00	5.00	5.00	0.90	0.05	0.05	1.00
13	90.00	5.00	5.00	1.10	0.06	0.06	1.22
14	89.00	5.00	6.00	0.90	0.05	0.06	1.01
15	88.00	5.00	7.00	0.90	0.05	0.07	1.02
16	87.00	5.00	8.00	0.90	0.05	0.08	1.03
17	86.00	5.00	9.00	0.70	0.04	0.07	0.81
18	86.00	5.00	9.00	1.00	0.06	0.11	1.17
19	85.00	5.00	10.00	0.70	0.04	0.08	0.82
20	85.00	5.00	10.00	1.00	0.06	0.12	1.18
21	84.00	5.00	11.00	0.80	0.05	0.11	0.96
22	83.00	5.00	12.00	0.80	0.05	0.12	0.97
23	82.00	5.00	13.00	0.70	0.04	0.10	0.84
24	82.00	5.00	13.00	0.80	0.05	0.13	0.98
25	81.00	5.00	14.00	0.60	0.04	0.11	0.75
26	80.00	5.00	15.00	0.60	0.04	0.12	0.76
27	79.00	5.00	16.00	0.60	0.04	0.13	0.77
28	78.00	5.00	17.00	0.50	0.03	0.10	0.63

Table 9: Flow meter regulation, three flow meters control unit. [NL = normal liter]

Tip ► If you need, ask Okolab for personalized Gas Percentage Tables. ◀

Tip ► Same color is equivalent to same gas percentage. ◀

Tip ► The first three lines, pink-colored, is the two gas lines case. ◀

- 'Target Gas Percentage' indicates the stream gas percentage that the operator wants during the experiment.
- 'Gas flow rate values to set', in Normal liter per minute [NL/min], are the values of gas flow rate to set on the graduated scale (see Figure 23).

- 'Total' indicates the measured total gas stream flow rate.

133

Example ► The target Air/N₂ percentage is 91.00%, the target CO₂ percentage is 5.00%, the target O₂/Other percentage is 4.00%. In Table 9 two possibilities that realize the required gas percentage are in the ninth and the tenth line. Notice that the values are a compromise between gas consumption, condensation (normally it decreases if Total gas stream flow rate increases) and medium evaporation (normally it decreases if Total gas stream flow rate decreases) and max percentage error. We could consider the ninth line in Table 9. So, we regulate the three flow meters to obtain the desired relative quantity of gas, as shown in Figure 23. Notice that the correct position of the indicator (black sphere) is about in the middle. The gas stream mix contains, now, 91.00% of Air/N₂, 5.00% of CO₂ and 4.00% of O₂/Other. ◀

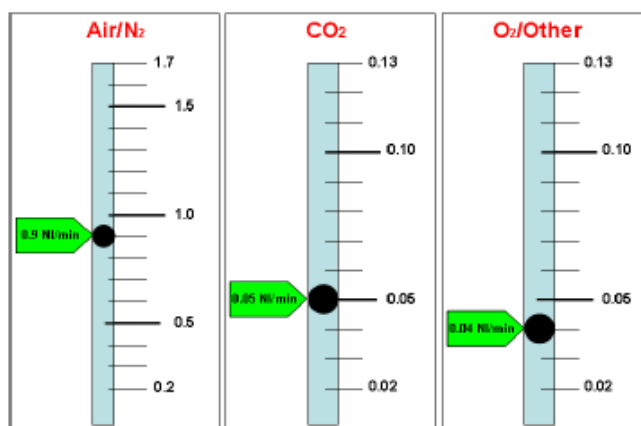


Figure 23. Flow meters graduated scales, example for three gas lines.

7. Electrical Microscope Stage Incubator USE

Depending on the system modality you choose (please, read carefully paragraph 4) follow the next instructions:

7.1. Chamber temperature feedback

7.1.1. Multi well adapters

Once fixed the multi well adapter (see Figure 17), to reduce thermal gradient inside the chamber, put the 1mm thickness glass inside the chamber, from the top, on the insert.

1. Insert the multi well plate in the chamber with the specimen. (See Figure 24)

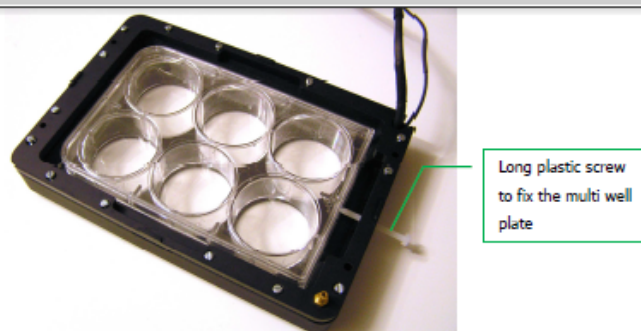


Figure 24: Chamber temperature feedback: 6 well configuration

2. Block it screwing the white plastic screw (Figure 12 and Figure 24).
3. Switch on the Control Unit.
4. Close the Chamber Base with the Lid.

7.1.2. Petri dish adapter (technically qualified personnel)

1. Insert the Petri dish adapter into its designed place then block it by using metal clip. (Figure 25).

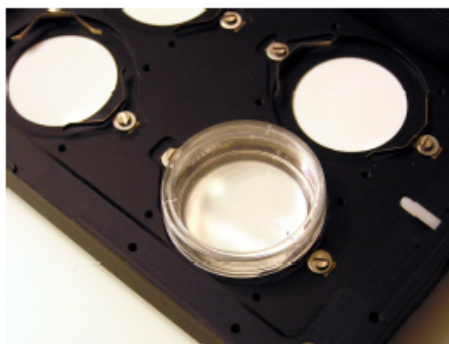


Figure 25: Petri dish adapter into its designed place

2. Switch on the Control Unit.
3. Close the Chamber Base with the Lid.

7.2. Specimen temperature feedback

To switch to this configuration, ONCE changed the controller parameters, starting from chamber temperature configuration, remove the temperature sensor from 'T1' connector (rear of Control Unit) and insert it in 'R.T.' connector. Insert in connector 'T1', the free temperature sensor (tagged 'SPECIMEN') as shown in Figure

26. The end of this sensor has to be properly inserted in the reference well. Please read carefully, the next paragraphs.

Notice: In this configuration the chamber Base temperature depends directly on the measured temperature in the reference well. Do not switch on the Control Unit if the free temperature sensor (tagged "SPECIMEN") is not in the correct configuration, which means in the reference well as shown in the next paragraph. **In case of OVERHEATING the Alarm rings and limits the base temperature.**

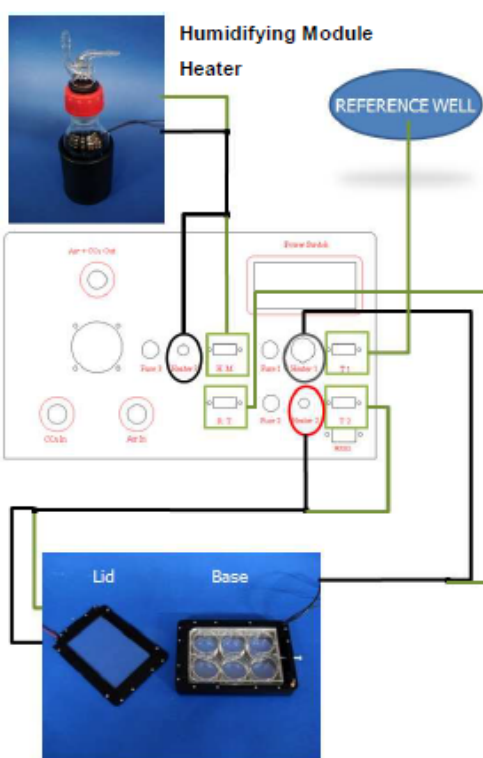


Figure 26: Complete cables scheme for Specimen control feedback configuration

7.2.1. Multi well adapter

Once fixed the multi well adapter (see Figure 17), to reduce thermal gradient, put the 1mm thickness glass inside the chamber, from the top, on the insert.

4. Scheme 1:

- a. Use a multi well plate different from the one where you will load the specimen, just to control the temperature during the start up of the experiment (reference Multi Well plate).
- b. Insert it in the Stage Incubator.
- c. Stick, using any common adhesive tape, the loose end of the Fine Gauge Thermocouple (sensor) to the bottom one well (reference well). Notice to leave the end of the sensor out of the adhesive tape. (See Figure 27).

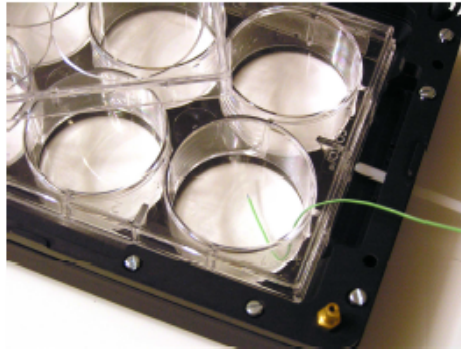


Figure 27: Specimen temperature feedback: 6 well configuration, particular.

- d. Fill the reference well hosting the thermocouple with distilled water, then close the Multi Well plate with its own cover and the Electric Micro Environmental Chamber, that fits the microscope stage, with its own lid.
- e. Prepare the specimen in another new Multi-Well. Remember to leave one of the wells for the Fine Gauge Thermocouple.
- f. Remember to stop the controllers before open the incubator, to avoid temperature overshoot, then re-start once you close the Electric Stage Incubator. See paragraph 5.5.
- g. Once the system has reached a temperature close to 37°C (i.e. 36.7°C, see below), remove the thermocouple from the provisory Multi-Well, and substitute the reference Multi Well plate with the Multi-Well plate where you have loaded your specimen.
- h. Inserting the thermocouple in a Multi-Well plate: the reference well
- i. Start the system following the next instructions:


Notice: Every time you start the Electrical Microscope Stage Incubator **REMEMBER** to monitor for 10-20 minutes the "Temperature 1" and "Temperature 2" to understand if everything was 'well done'.


Switch on the Control Unit.

Stand by the controllers 'Temperature' 1 and 'Temperature 2' by clicking for 2 seconds <P/S button. The message 'Stop' will appear.

Close the Chamber Base with the Lid.

Start the controllers 'Temperature' 1 and 'Temperature 2' by clicking for 2 seconds <P/S button. The current measured temperature will appear.

 **Notice:** Every time you open the Electrical Microscope Stage Incubator **REMEMBER** to stand by the controllers "Temperature 1" and "Temperature 2" to avoid temperature overshooting.

 Remember to fill the reference well with enough water: the end of the fine gauge thermocouple HAS to be under the water level. If this condition is not respected, could be present thermal instability in the thermal profile.

5. Follow the scheme 2: Minimize contamination.

- j. Get free the Thermocouple sensor:
- k. Disconnect the Thermocouple connector from the control unit.
- l. Prepare the Multi-Well plate under sterile wood.
- m. Stick, using any common adhesive tape, the loose end of the Fine Gauge Thermocouple (sensor) to the bottom one well (reference well). Notice to leave the end of the sensor out of the adhesive tape.
- n. Fill the reference well hosting the thermocouple with distilled water
- o. Prepare the Multi-Well plate
- p. Fill the space present among the well of the Multi-Well plate, in order to improve the gas saturation, with distilled water. Please remember to control the distilled water level in these interstitial spaces before starting and during the experiment.
- q. Close the Multi-Well plate with its own lid, always under sterile wood.
- r. Quickly, come back to the microscope with the specimen and the Fine Gauge thermocouple.
- s. Open the Electric Stage Incubator.
- t. Insert the multi Well Plate in the Stage Incubator that fits the microscope stage. Let the thermocouple cable pass between the Stage incubator cover and basis.
- u. Close the Electric Stage Incubator.
- v. Connect the thermocouple connector in position T 1 according to paragraph
- w. To fix the Multi-Well plate turn the white plastic screw as shown in Figure 12.
- x. Start the system following the next instructions:

- 🔊 **Notice:** Every time you start the Electrical Microscope Stage Incubator **REMEMBER** to monitor for 10-20 minutes the "Temperature 1" and "Temperature 2" to understand if everything was 'well done'.

Switch on the Control Unit.

Stand by the controllers 'Temperature' 1 and 'Temperature 2' by clicking for 2 seconds <P/S button. The message 'Stop' will appear.

Close the Chamber Base with the Lid.

Start the controllers "Temperature" 1 and "Temperature 2" by clicking for 2 seconds <P/S button. The current measured temperature will appear.

- 🔊 **Notice:** Every time you open the Electrical Microscope Stage Incubator **REMEMBER** to stand by the controllers "Temperature 1" and "Temperature 2" to avoid temperature overshooting.
- 🔊 Remember to fill the reference well with enough water: the end of the fine gauge thermocouple HAS to be under the water level. If this condition is not respected, could be present thermal instability in the thermal profile.

7.2.2. Petri dish adapter

1. Stick, using any common adhesive tape, the loose end of the Fine Gauge Thermocouple (sensor) to the bottom one well (reference well). Notice to leave the end of the sensor out of the adhesive tape. (Figure 28).



Figure 28: Sensor placement and fixing

2. Insert the Petri dish in its designed place then block it by using metal clip.

3. Fill the reference well hosting the thermocouple with 4 ml of distilled water, then close the Petri dish with its own cover to avoid water evaporation, and the Electric Micro Environmental Chamber, that fits the microscope stage, with its own lid.

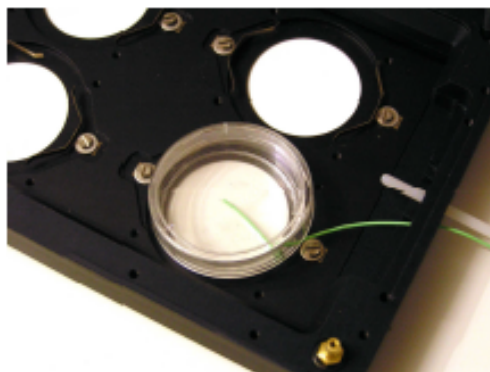


Figure 29: Petri dish (reference well) placement

4. Start the system

- ⓘ **Notice:** Every time you start the Electrical Microscope Stage Incubator **REMEMBER** to monitor for 10-20 minutes the "Temperature 1" and "Temperature 2" to understand if everything was 'well done'.

Switch on the Control Unit.

Stand by the controllers "Temperature" 1 and "Temperature 2" by clicking for 2 seconds <R/S button. The message 'Stop' will appear.

Close the Chamber Base with the Lid.

Start the controllers "Temperature" 1 and "Temperature 2" by clicking for 2 seconds <R/S button. The current measured temperature will appear.

- ⓘ **Notice:** Every time you open the Electrical Microscope Stage Incubator **REMEMBER** to stand by the controllers "Temperature 1" and "Temperature 2" to avoid temperature overshooting.

- ⓘ Remember to fill the reference well with enough water: the end of the fine gauge thermocouple HAS to be under the water level. If this condition is not respected, could be present thermal instability in the thermal profile.

8. Support

8.1. Web conference for assistance and training

In case you requested on line support and/or web conference assistance for system assembling and experiment support, you received a web cam. Please follow these rules to receive a good service:

- Webcam Installation (Instruction and Cd rom Included)
- Last MSN Messenger ® installed (www.msn.com)
- Register yourself on www.msn.com to have an account (MSN passport)
- Set the audio and video and test them using MSN Messenger.
- If you have problem with MSN Messenger you can choose Skype ® software (www.skype.com).
- Contact our technical support (sibilo@oko-lab.com) by e-mail to take an appointment for the web assistance.

8.2. Technical Support.

Please, do not hesitate to contact Okolab should you need any further commercial information or technical support.

Please, check Okolab web site www.oko-lab.com for news, events, new products and general FAQ.

For	COMMERCIAL SUPPORT:	lanzaro@oko-lab.com	
		Phone	+39 081 806 2624
		Fax:	+39 081 876 4410
		Mobile:	+39 348 96807 17
For	HARDWARE SUPPORT:	sibilo@oko-lab.com	
		Phone	+39 081 806 3470
		Fax:	+39 081 876 4410
		Mobile:	+39 348 96807 18

Published by Okolab S.r.l., Via G. Di Prisco, 152, 80040 Ottaviano (NA), ITALY

8.3. Technical Specifications

System Specifications	
Ambient temperature range	20°C+30°C (23°C suggested)
Chamber temperature range	25°C+50°C
Specimen temperature range	3°C above ambient temperature to 45°C
Regime temperature Time:	about 40 min
Regime Temperature Stability	± 0.3°C (chamber temperature feedback)
	± 0.2°C (specimen temperature feedback)
Set point value range	30+45
Offset value range	-15+5
Weight	About 400 g (It depends on configuration)

Precision fine wire thermocouples: type K; Chromega-Alomega.

8.4. Troubleshooting

Incorrect operations are often mistaken for trouble and malfunctions. If you think that there is something wrong with a component, check the points below. Sometime the trouble may lie in another component. Investigate the others components, electrical appliance. If the trouble cannot be rectified even after exercising the checks listed below, ask Okolab Technical Support.

Symptom	Probable cause	Remedy
Device off	Supply cable disconnected	Properly connect the cable
	Supply cable damaged	Substitute the cable
	Blown fuse	Replace the fuse (see Technical Specifications)
No temperature displayed	Thermocouple cable disconnected	Properly connect the cable
	Thermocouple cable damaged	Contact Okolab to receive assistance
Specimen temperature differ from set point	Ambient temperature too low or too high	Regulate the ambient temperature
		Change the Offset value
Chamber Base and Lid cold	Low set point value	Change the set point
	Heater ½ and/or cable disconnected	Connect the cable
	Heater ½ and/or cable damaged	Contact Okolab to receive assistance
	Resistances damaged	Contact Okolab to receive assistance
Alarm rings (for specimen temperature feedback)	Chamber Base at high temperature (for specimen temperature feedback)	Quickly shoot down the control unit and properly set the system. Please, check below
Chamber Base at high temperature (for specimen temperature feedback)	Control thermocouples connection	Check the connection scheme
	Damaged thermocouple	Ask Okolab for replacement
	Sensor out of the reference well	Properly set the reference well
I check the previous troubleshooting but I cannot solve the problem	Contact Okolab to receive assistance	

9. Appendix: Controller manual

4. PARTS DESCRIPTION

(1) Measured value (PV) display (Green)
Displays PV or various parameter symbols.

(2) Set value (SV) display (Orange)
Displays SV or STEP set value (SV1, SV2).
Displays various parameter set values.

(3) Indication lamps
AutoStart (AT) lamp (Green)
Flashes during autoStart activation.
(After autoStarting is completed, AT lamp will become OFF)

Output lamps (OUT1, OUT2) (Green)
OUT1: Lights when output 1 is turned on.
OUT2: Lights when output 2 is turned on.

STEP set value (SV2) lamp (Orange)
Lights when the SV2 of STEP function is selected.

Alarm lamps (ALM1, ALM2) (orange)
ALM1: Lights when alarm 1 is turned on.
ALM2: Lights when alarm 2 is turned on.

(4) UP key
Increase numericals.

(5) DOWN key
Decrease numericals.

(6) SHIFT & RS key
Shift digits when settings are changed.
Selects the RUN/STOP function.

(7) SET key
Used for parameter calling up and set value registration.

To avoid damage to the instrument, never use a sharp object to press keys.

5. SETTING

Parameter Setting Mode

- Lb** Control loop (loop gain) (0.04)
Setting range: 0 to 999.999
Factory set value: 0.3
- AL1** Alarm 1 (ALM1)
Setting range: Process alarm, SV alarm, Sensor input alarm, Derivative alarm, AutoStart alarm
Factory set value: Temperature input: 0.0000, Voltage input: 0.0
- AL2** Alarm 2 (ALM2)
Setting range: Process alarm, SV alarm, Sensor input alarm, Derivative alarm, AutoStart alarm
Factory set value: Temperature input: 0.0000, Voltage input: 0.0
- HCU** AutoStarting (AT)
Setting range: ON: AT sensor excitation, OFF: Not during operation
Factory set value: OFF
- ST** Self-Starting (ST)
Setting range: ON: Self-starting ON, OFF: Self-starting OFF
Factory set value: OFF
- Head-side proportional band (P)**
Setting range: 0 to 999.999 (0.0: 0.0000) value
Factory set value: 100.0000
- Integral time (I)**
Setting range: 0 to 999.999 (0.0: 0.0000)
Factory set value: 5.0
- Derivative time (D)**
Setting range: 0 to 999.999 (0.0: 0.0000)
Factory set value: 0.0

Gain

- 000: No gain (0.0000)
- 001: 0.0000
- 002: 0.0000
- 003: 0.0000
- 004: 0.0000
- 005: 0.0000
- 006: 0.0000
- 007: 0.0000
- 008: 0.0000
- 009: 0.0000
- 010: 0.0000
- 011: 0.0000
- 012: 0.0000
- 013: 0.0000
- 014: 0.0000
- 015: 0.0000
- 016: 0.0000
- 017: 0.0000
- 018: 0.0000
- 019: 0.0000
- 020: 0.0000
- 021: 0.0000
- 022: 0.0000
- 023: 0.0000
- 024: 0.0000
- 025: 0.0000
- 026: 0.0000
- 027: 0.0000
- 028: 0.0000
- 029: 0.0000
- 030: 0.0000
- 031: 0.0000
- 032: 0.0000
- 033: 0.0000
- 034: 0.0000
- 035: 0.0000
- 036: 0.0000
- 037: 0.0000
- 038: 0.0000
- 039: 0.0000
- 040: 0.0000
- 041: 0.0000
- 042: 0.0000
- 043: 0.0000
- 044: 0.0000
- 045: 0.0000
- 046: 0.0000
- 047: 0.0000
- 048: 0.0000
- 049: 0.0000
- 050: 0.0000
- 051: 0.0000
- 052: 0.0000
- 053: 0.0000
- 054: 0.0000
- 055: 0.0000
- 056: 0.0000
- 057: 0.0000
- 058: 0.0000
- 059: 0.0000
- 060: 0.0000
- 061: 0.0000
- 062: 0.0000
- 063: 0.0000
- 064: 0.0000
- 065: 0.0000
- 066: 0.0000
- 067: 0.0000
- 068: 0.0000
- 069: 0.0000
- 070: 0.0000
- 071: 0.0000
- 072: 0.0000
- 073: 0.0000
- 074: 0.0000
- 075: 0.0000
- 076: 0.0000
- 077: 0.0000
- 078: 0.0000
- 079: 0.0000
- 080: 0.0000
- 081: 0.0000
- 082: 0.0000
- 083: 0.0000
- 084: 0.0000
- 085: 0.0000
- 086: 0.0000
- 087: 0.0000
- 088: 0.0000
- 089: 0.0000
- 090: 0.0000
- 091: 0.0000
- 092: 0.0000
- 093: 0.0000
- 094: 0.0000
- 095: 0.0000
- 096: 0.0000
- 097: 0.0000
- 098: 0.0000
- 099: 0.0000
- 100: 0.0000

MRD1001-E8

■ Changing Parameter Settings

Procedures to change parameter settings are shown below.

To store a new value for the parameter, always press the SET key. The display changes to the next parameter and the new value will be stored.
 - A new value will not be stored without pressing SET key after the new value is displayed on the display.
 - After a new value has been displayed by using the UP and DOWN keys, the SET key must be pressed within one minute, or the new value is not stored and the display will return to the PWSV display mode.

When the set data is locked, the digits on the SV display are brightly lit and the set value cannot be changed.

● Change the set value (SV)

Change the set value (SV) from 0 °C to 208 °C

1. select the SV editing mode

Press the SET key 2 times. The PWSV monitor screen until SV setting screen is displayed.

2. Start the blinking digit

Press the -R/S key to blink the hundreds digit. The blinking digit indicates which digit can be set.

3. Change the set value

Press the UP key to change the number to 2.

4. Store the set value

Press the SET key to store the new set value. The display returns to the PWSV display mode.

● Change parameters other than the set value (SV)

The changing procedures are the same as those of example 2. to 4. in the above. ● Change the set value (SV). * Pressing the SET key after the setting and shifts to the next parameter. When an parameter setting is required, return the instrument to the PWSV display mode.

6. OPERATION

6.1 Operating Precautions

- (1) All modeling and wiring must be completed before the power is turned on.
- (2) The settings for the SV and all parameters should be appropriate for the controlled object.
- (3) A power supply switch is not furnished with this instrument. It is ready to operate as soon as the power is turned on.
 [Factory set value: RUN (operation start)]

Connect the input signal wiring and turn the power on. If the input signal wiring is not complete prior to turning the power on, the instrument determines that a fault has occurred.

A power failure of 20 ms or less will not affect the control action. When a power failure of more than 20 ms occurs, the instrument assumes that the power has been turned off. When power returns, the controller will retain the conditions that existed prior to shut down.

The alarm reset action is activated when the power is turned on or the SV is changed, including an SV change made with the STOP function.

6.2 RUN/STOP

RUN/STOP can be selected by contact input (option) other than the key operation. In addition, at STOP, the key operation and contact state are displayed on the PV display. Relationships between key operation, RUN/STOP and the characters to indicate the STOP state are shown in the following.

		RUN/STOP with Contact Input ¹⁾	
		RUN (Contact closed)	STOP (Contact open)
RUN/STOP with Key Operation	RUN	RUN	STOP
	STOP	STOP is not displayed	STOP ²⁾ (STOP) ³⁾
		STOP ⁴⁾ (STOP) ⁵⁾	STOP ⁴⁾ (STOP) ⁵⁾

- ¹⁾ Contact input: Terminal No. 10, 12
 - ²⁾ Characters in parentheses are those shown on the PV display.
 - ³⁾ STOP: Only contact input is in the STOP mode
 - ⁴⁾ STOP: Only key operation is in the STOP mode
 - ⁵⁾ STOP: Both key operation and contact input are in the STOP mode
- Conditions which changed to STOP mode:
- Control, Alarm: Control OFF, Alarm OFF
 - Output: OUT1 output OFF (OPEN), OUT2 output OFF (OPEN)
 - Autotuning (AT): AT canceled (The PID constants are not updated)

■ RUN/STOP transfer by key operation

1. Press the -R/S key for 1 second in PWSV display mode.
2. The mode is changed to STOP from RUN. The PV display shows the characters of showing the relevant STOP state.

Also when changing from STOP to RUN, press the -R/S key for 1 second while in the PWSV display mode.

■ RUN/STOP transfer by contact input

RUN/STOP can be selected according to the open or closed state of the terminal numbers 10 to 12.

Terminal No.	RUN	STOP
10 - 12	Contact closed	Contact open

6.3 Set Data Lock (LCK)

The set data lock restricts parameter setting changes by key operation. The function prevents the operator from making errors during operation.

Set value	Parameters which can be changed
0000	All parameters (except set value)
0001	SV, Alarm (ALM1, ALM2)
0010	All parameters except for Alarm (ALM1, ALM2)
0002	All parameters except for SV
0011	SV
0001	Alarm (ALM1, ALM2)
0010	All parameters except for SV and Alarm (ALM1, ALM2)
0011	No parameter (ALL LOCK)

Set Data Lock can be changed in both RUN and STOP mode. Parameters protected by Set Data Lock function are still displayed for monitoring.

6.4 Autotuning (AT)

Autotuning (AT) automatically measures, calculates and sets the optimum PID and LSA constants. The following conditions are necessary to carry out autotuning and the conditions which will cause the autotuning to stop.

Caution for using the Autotuning (AT)
 When a temperature change (UP and/or Down) is 1 °C or less per minute during autotuning, autotuning may be cancelled before calculating PID values. In that case, adjust the PID values manually. It is possible to happen when the set value is around the ambient temperature or is close to the maximum temperature controlled by the load.

■ Requirements for AT start

- Start the autotuning when all following conditions are satisfied:
- Prior to starting the AT function, all the parameter settings other than PID and LSA.
 - Confirm the LCK function has not been engaged.
 - When the autotuning is finished, the controller will automatically return to PID control.

■ Requirements for AT cancellation

- The autotuning is canceled if any of the following conditions exist.
- When the set value (SV1, SV2) is changed.
 - When the power is turned off.
 - When the PV bias value is changed.
 - When the RUN/STOP mode is changed to the STOP mode.
 - When the PV becomes abnormal due to bumpout.
 - When the AT does not end in 5 hours after autotuning started.
 - When power failure longer than 20 ms occurs.

If the AT is canceled, the controller immediately changes to PID control. The PID values will be the same as before AT was activated.
 When AT is completed, the controller immediately changes to PID control. If the control system does not allow the AT cycling process, set each PID constant manually to meet the needs of the application.

6.5 Self-tuning (ST)

The ST function is used to automatically calculate and set adaptive PID constants anytime the power is turned on, the SV is changed or the controller detects unstable control conditions.

- The ST function should be turned off when the controlled system is affected by ripples that occurs due to periodic external disturbances.
- The power to the controlled system must be turned on before the power to the instrument is turned on or SV is changed. This is required when ST function is on.
- To activate the ST function, the following parameters must not be set to zero: Pw0, Sw0, Dv0, ARWw0.
- When heuristic PID action is selected, the ST function cannot be activated.
- When the AT function is activated, the ST function can not be turned on.
- When the ST function is activated, the PID and ARW settings can be monitored, but not changed.

Figures

FIGURE 1. SYSTEM OVERVIEW	5
FIGURE 2: COMPLETE GAS LINES SCHEME.....	8
FIGURE 3: PRESSURE GAUGE (PROVIDED BY OKOLAB): CORRECT GAS INPUT – OUTPUT.....	9
FIGURE 4: AVOID GAS LEAK: STRONGLY PUSH THE TUBE INTO THE SWIFT-FIT CONNECTOR	9
FIGURE 5: CONNECTING THE BLUE RIGID PLASTIC TUBE.....	10
FIGURE 6. FRONT PANEL	10
FIGURE 7. BACK PANEL	11
FIGURE 8: COMPLETE CABLES SCHEME FOR CHAMBER CONTROL FEEDBACK CONFIGURATION.....	12
FIGURE 9. ELECTRIC MSI OVERVIEW, BASE PLATE AND LID WITHOUT ADAPTERS.....	13
FIGURE 10: ELECTRIC MSI OVERVIEW, BASE PLATE AND LID WITH 6 WELL ADAPTER.....	13
FIGURE 11: INTERCHANGEABLE PLATE ADAPTERS FOR 2 WELL, GLASS SLIDES AND 96 MULTIWELL.....	13
FIGURE 12. STANDARD BASE.....	15
FIGURE 13. ADDITIONAL BODY FOR STANDARD BASE. SPACER TO INCREMENT THE BASE VERTICAL HEIGHT.....	15
FIGURE 14. STANDARD BASE WITHOUT BARB FITTING.....	15
FIGURE 15. PUT THE ADDITIONAL BODY ON THE STANDARD BASE.....	16
FIGURE 16. TIGHTEN THE M2 SCREWS.....	16
FIGURE 17. STAGE INCUBATOR BASE AND LID INSERTS.....	16
FIGURE 18: CALIBRATION DOCUMENT, FACSIMILE	18
FIGURE 19. TEMPERATURE PROFILES, AMBIENT 23.0°C, SET POINT 37.0°C AND 'SECONDARY OFFSET 1'=-2.0°C. 21	21
FIGURE 20. TEMPERATURE PROFILES, AMBIENT 23.0°C, SET POINT 37.0°C AND 'SECONDARY OFFSET 1'=-4.2°C. 21	21
FIGURE 21. DISPLAY DESCRIPTION	24
FIGURE 22. FLOW METERS GRADUATED SCALES, EXAMPLE FOR TWO GAS LINES.....	28
FIGURE 23. FLOW METERS GRADUATED SCALES, EXAMPLE FOR THREE GAS LINES.....	30
FIGURE 24: CHAMBER TEMPERATURE FEEDBACK: 6 WELL CONFIGURATION	31
FIGURE 25: PETRI DISH ADAPTER INTO ITS DESIGNED PLACE	31
FIGURE 26: COMPLETE CABLES SCHEME FOR SPECIMEN CONTROL FEEDBACK CONFIGURATION.....	32
FIGURE 27: SPECIMEN TEMPERATURE FEEDBACK: 6 WELL CONFIGURATION, PARTICULAR.	33
FIGURE 28: SENSOR PLACEMENT AND FIXING	35
FIGURE 29: PETRI DISH (REFERENCE WELL) PLACEMENT.....	36

WARRANTY

Okolab S.r.l. warrants the "Okolab electrical stage incubator" to be free of defects in materials and workmanship for a period of two (2) years starting from invoice date. If the unit malfunctions, it must be returned to the factory for evaluation. If the equipment has to be returned to the factory, please ensure that is carefully and properly packed. Okolab S.r.l. accepts no responsibility for damage due to unsatisfactory packing. Upon examination of Okolab S.r.l., if the unit is found to be defective, it will be repaired or replaced at no charge. This warranty does not apply to defects resulting from any actions of the purchaser. Components which wear are not warranted. Okolab S.r.l. neither assumes responsibility for any omissions or errors nor assumes liability for any damages that result from the use of its products in accordance with information provided by Okolab S.r.l.. Okolab S.r.l. warrants only the parts manufactured by it will as specified and free of defects. Okolab S.r.l. makes no other warranties or representations of any kind whatsoever, express or implied, except that of title, and all implied warranties including any warranty of merchantability and fitness for a particular purpose are hereby